INDIAN RIVER INLET BRIDGE AND BATHYMETRY SCOUR MONITORING SYSTEM

BY

JESSE T. HAYDEN

AND

JACK A. PULEO

RESEARCH REPORT NO. CACR-09-02
JULY 2009

CENTER FOR APPLIED COASTAL RESEARCH

Ocean Engineering Laboratory
University of Delaware
Newark, Delaware 19716

ACKNOWLEDGEMENTS

This project was funded by the Delaware Department of Transportation and University of Delaware.

TABLE OF CONTENTS

LIST OF FIGURES

LIST OF TABLES

ABSTRACT

Mention the Indian River Inlet Bridge to any Delawarean and they will surely ask if it is safe to use. The scour problems that have plagued the current bridge for the past 30 years are common knowledge, and public concern over the safety of the bridge pushed the Delaware Department of Transportation (DelDOT) to team up with the University of Delaware to design and install a custom system to monitor the bridge. The Indian River Inlet Bridge and Bathymetry Scour Monitoring System (BBSMS) employs tilt sensors, scanning sonar, and current profilers to return a variety of information that DelDOT engineers can use to determine the bridge integrity and ensure the safety of the public.

Results from the BBSMS are combined with earlier field surveys to analyze the morphodynamics associated with the giant scour holes. Observations from two different current profiler deployments and a thermal camera investigation corroborate the presence and significance of macroturbulence in suspending and transporting sediment out of the inlet. The flow pattern behind the rise in bathymetry located under the bridge is studied in detail during ebb tide, as the macroturbulence generated by the ebbing tide is thought to be responsible for the ongoing local scour threatening the bridge.

The two sonars of the BBSMS are able to return bathymetry data from approximately $25,000m^2$ of the channel bed twice per day; and the resulting maps of the channel are geo-referenced for viewing in Google Earth to give DelDOT engineers a powerful, yet easy to use, decision making tool. Transfer and processing of all of the BBSMS data are performed automatically, returning high value information

while reducing the daily cost of operation of the near-real time system. The BBSMS will be a vital tool for DelDOT engineers until the replacement bridge completely spanning the Indian River Inlet is completed in late 2011.

INTRODUCTION

The two most common methods of combating bridge pier scour in the USA are scour hole monitoring and channel bed armoring with riprap [23, p. 320]. Traditional in situ bridge scour monitors focus on the immediate vicinity of the foundation or abutments, and are generally limited to single point observations. When that immediate vicinity is armored with riprap, it becomes prudent to observe the entire armored area. Riprap stones are designed to resist movement under a certain design velocity and can retard sediment loss from large areas of flow channels at relatively low cost [18]. However, Chiew [2; 4] and Lauchlan and Meville [19] describe how local armoring can fail, even if the stones are sufficiently massive to resist the flow themselves.

If a bridge spans sufficiently deep water, then in situ sonar monitors can still be used to observe the riprap blanket. The single echosounder methods of Schall et al [32] could be adapted by aiming transducers at a more oblique angle in order to observe a single point some distance from the bridge pier. However installing multiple transducers to observe every point of interest complicates the simple logistics of Schall's design. A better approach employs a scanning sonar to observe wide areas of the channel using only a single transducer. Some scanning instruments and methods, restricted to portable scour monitors only, are presented in NCHRP Report 515 *Portable Scour Monitoring Equipment* [33]. The Sonar Scour Vision System (SSVS), a 675kHz scanning transducer system developed by American Inland Divers, Inc. and operated during the 1993 flooding of the upper Mississippi River met the performance demands of observing large spatial areas (up to a $100m$

radius) using a single transducer deployed at one location [31]. While other sonar instruments such as side scan sonar can cover large areas, they do not return depth information like the scanning profiling sonar. The SSVS and similar portable systems are deployed using a small crane [33], which requires traffic lane closure and dedicated personnel. These requirements limit applicability to severe storm events with substantial flooding.

Advanced scour monitoring becomes a significant priority when a bridge is classified as scour critical. To ensure public safety, the engineers that make decisions about bridge operation need to be armed with as much information as is available. Ideally, they should have access to multi-dimensional data which consider both the bridge and its relationship with the channel. A bridge and bathymetry scour monitoring system - BBSMS, as will be described in this thesis, can provide a wealth of information giving engineers the ability to make daily bridge safety decisions based on a variety of high quality data.

Delaware's Route 1 State Highway Bridge over the Indian River Inlet is in danger of being rendered unfit for public use. In recent years, as giant scour holes expanded toward the bridge substructure, Delaware Department of Transportation (DelDOT) engineers were forced to take defensive actions to ensure the continued safety of the public until a replacement bridge is completed. Part of this defense began in 1989 with the armoring of the channel bed in the vicinity of the underwater bridge substructure with large riprap stones. The plan continues with the efforts presented here: monitoring of the bridge and the surrounding bathymetry for telltale changes that could indicate a decline in the stability of its foundation.

The system presented employs a number of instruments and techniques to process data multiple times per day, giving DelDOT engineers the power to make decisions on time scales comparable with storm events. This enhanced ability to

monitor the existing bridge should ease the tension created by the delays in constructing a replacement along with the collective public concern over the progressing scour.

The Indian River Inlet is predominantly navigated by recreational fishermen and boaters, though the US Coast Guard has a base just inside the inlet and a number of charter boats operate out of the Indian River Marina. The Indian River Inlet Bridge, carrying an average annual daily traffic load of more than 13,000 cars, is supported by two piers in the channel and two piers outside the channel.

The dual bay and inlet system is located about 160km east of Washington, DC and 160km south of Philadelphia on Delaware's short stretch of Atlantic coast. The bays cover approximately $31km^2$ each, with catchment area of $650km^2$ [9]. Delaware's coastline stretches from Cape Helopen at the north to the town of Fenwick Island at the state line, 40km to the south. The Indian River Inlet breaks this otherwise continuous reach of sandy beaches just south of the midpoint. The armored channel is oriented about 5 degrees from true east-west, as can be seen in Figure 1.

The two bays are connected through a narrow throat known as *The Ditches* or as *Massey's Ditch* by some locals. *Middle Island* splits this communicating throat into a major (*Big Ditch*) and minor (*Little Ditch*) channel, in addition to inhibiting flow between the bays by adding friction. The land surrounding both bays is very low elevation, with some marsh and farmland. The Assawoman Canal links Indian River Bay to Assawoman Bay to the south with a narrow and shallow channel. The Rehoboth Canal links Rehoboth Bay to the Delaware Bay to the north with a slightly more significant channel. These canals have had very little influence on the two bay and inlet system, even prior to the improvements to the inlet [14].

Today, the bays have a collective average depth of 1.5m at low tide, though Rehoboth Bay is generally slightly shallower than Indian River Bay. The tidal

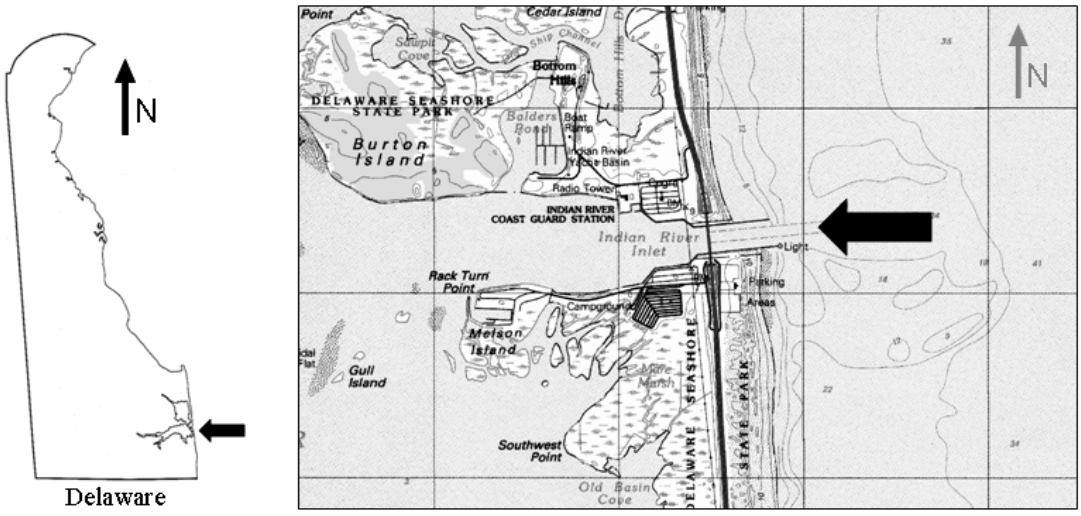

Figure 1: Map of Delaware showing location of Indian River Inlet, with regional view of Inlet and Bays inset. Note the orientation of the channel is not perfectly east-west.

range in the bays has increased steadily since the US Army Corps of Engineers armored the channel walls, now Indian River Bay sees tides of 0.64m while water in Rehoboth Bay oscillates about half that distance at 0.3m. The salinity in most of the bay waters matches the salinity of the ocean, only dropping near the inflow of the Indian River [9].

The tidal prism has changed from $778,000m^3$ in 1931 when the inlet was a natural opening to the 1986 value of $42,500,000m^3$ and beyond; permanent tide gages do not exist in the bays, so accurate measurements of the change in tidal prism only accompany field experiments. The *inlet tide* is considered at the Coast Guard Station just inside the channel, while values for the bay tides are considered to be far from the inlet [20]. A 1.25m ocean tide range has been constant throughout the period of history considered in this investigation, and it is the gradient in free surface elevation through the inlet that drives the intense currents observed since the first improvements were made to the natural channel.

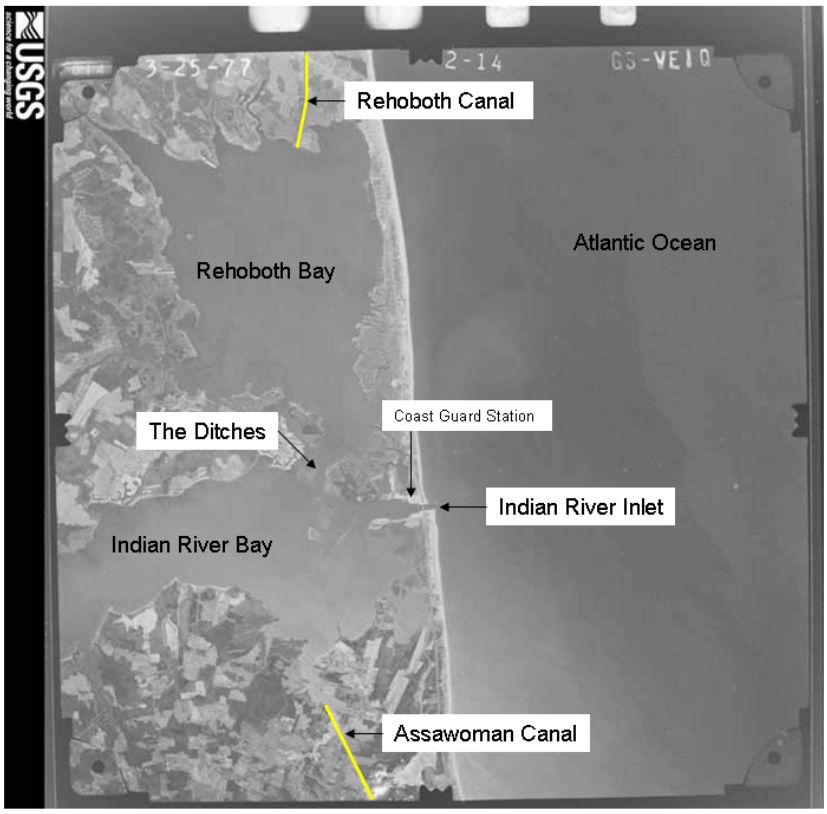

Figure 2: USGS aerial photograph from 1977 showing the dual bays, the inlet, and the two canals.

Chapter 1

A BRIEF HISTORY OF INDIAN RIVER INLET

1.1 Geologic History

During the Wisconsin Glacial Period, the local sea level reached an elevation estimated at $70m$ to $90m$ lower than Present Day — placing the coastline $100km$ east of its present location. The Delaware River migrated northward, and deposited thick layers of mud and silt along the present Delaware coastline. That mud was subsequently covered with about 10m of modern coastal sand, which is the sand we now see when we visit the beach [34]. Reliable geotechnical data in the vicinity of the present day inlet is sparse, but evidence suggests that under the $10m$ layer of modern coastal sand sits $20m$ of silty mud containing some organic materials, all on top of compacted Pleistocene era sand below extending to an indefinite depth [34]. Prior to anthropogenic "improvements" the Indian River Inlet periodically opened and closed and migrated along Delaware's coast.

1.2 Early Improvement Efforts

Locals were interested in maintaining an inlet to support the fishing industry that developed in the bays, see the photo in Figure 1.1. During times when the natural inlet closed from sedimentation or shoaling, the water quality in the bays degraded and fishermen and traders could not navigate between the bays and the Atlantic. In the early 1910's the inlet was silted closed; a few hundred local farmers attempted to reopen the inlet with shovels. Their labors were not rewarded as the

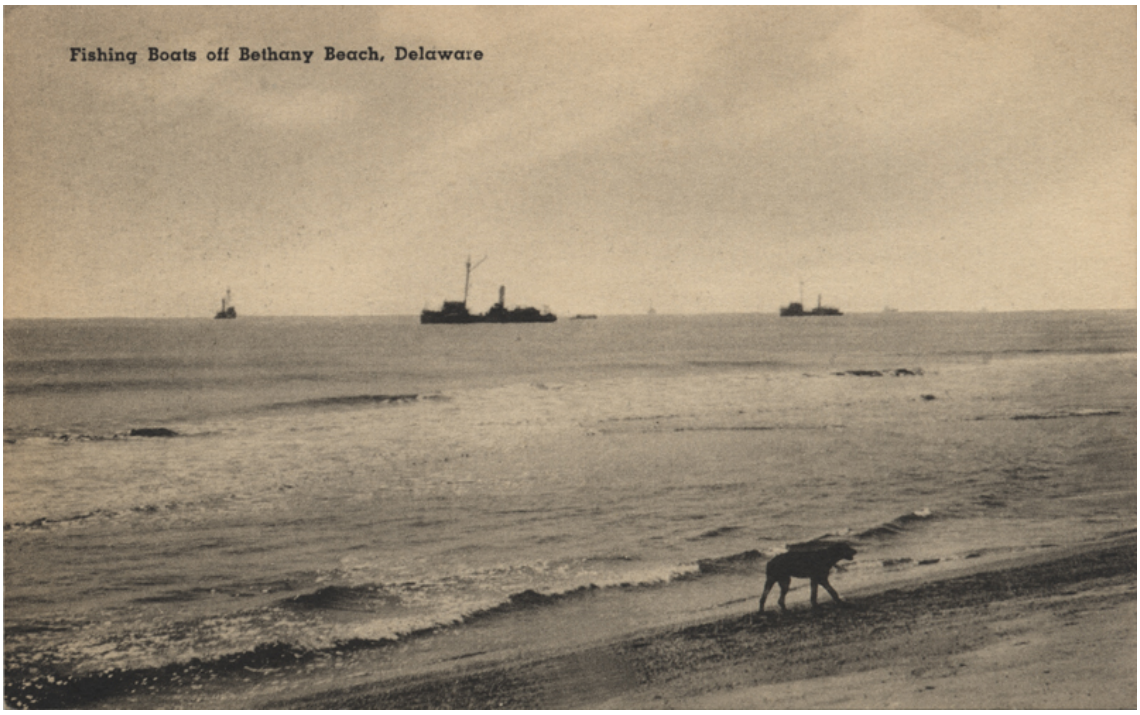

Figure 1.1: 1900's era postcard showing large fishing boats off the coast just outside the Inlet.

opening they created was too small and quickly closed again [24]. In 1919, the 97th General Assembly of the State of Delaware created the first Indian River Inlet Commission, indicating that the desire to maintain a navigable inlet extended to the entire state. The Commission was given some state funds, but the General Assembly suggested applying for federal assistance for creating a permanent inlet [10]. Nine years later, in 1928, the Commission had not yet received federal aid, but they were ready to try to open the inlet again. This time, under the engineering guidance of the Chief Engineer of the State Highway Department, a $1.25m$ deep and $20m$ wide cut was made through the dunes to within about 30m of the ocean water. This remaining section was to be cut by blasting experts using 1000 pounds of dynamite donated by the Hercules Powder Company. The dynamite-blasted channel initially allowed water to flow freely, but in a short time the sides of the channel slumped

inwards and the flow of water was restricted once more [24].

The sixth Indian River Inlet Commission appointed by the Delaware General Assembly published a report in 1931 regarding their efforts toward opening the inlet, as well as observations of the conditions and future plans. Following the 1928 attempt with dynamite, heavy rains in the winter and spring of 1929 raised the levels of the bays significantly. Again, locals cut through the dunes and beach, and aided by the $1m$ super-elevation of the bays, a $30m$ wide and $1.25m$ deep channel was created. This reopening of the inlet allowed water exchange with the ocean for a time, and local fishermen were rewarded with catches of saltwater species; however once the elevation of the bays returned to normal levels the channel began to shoal and it closed completely by the end of the summer of 1929 [14]. Figure 1.2 shows an aerial photograph of the inlet at a time when it appears non-navigable, the photograph is dated from 1931.

Pages 30 and 31 of the IRI Commission report contain observations on the duration of ebb or flood tide and the direction and speed of the prevailing wind during the observation. The notes cover June 15, 1930 through September 12, 1930 and required the direct attention of an observer. The original goal of these studies was to disprove the popular public opinion that the Rehoboth and Assawoman Canals were dominant factors in the periodic closing of the Indian River Inlet. The Commission concluded that the flow through the canals was insufficient to affect the elevation of water in the bays enough that the inlet should be negatively affected. They also noted that without the canals, the bay water would rise even further during periods of heavy rains and submerge and degrade nearby land [14].

One important note for comparison with future conditions is the observation that prior to 1938 the bays have no regular tide. During the study period in 1930 the average inflow through the inlet was $481,000m^3$ while the average outflow was observed to be $778,000m^3$. Given the wide surface area of the bays, this was only

Figure 1.2: 1931 aerial photograph showing the natural inlet with remnants of a previous cut through the dunes.

sufficient to raise or lower the bay water by $0.006m$ and $.01m$ respectively.

1.3 Engineered Inlet

Not until the federal government, in the form of the US Army Corps of Engineers (USACE), provided assistance was the anthropogenic inlet a permanent fixture on the coast. Initially, a dredged channel was cut through the dunes as before, and as with prior cuts this one shoaled closed in a short time. Beginning in 1935 studies were undertaken by the USACE Philadelphia District and the Shore Protection Board to design a permanent inlet with reinforced sides. The initial inlet design was based on Col. E.I. Brown's design methods found in his book "Inlets on Sandy Coasts" written in 1928.

Brown's method assumes that the water entering a bay is a function of the elevation of water in the ocean and the head loss along a prismatic channel. Possible channel dimensions were selected in the range of $76m$ wide by $2.4m$ deep to $152m$ wide by $3m$ deep, which according to Brown's method were associated with design peak velocities of $1.1m/s$ and $1.28m/s$ respectively. An ominous footnote in the history of the inlet: the initial 1935 Philadelphia District design of a $200m$ wide inlet was reduced to about $150m$ wide after recommendations from the Shore Protection Board in 1936 - in order to avoid future dredging by ensuring design velocities were high enough to maintain a self-scouring channel [9].

In 1938 construction began when the initial channel was dredged $150m$ wide and $3m$ deep, and work began on armoring the channel walls. In 1939 the $200m$ of outer stone jetty and $300m$ of inner sheet pile walls of the original design were completed, and immediately the sheet pile was outflanked by bank erosion. Years of reactionary construction extended and widened the initial channel to its present dimensions (visible in the aerial photograph in Figure 1.8). The longer armored length decreased the effective channel friction and in turn increased the tidal prism. Both the maximum velocity and the tidal prism continued to grow up until the latest comprehensive study which started in 1988, and was performed jointly by the USACE Philadelphia District and the Coastal Engineering Research Center (CERC) [22].

Immediately following the completion of the inner sheet pile inlet wall in 1939, the interior banks of the channel began to erode. This outflanking of the channel walls proved a persistent problem, as the construction raced to keep pace with nature until the length of armored channel stretched from the original $500m$ to a total of $900m$ [9]. From the completion of the jetties and first leg of sheet pile in 1941 to the last piecewise expansion of the channel, the distinct shape of the Inlet was born — a narrow main channel extending between two jetties into the ocean,

expanding twice with 45° flares and armored along the entirety of each bank before opening into the bay.

In addition to the lateral bank erosion issues, an inconvenient flood shoal was growing rapidly, periodically threatening to limit the effective navigation through the Inlet. This sink for sand became an attractive mining prospect to supply the outer shoreline north of the inlet with much needed nourishment, during a number of years it had eroded to the point where it threatened the highway paralleling the coast. A series of mining operations between 1972 and 1990 removed sand from the flood shoal for use as north shore nourishment; prior to 1972 other Rehoboth Bay sites were used as sand sources [9].

From the construction of the jetties in 1938 until 1975 the northern interior shoreline eroded at a rate of $4.6m$ per year, and the southern shoreline eroded at $3m$ per year until 1968 when "construction rubble" (possibly from the partial demolition of the old Inlet bridge) was used to reconstruct some of the southern shoreline. These steady erosion rates were coupled with the development of the same area: the northern shoreline saw the construction of a new Coast Guard Station and state marina and the southern shoreline became home to a trailer park, a campground, and private marina. Figure 1.3 shows the new state marina as well as a makeshift fishermen's campground on the northern shore west of the Coast Guard Station. Note that at this time the shoreline was natural, by 1989 this entire stretch would be armored with sheet pile, riprap, or both [9].

The coupled erosion and armoring of the interior shorelines effectively reduced both the length and the resistance to flow that had originally been a component of the design of the Inlet. Additionally, the final inlet shape, which is visible in Figure 1.8 created a venturi effect on the ebbing tide and quite possibly contributed to the scour problem discussed in Chapter 2 [31]. Figures 1.4 through 1.8 show the evolution of the interior shorelines, the flood shoal, the jetty-induced shoreline

Figure 1.3: Aerial photograph found on a postcard in the 1970's showing developments along the rapidly eroding northern interior shoreline of the Indian River Inlet.

erosion north of the inlet, and the bridges described in Section 1.4.

1.4 Bridges

The first state funded bridge across the inlet spanned the natural inlet with a wood trestle design. Completed in 1934, it crossed a differently oriented channel than subsequent bridges — as seen in Figure 1.9 the natural channel's orientation was dictated by the northward growing spit [7]. This map is dated from 1942, and as can be seen in Figure 1.10 it was prepared by USACE personnel; it is puzzling, then, why the map does not reflect the inlet that was completed by the USACE in 1939.

The 1934 wood bridge was damaged by storms and its replacement, the C. W. Cullen Bridge, was completed in 1938 [26; 7] or 1940 [5] depending on the

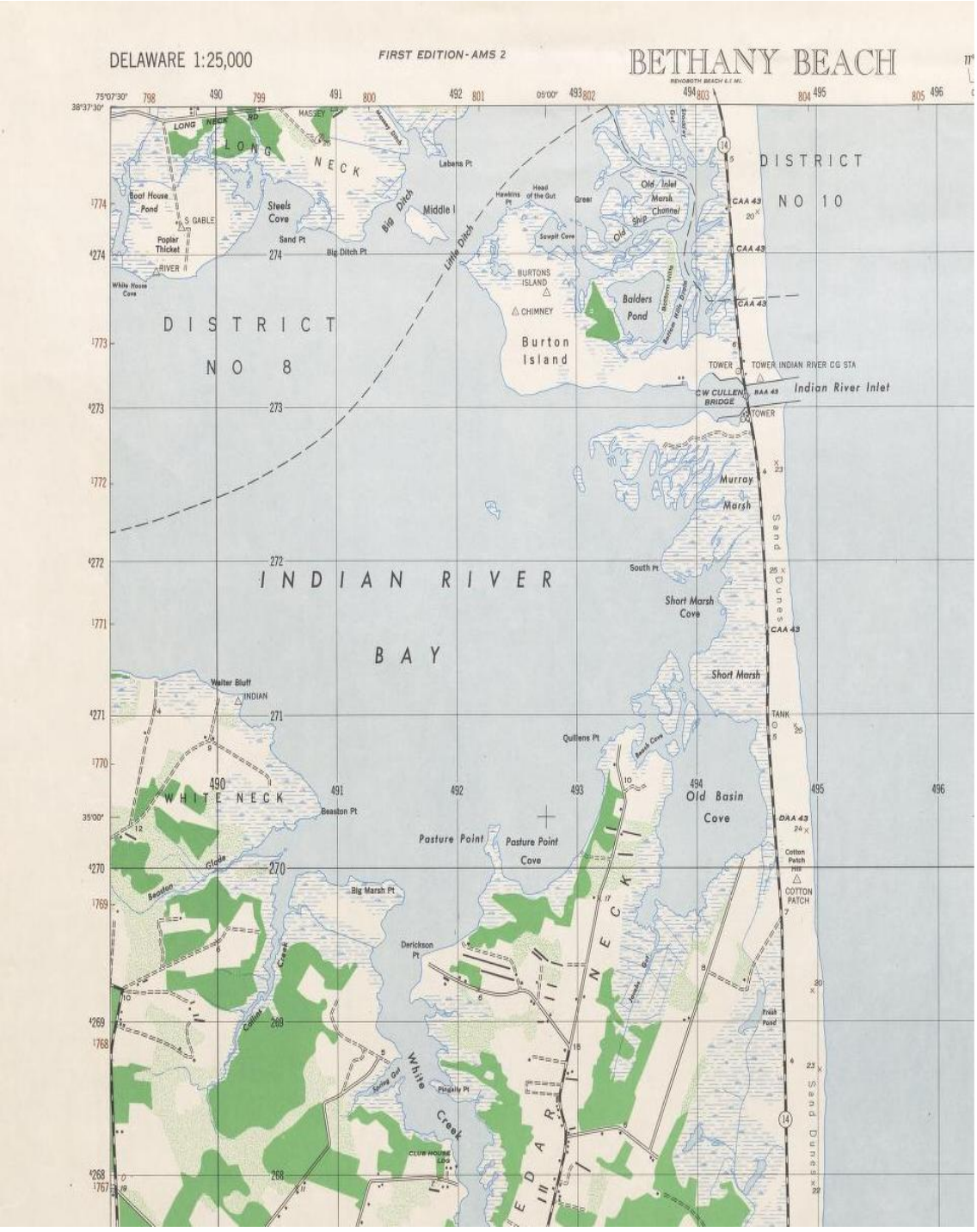

Figure 1.4: 1948 map of the inlet and bays, notice the detail of the interior shoreline erosion and countermeasures.

Figure 1.5: 1953 aerial photograph inlet area, notice the completion of the second set of 45° flares.

Figure 1.6: 1973 aerial photograph inlet area, notice the significant erosion of the interior shoreline, since the 1953 photograph, west of the Coast Guard Station.

Figure 1.7: 1989 satellite photograph inlet area, notice the extent of the channel bank armoring west of the Coast Guard Station and the severe beach erosion north of the jetties.

Figure 1.8: 1992 digital quadrangle of the inlet area, notice the flood shoal, the developments visible in the area since Figure 1.5, and the apparent health of the beach north of the jetties. This beach improvement is a result of the sand bypassing system installed in 1990.

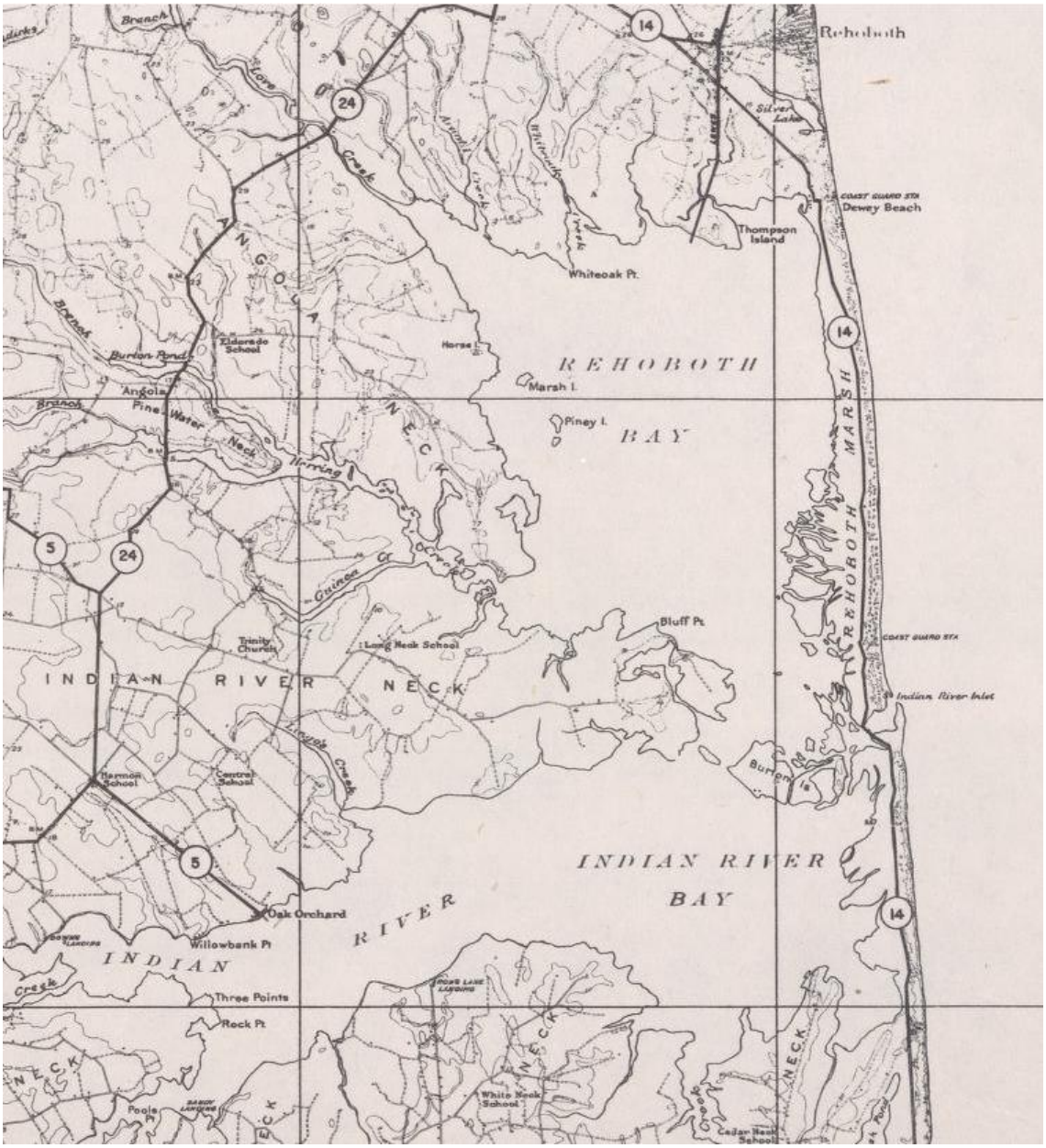

Figure 1.9: A 1942 map that was apparently created using pre-1938 information, as it shows the natural inlet and the state highway bridge from 1934.

information source. Aerial photographs from the period suggest that indeed the bridge was complete in 1938 prior to the completion of the inlet walls — though it is impossible to tell if it was open to traffic at this time.

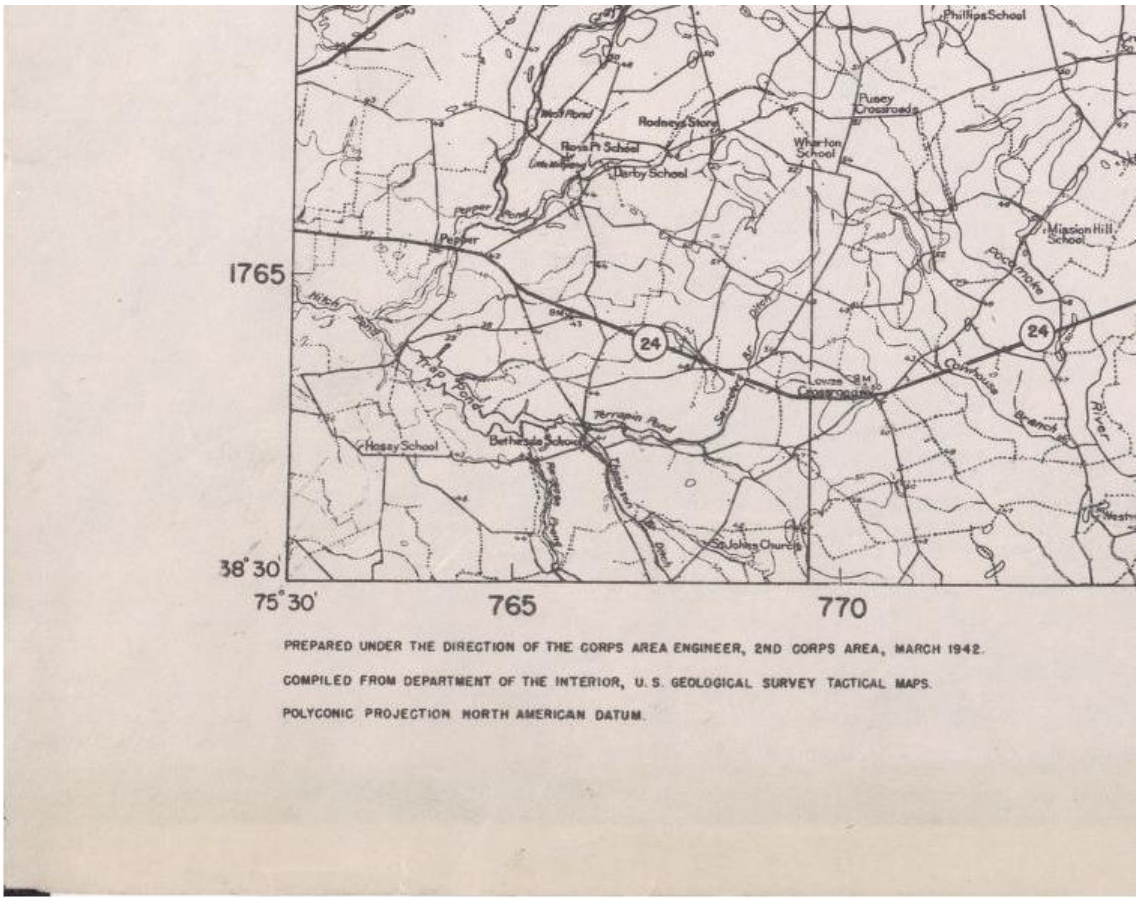

Figure 1.10: Comments from the map in Figure 1.9 showing the date created and attributing it to the USACE, who also built the Indian River Inlet in 1938-39.

This concrete and steel swing bridge was originally constructed on multiple timber piles, as can be seen in the postcard illustration in Figure 1.12. In 1948 the southern half of this structure was destroyed by ice flows and storm tides, and by 1952 was repaired this time using two concrete piles [26]. The debris from the demolished portion of the structure remained on the channel bottom, and modern sub-bottom soundings reveal that debris from this first structure still resides below the channel bed [31].

In light of the previous collapse, a hurricane in 1956 that severely damaged the coastline and a nor'easter in 1962 that caused the C. W. Bridge to close (at

Figure 1.11: Aerial photograph from 1938 showing construction of the inlet walls and the original timber-pile swing bridge.

least temporarily [7]) provided the impetus for constructing a replacement bridge. The substructure for the new twin span bridge was constructed in 1965, along with the east span (Phase I). The west span was completed in 1976 (Phase II) along with the removal of the old bridge—though debris, and possibly timber pilings, remain beneath the mud line at the location of the old bridge [5]. The presence of this debris appears to have armored the bed in this area [31]. One bizarre design choice aligned the new Indian River Inlet Bridge $75m$ east of the Cullen Bridge, forcing the highway to be relocated closer to the eroding shoreline north of the inlet [9]. This choice was made in an effort to minimize the length and cost of the main span by bridging the narrowest portion of the inlet. However, this part of the inlet also contains the highest flow velocities so scour problems were imminent from the time of construction.

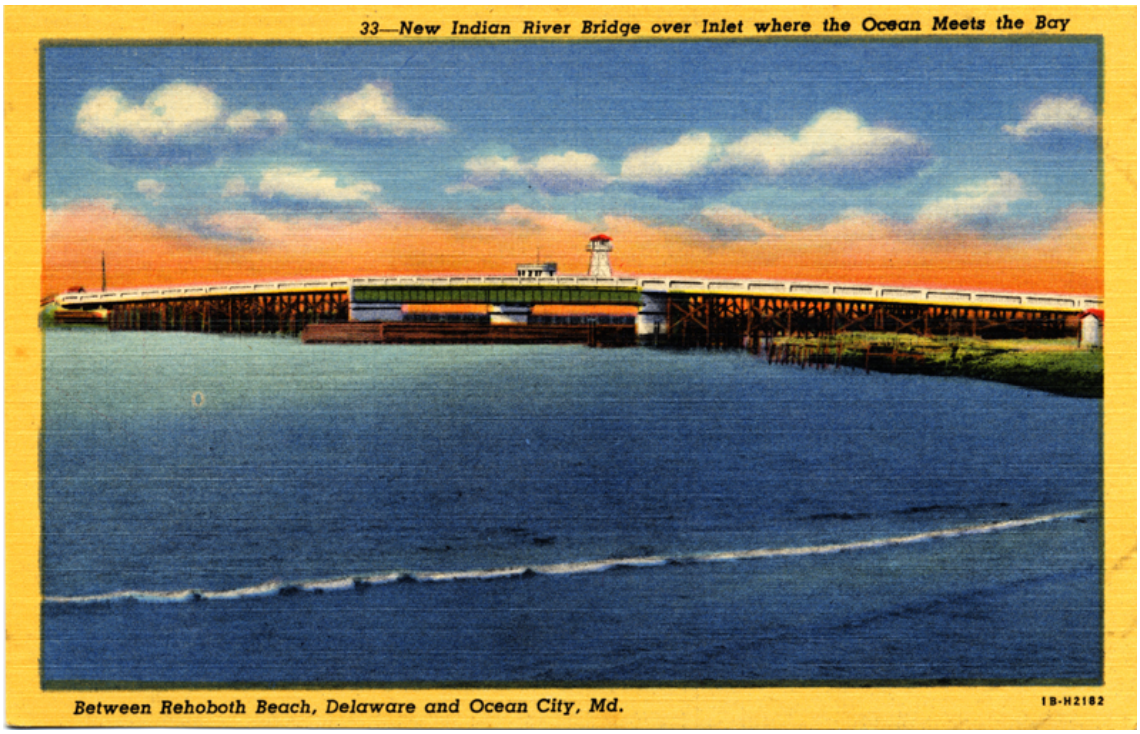

Figure 1.12: Postcard image from the late 1930's showing a drawing of the first State Highway swing bridge spanning Indian River Inlet.

The current bridge was constructed first by driving steel H-piles that would support the weight of the bridge. After some trouble achieving the desired bearing capacity on the test piles at the desired drive depth, the choice was made to attach timber wedges to the H-piles so that the proper bearing capacity was reached at the desired depth [11]. This choice appears to have been motivated by the additional cost of driving deeper piles. The steel sheet pile cofferdam was left in place around the pile group as an additional barrier to environmental forces after a concrete tremie seal was poured that collectively capped the H-piles [7].

The Philadelphia District of the USACE claims to have contacted DelDOT as early as 1979 about the beginnings of scour holes forming around the two rectangular concrete bridge piers, with undermining of the north pier's cofferdam apparently imminent [9]. Depth soundings performed by the Delaware Department of Natural

Figure 1.13: Aerial photograph from 1968 showing completed construction of Indian River Inlet Bridge Phase I, along with partial demolition of the old bridge.

Resources and Environmental Control (DNREC) in 1984 and 1985 revealed that scour had indeed reached the bottom of the steel sheet pile at the southwest corner of the northern pier [6]. DelDOT makes no reference to an awareness of scour problems prior to these soundings by DNREC.

The 1988 *Condition Report on Indian River Inlet Bridge* [6] describes the first three underwater surveys contracted by DelDOT that revealed the alarming degradation of the bed. The first study was in October 1985 and it revealed a 12m by 7m cavity under the tremie seal of the northern pier and that 21 steel H-piles were exposed to the salt water. A May 1986 survey revealed the same conditions and noted little change. One and a half years later in December 1987 the third study found the cavity 2.5m deeper, significant deterioration of the steel

sheet pile cofferdam that had been left in place, and led to the development of a cathodic protection plan for the underwater steel. This series of three underwater studies represent the first alarm for DelDOT that the bridge was in serious trouble. It is worth noting here that a cathodic protection system was installed to try to mitigate corrosion of the steel exposed to salt water, it never operated properly [7] but currently supplies the BBSMS with electric power.

1.5 Riprap Remediation

In 1989 DelDOT took action against the scour, placing a 2m thick blanket of armor in the form of loose riprap over a filter layer of graded stone. Hu [12] describes the sizes of riprap stones, though inspection of the *in situ* armoring does not agree with the measurements listed. It is presumed that the units are incorrect in the DelDOT report, and that dimensions of the stones are in fact given in meters . Three different sizes of stones were used to achieve a filter layer underneath a more resistant armor layer [12]. The filter layer is designed to prevent winnowing of the fine natural sediments through the large voids between the armor stone, and is required when $\frac{d_{15riprap}}{d_{85base}} > \frac{d_{15riprap}}{d_{15base}} > 40$ and $\frac{d_{50riprap}}{d_{50base}} > 40$. Since the sand and silty mud is much smaller than the designed riprap, DelDOT used two layers of smaller natural stone satisfying $5 < \frac{d_{15filter}}{d_{15base}} < 40$. These filter layer requirement are taken from Gregorius (1985) as cited in [23], and differ slightly from the equations listed in the 1989 DelDOT report, though it is assumed that these are the requirements that were used in design.

At the same time the channel armoring riprap was placed, the USACE installed shoreline protection along the length of the inlet walls also in the form of riprap. These stones blend with the DelDOT armoring in the vicinity of the bridge, and range between 90 and 1500 pounds, which is on the same order of size as the stone used to armor the channel [9].

Since the placement of riprap, scour has continued —see Figures 2.2 and 2.3 in Section 2.2. Though the local armoring successfully slowed the degradation of the bed under the bridge, it appears to have played a part in enhancing erosion elsewhere, particularly at the edge of the riprap blanket. DelDOT admitted that the riprap was not performing properly in 2004 [7]. It is doubtful that the large armor stones themselves are failing, though it is interesting to note that updated design parameters published in 1993 would have sized the stones about thirty percent larger based on flow interactions with the rectangular pier footings [28].

There is no information on the amount of backfill or depth of filter stone used underneath the armor stones, but it is evident in Figures 2.2 and 2.3 that a substantial volume of material was used to try to recover some of the bed lost to scour. It is also unknown if backfilled material applies any significant friction force to the piles, and therefore it is unknown if any pile bearing capacity was regained during the remediation.

1.6 Current Conditions

The current state of the inlet can be characterized by the giant scour holes flanking both sides of the bridge and by the complex and turbulent tidal currents still coursing through the channel. The complete channel is surveyed using multibeam sonar by the US Army Corps about every two years, with the most recent survey in 2007l. Figure 1.14 shows some of the survey results from 1986 to 2007 that reveal the progression of the scour problem. Figure 1.15 contains a detail of the most recent 2007 multibeam survey which revealed continuing degradation near the bridge piers and at some points along the channel walls.

The cathodic protection system installed in 1990 does not work to slow the corrosion of the steel H-piles exposed to the salt water, rather yearly inspections by divers ensure that these bridge supports have not deteriorated to unsafe levels [26].

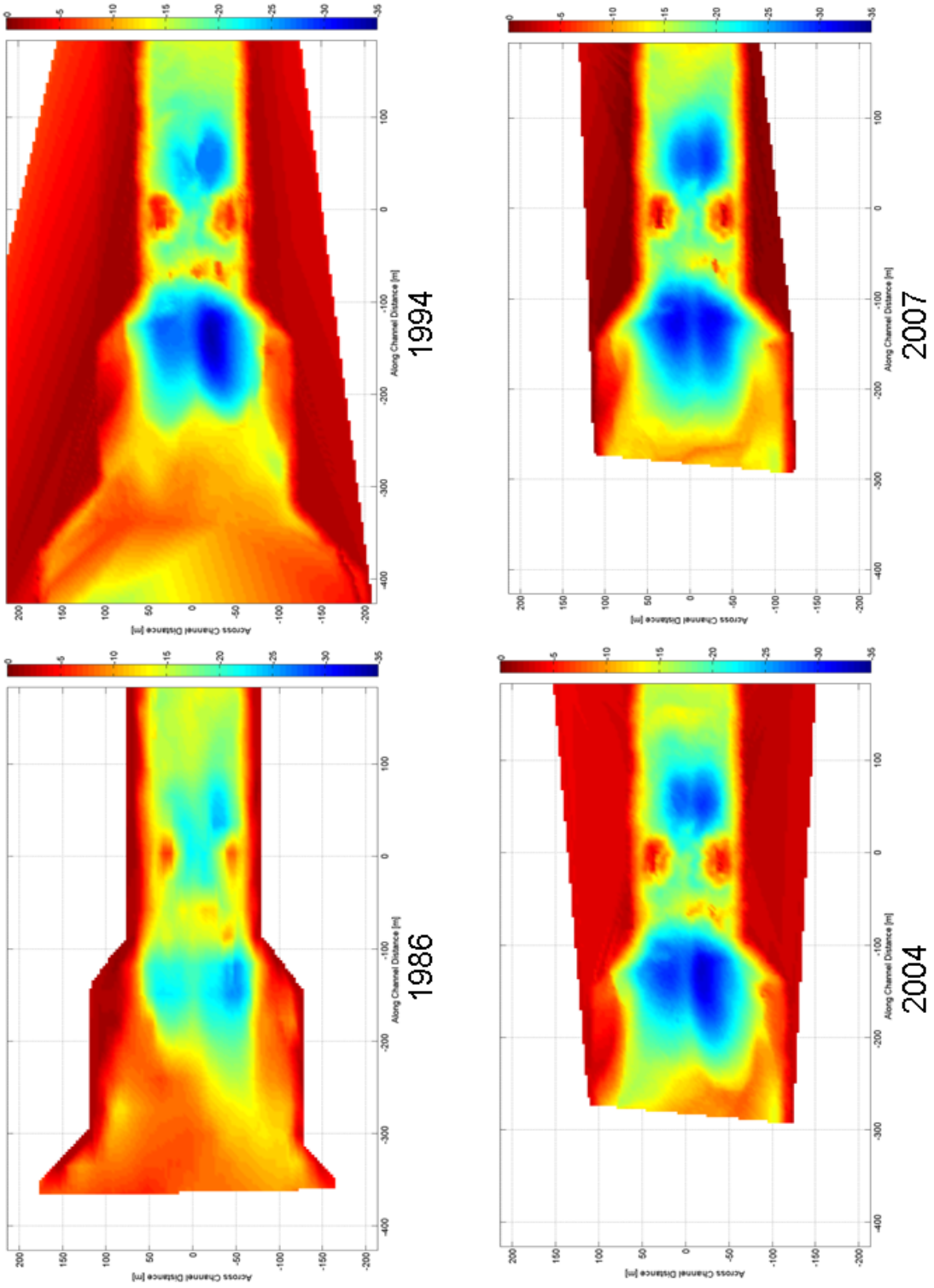

Figure 1.14: Progression of multibeam bathymetry surveys from the USACE showing the spreading of the scour holes from 1986 through 2007.

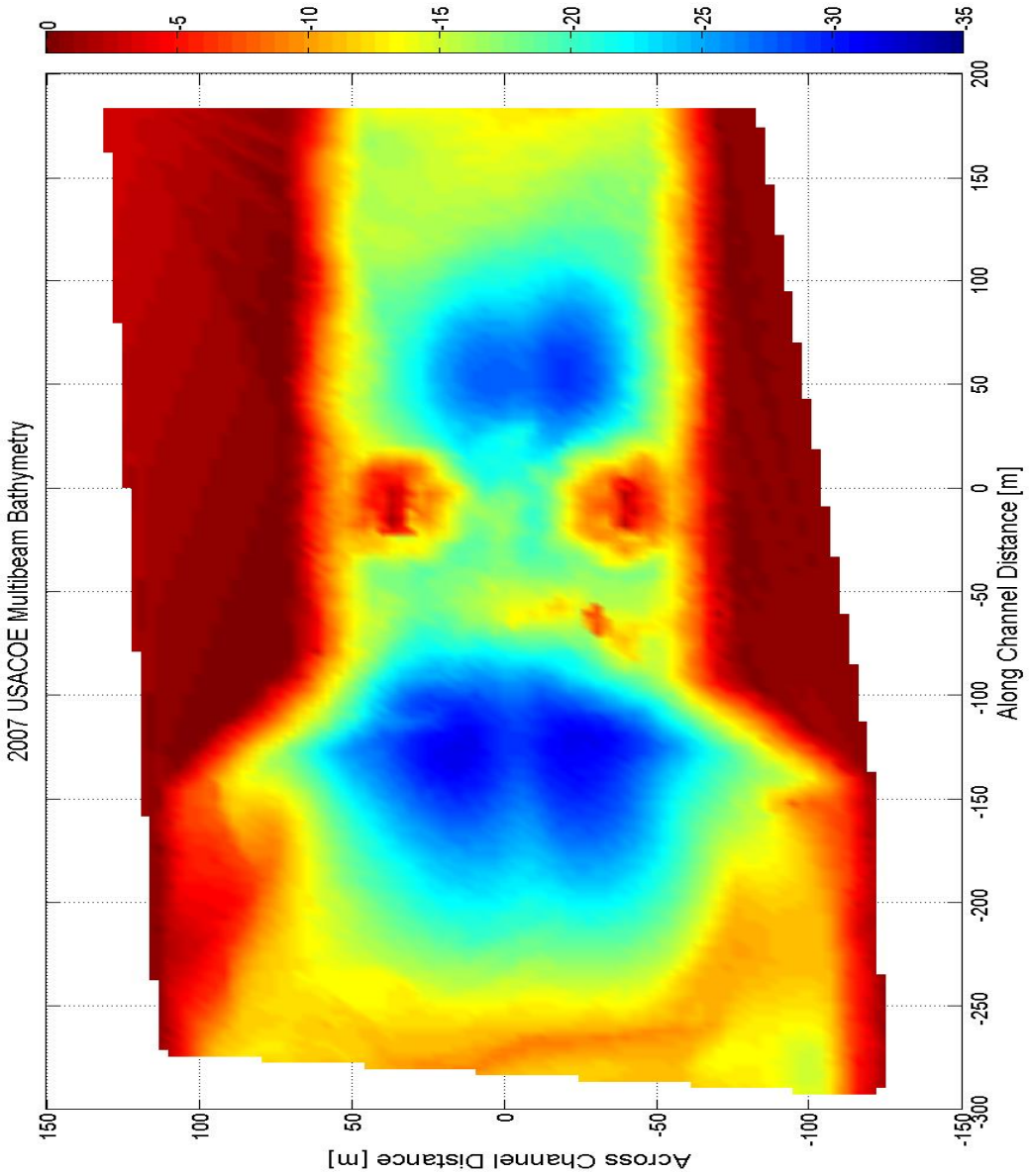

Figure 1.15: USACE multibeam bathymetry data from 2007 represented on a 1m by 1m square grid, illustrates the two deep scour holes in blue. The colorbar is depth in meters.

The electricity originally powering this system has been routed to power the new BBSMS described in this thesis.

Sand bypassing has successfully maintained a safe width of the beach north of the jetties, and eliminated the need to mine sand from the inlet shoals. About 100,000 cubic yards of sand are bypassed yearly from just south of the southern jetty to a point just north of the northern jetty [5].

Since 2004 politicians and Delaware Department of Transportation officials have been working toward the goal of replacing the Indian River Inlet Bridge, though two attempts between 2004 and 2008 failed because of budget and labor issues respectively. The third attempt is currently underway; as of the writing of this thesis a design-build contract has been awarded to Skanska USA Civil Southeast, Inc and that company has begun driving test piles to ensure proper bearing capacity. Scheduled completion of this replacement bridge, which completely spans the inlet, is Spring or Summer 2011 [13].

Chapter 2

INLET SCOUR

The loss of channel material has been well documented since the US Army Corps of Engineers first constructed the inlet walls and scour began, though a complete understanding of the mechanics that have caused such severe scour is elusive. The most important comprehensive study, in terms of channel scour, is the 1994 Committee on Tidal Hydraulics (CTH) report [5]. This report aimed to answer the questions, "What factors caused the accelerated scour to begin during the mid 1970's?", "What course of action is recommended?", and "What modeling tools and/or prototype data are needed to design a stabilization scheme?" The significant result of the study is the fact that equilibrium is not expected at the Indian River Inlet, even if the cross section grows large enough that the peak velocity will begin to fall — that velocity will still be capable of scouring the channel bed [5]. Even if scour were to deepen the inlet uniformly by $6m$, an equilibrium condition would not exist [9].

2.1 General Scour

It is prudent to reiterate that the original design of the inlet was selected to ensure velocities would be high enough to maintain a navigable channel [9]. Now 70 years later, the average peak velocity is still increasing from the baseline $1.28m/s$ design peak velocity. The CTH document reports results from a 2D hydrodynamics model that hindcasted the 1941 peak tidal discharge of $0.9m/s$, noting that in 1988 that value more than doubled to $2m/s$. The model also predicted that the 1988

velocities represented the maximum flow conditions, and the future would see a drop in peak velocities as the channel cross section continued to grow [5]; however, the channel cross section *and* the velocities both continued to grow.

Early on, the high velocities were not a problem, as general scour of the channel meant more exchange between the ocean and bays and promised to maintain navigability of the inlet—something that had not been guaranteed before. Even as late as 1974 when the mean inlet depth was $7.62m$ below mlw, the only scour considered to be a problem was the hole that was swallowing the seaward end of the northern jetty [9]. The mid 1970's represented a turning point in the attitude toward scour, as the rate of scour doubled from approximately $0.15m/year$ to $0.3m/year$ [5].

One of the goals of the CTH report, as mentioned above, was to determine the cause of this inflection point. Ultimately the acceleration was attributed to a combination of the first significant sand mining from the flood shoal in 1972, the reduction in flow resistance following the removal of the C. W. Cullen Bridge, and the exposure of the silty mud layer found under the $10m$ layer of coastal sands [5].

2.2 Local Scour

The puzzle remains, though, as to the physics that caused the giant scour holes to initially form in their respective locations. The CTH report, on page 25, asserts that the local severe scour could be the result of the convergence of turbulent flow structures — a suggestion supported in this thesis in Section 2.5. As discussed in that section, turbulent flow structures shed from the bathymetry and/or bridge piers are likely responsible for maintaining and expanding the holes, but little is still known about the initial cause of their formation.

Considering the significant resistance to flow that the multiple timber piles of the C. W. Cullen Bridge provided, the fluid's energy was likely transferred into turbulent eddies as flow passed the piles. Investigation of the historical USACE

bathymetry data shown in Figure 2.1 reveals that the original anomalous scour holes first appeared flanking the C. W. Cullen Bridge. Only after the 1978 survey does the ocean-side hole appear in its current familiar location, meaning the shift followed the removal of the old bridge, which was executed in 1976. The 1978 line also represents the first time the majority of this profile line fell below the sand/mud transition line, and subsequent surveys reveal that scour through this mud layer occurred faster than through the sand above. Once the finer mud and silt is suspended, redeposition within the inlet is unlikely, this is a drastic contrast to the sand which can redeposit as flow conditions change [5].

Figure 2.1 also reveals that scour continued to flank the Cullen Bridge remnants, and it was not until the placement of the riprap armoring in 1989 that the ocean side scour hole took hold at its current location. Once that area around the Indian River Inlet Bridge was armored, it became an ejection point for turbulence, much like the Cullen Bridge had been, causing enhanced scour in its lee during ebb tide. Evidence that this type of wake turbulence can indeed contribute to remote local scour can be found in Section 2.5.

As was discussed in Sections 1.5, the scour near the bridge raised alarms for officials and engineers at DelDOT. During the late 1980's, the threat became very real that the foundation of the bridge could be compromised due to undermining. An unpublished study by Greiner, Inc. of Maryland, performed under a contract for DelDOT, revealed that the critical bed depth for safe bearing capacity, according to AASHTO requirements, is approximately $21m$ below NAVD88 [11]. This depth was exceeded along the centerline profile in the 1988 survey, prior to the placement of riprap, though it was never reached under either of the piers. Figure 2.2 shows the historical profiles along the along–channel axis of the north pier of the current Indian River Inlet bridge, generated by interpolating USACE bathymetry surveys. Figure 2.3 shows similar data along the along–channel axis of the south pier.

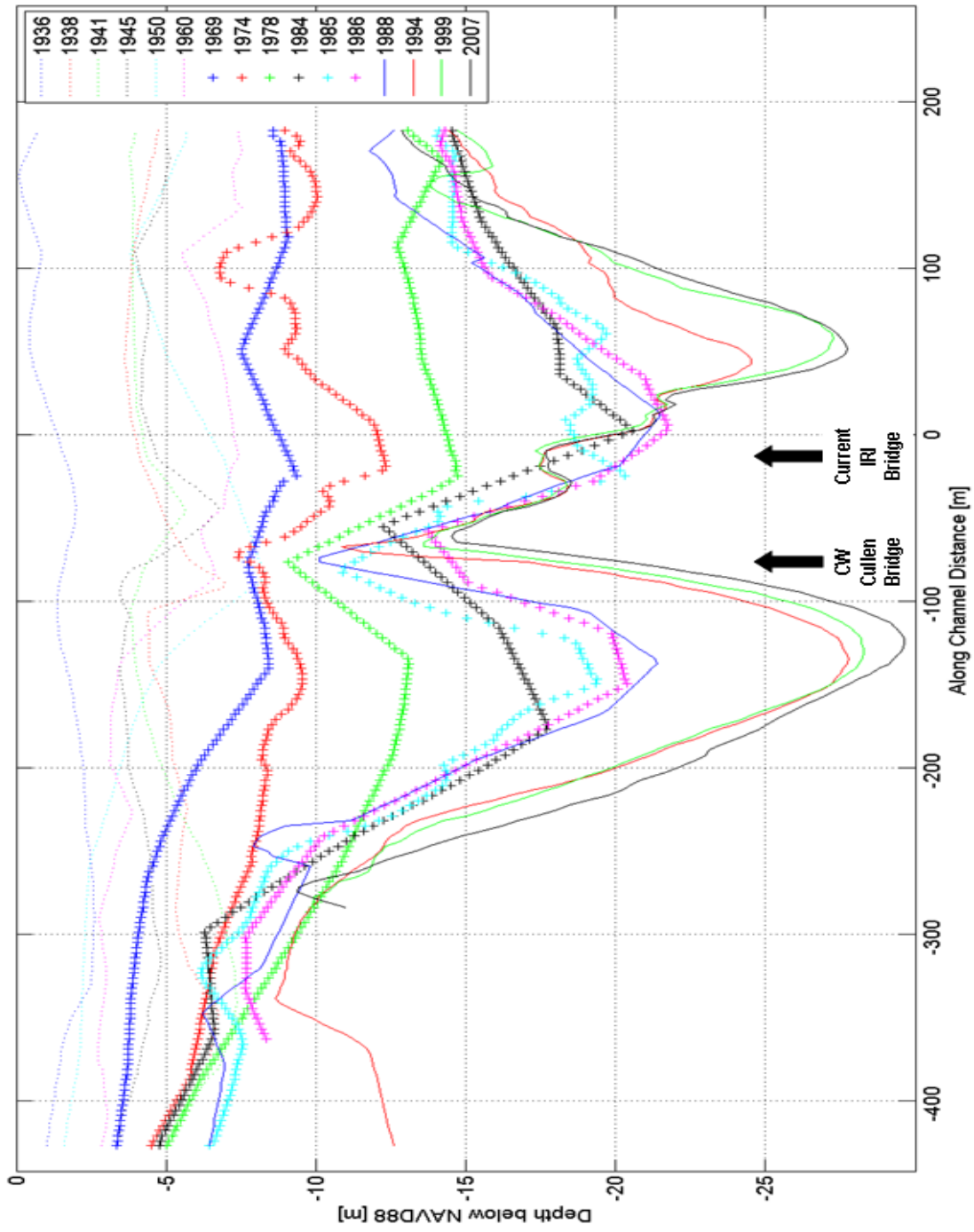

Figure 2.1: A history of the centerline profile of the Inlet according to USACE surveys. Arrows indicate locations of Cullen Bridge and current Indian River Inlet Bridge.

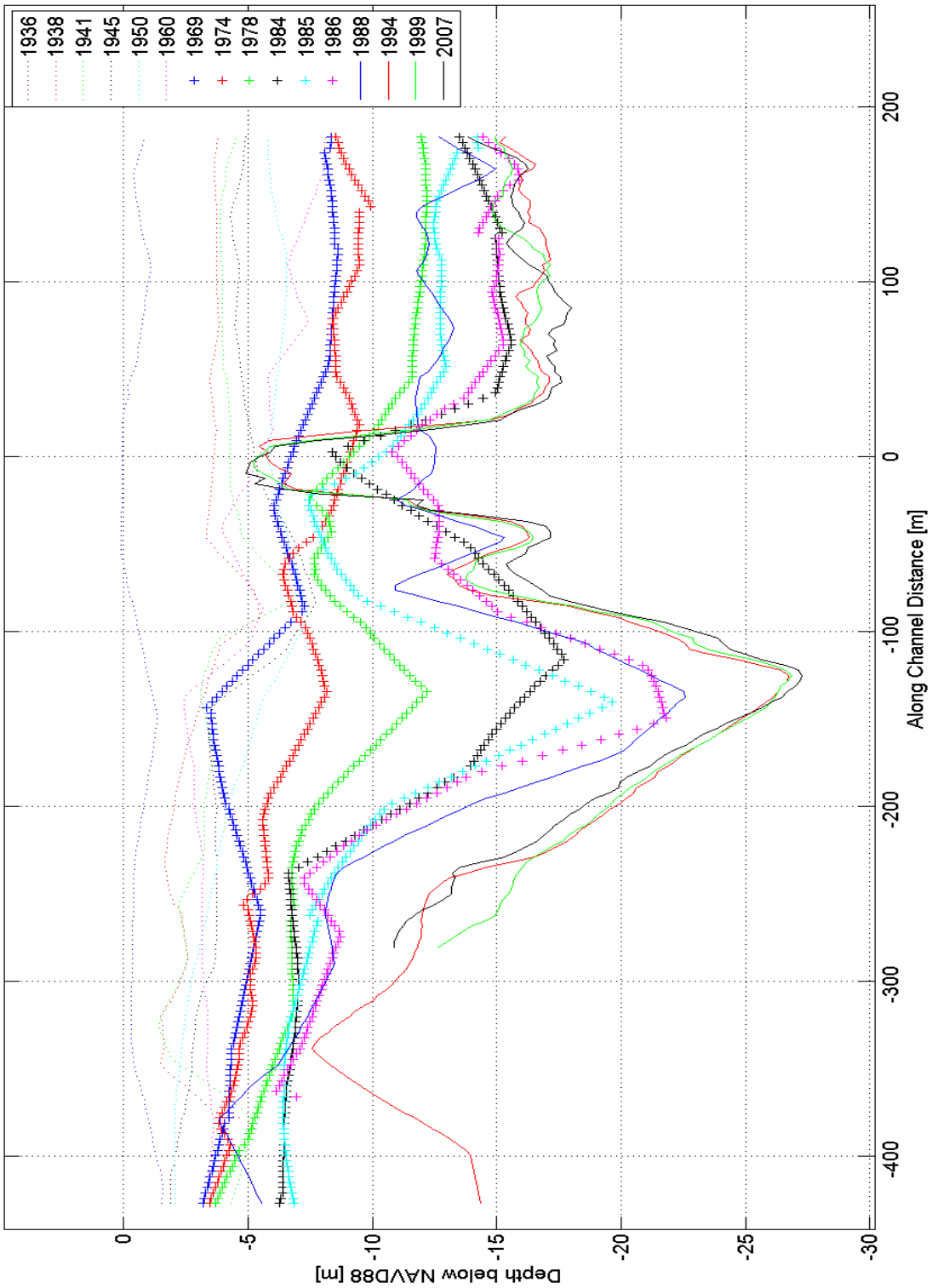

Figure 2.2: A history of the profile line along the axis of the north pier of the current bridge, according to USACE surveys.

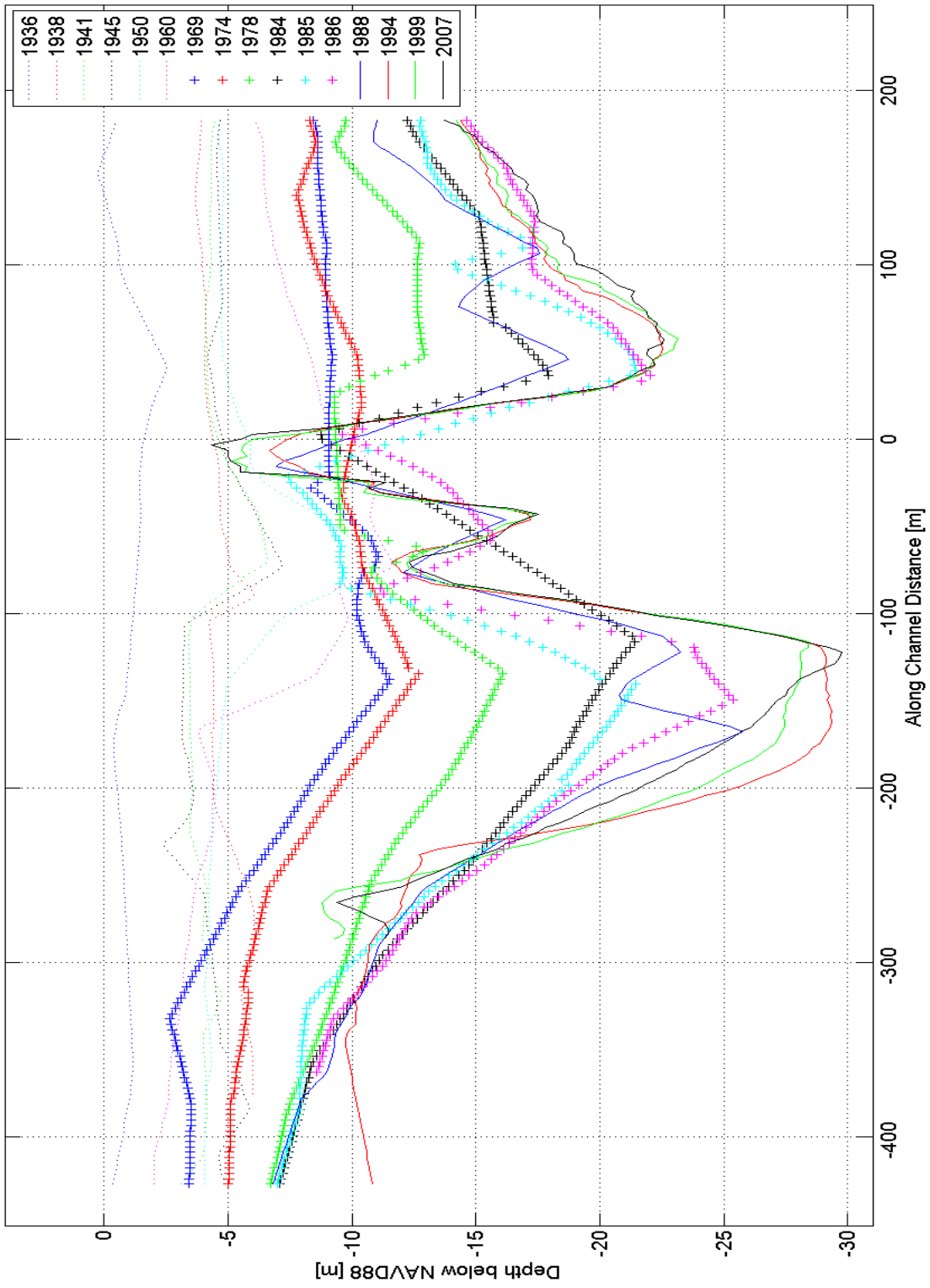

Figure 2.3: A history of the profile line along the axis of the south pier of the current bridge, according to USACE surveys.

DelDOT installed the riprap blanket only as a means of temporary bed armament. Visible in Figures 2.1 through 2.7 as the difference between the solid red and solid blue lines in the along channel area of $-30m$ to $0m$, and initially considered a success, documents released by DelDOT after 2004 reveal that this armor layer has not performed adequately and is in danger of failing. Chiew (1995, 2000) and Lauchlan and Meville (2000) provide scenarios under which riprap armoring can fail even if the stones are sized properly to resist flow, such as edge failure which occurs when the interface between the armor and the natural bed degrades.

If the depth of scour is not alarming alone, the slope that the bed achieves (up to 30% in Figures 2.2 and 2.3) as material continues to scour around the riprap is considerably unsettling. Catastrophic avalanching failure of the riprap layer appears inevitable. Figure 2.4 shows the channel cross sectional profile at the location of the current bridge, revealing the truly precarious perch the bridge occupies. DelDOT engineers were comparably concerned with the scour, and so in addition to moving forward on the construction of a new bridge, they partnered with the Center for Applied Coastal Research to design and install an enhanced scour monitoring system. This monitoring system is described in detail in Chapter 3.

2.3 Equilibrium Inlet Size

The CTH report also presented the results of models and calculations that attempted to predict the equilibrium cross section of the inlet, in hopes that at some point scour would subside. Such a figure could ease the tension of USACE and DelDOT engineers who see the inlet as a self-destructive entity—if such a figure did indeed exist. No single model could responsibly pinpoint a terminal cross sectional area, especially given the fact that a representative cross sectional area of the existing bathymetry is remarkably difficult to calculate given the undulating bathymetry. Results from the Keulegan hydrodynamic method [17], the Jarret-O'Brien tidal prism versus inlet area method [15] (used as an estimator since the sand bypassing

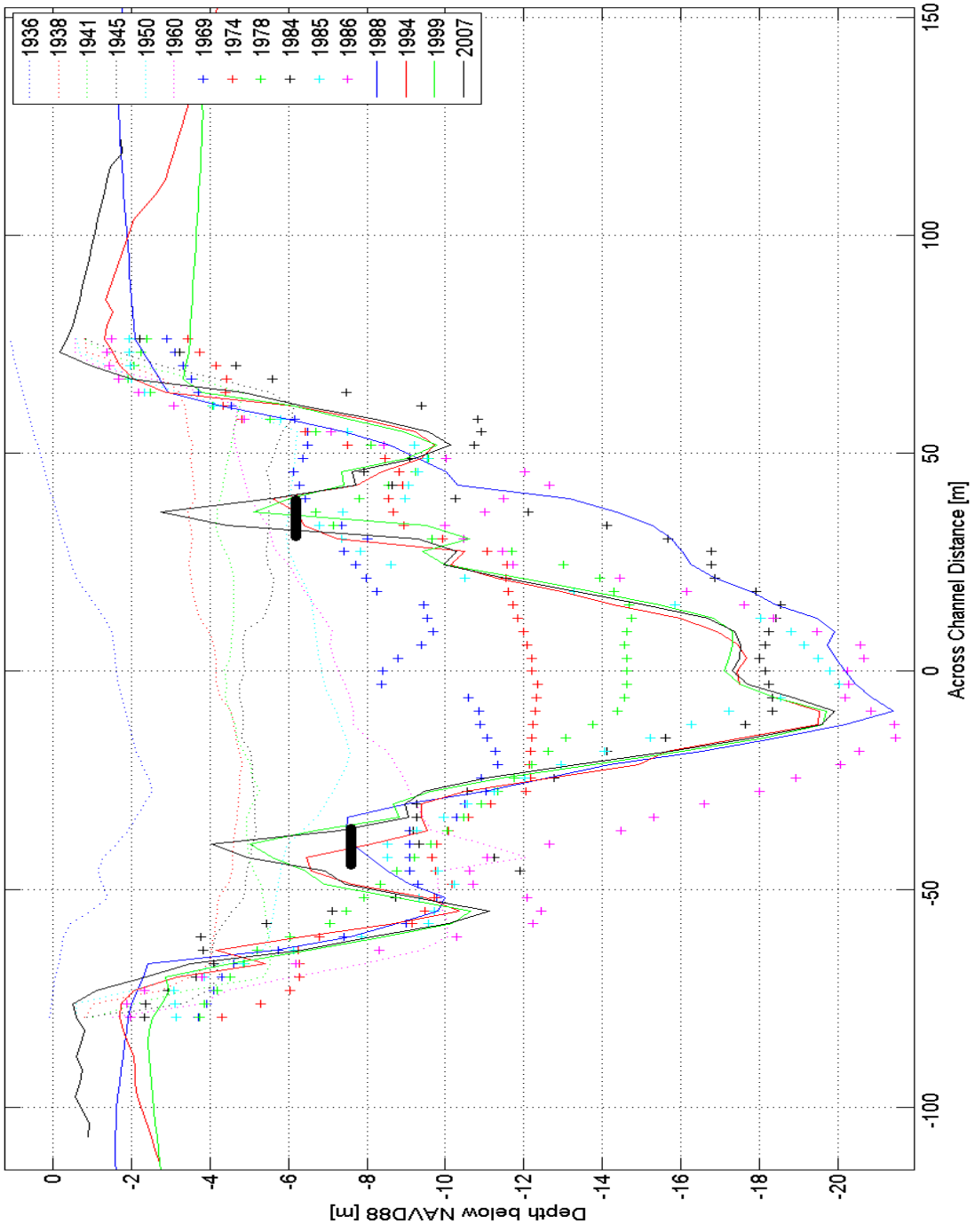

Figure 2.4: Cross sections of the inlet at the bridge, from USACE data 1936-2007. Thick solid black lines show the tops of the pier footing concrete.

system prohibited its predictive accuracy), and the O'Brien-Dean velocity versus cross sectional area method [25] were compared. A best-guess at the stable cross sectional area was computed as $3200m^2$, where the effective cross section at the time of the 1988 study was $1850m^2$ [5]. The report emphasizes that even their best-guess is probably low because it relies on adequate sediment supply into the inlet, which the sand bypassing system prevents.

Even if the size of the inlet equilibrates at this predicted cross sectional area, the peak velocities are still above the critical values needed to scour sediment [20] and so an adequate supply of sand would be required to prevent ongoing scour. The dominance of silt and mud in the channel profile suggests that a stable bed will not be feasible until either it is all removed or enough sand is let into the system to create an erosion buffer. In this mindset, the sand bypassing system that protects the shoreline north of the jetties could also contribute to the inability of the inlet to achieve equilibrium [5].

Figures 2.5 through 2.7 show the true historic cross sections, directly surveyed during almost all of the USACE bathymetry surveys, dating back to the natural inlet in 1936. These survey cross sections are traditionally used to compute the effective cross sectional area that characterizes the inlet in historic studies and reports.

The historic increase in cross sectional area is directly proportional to the historic increase in tidal range in the bays. Unchanged is the $1.25m$ ocean tidal range, which provides the forcing head potential for all of the subsequent velocity and morphologic changes. Simply, once a reliable channel was created, the head difference between the ocean and the bay drove a current that created a larger channel. The larger channel allowed a greater volume of water to enter the bay during any given tidal cycle, increasing the tidal prism associated with the inlet. Though the bay tides have increased, they are still only a fraction of the ocean tide,

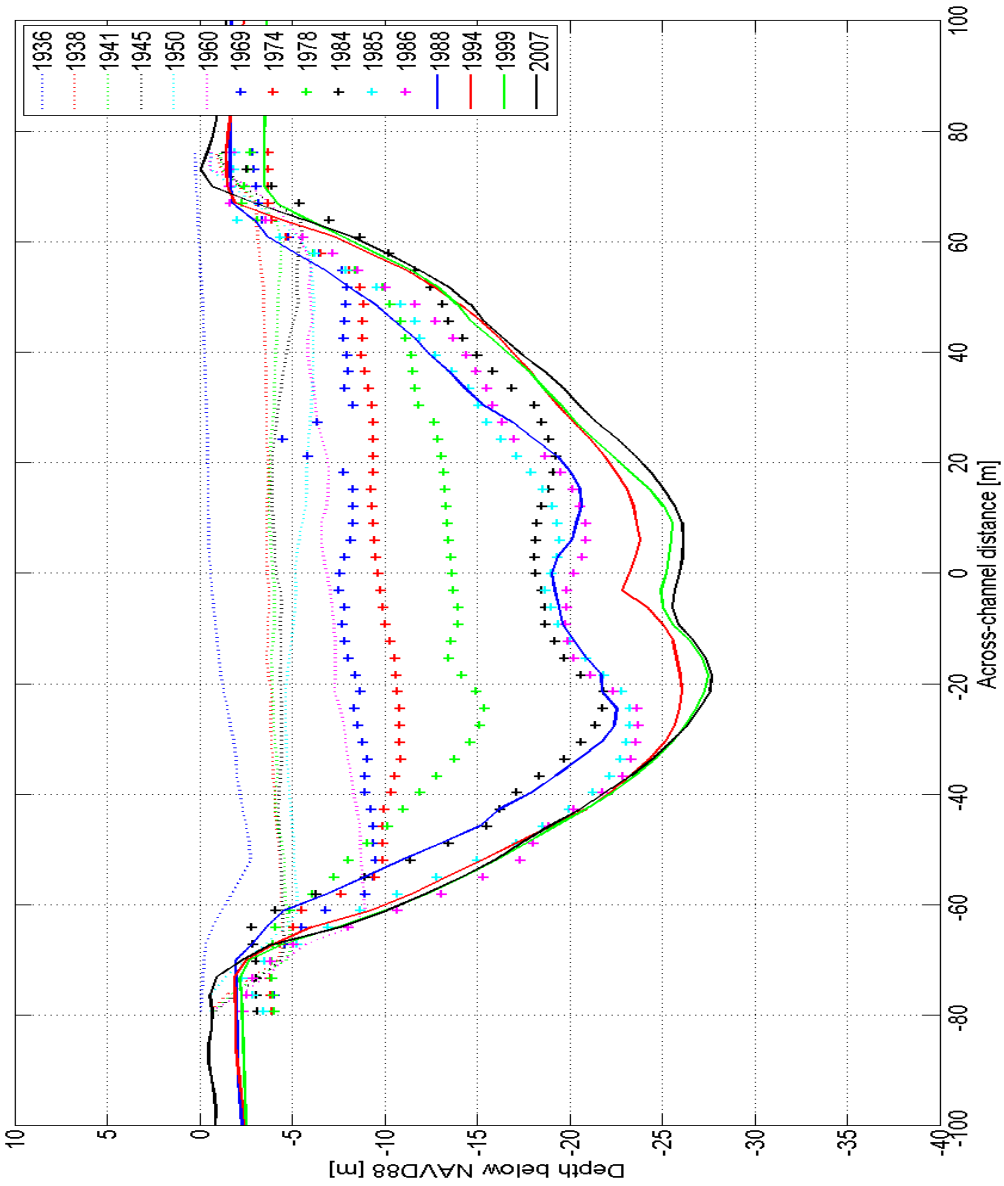

Figure 2.5: Cross sections of the inlet 40m east of the bridge, from USACE data 1936-2007.

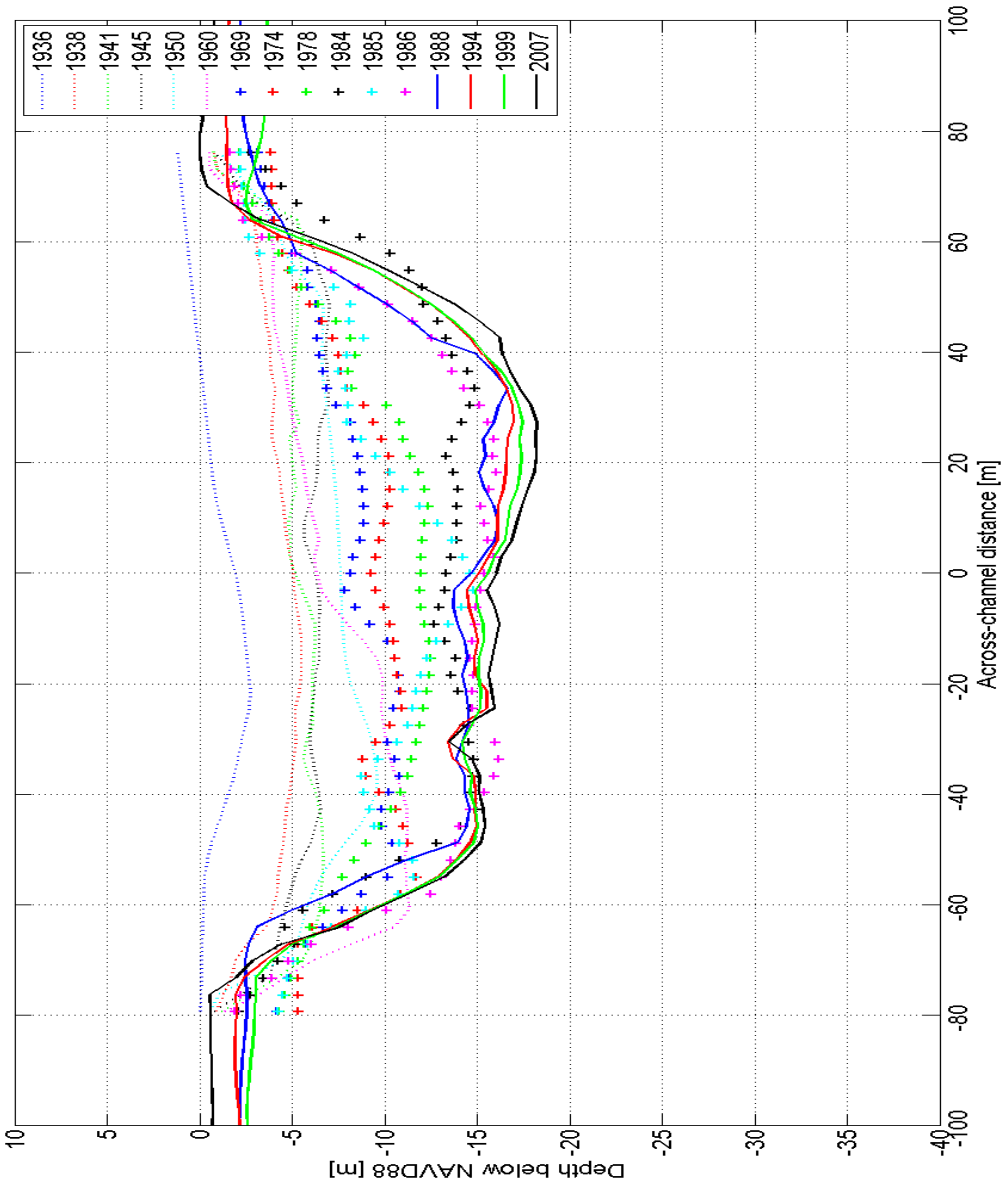

Figure 2.6: Cross sections of the inlet 50m west of the bridge, from USACE data 1936-2007.

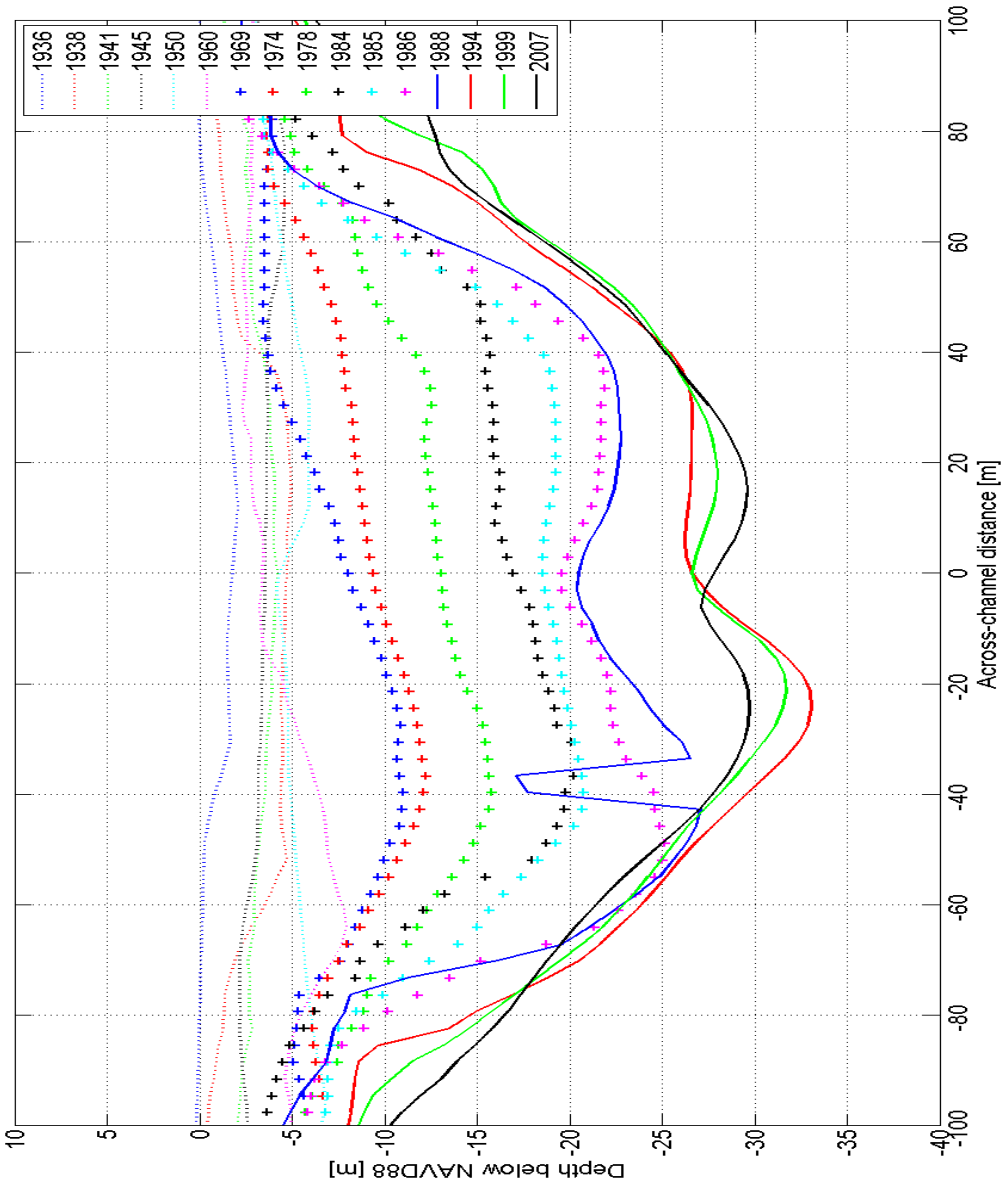

Figure 2.7: Cross sections of the inlet 150m west of the bridge, from USACE data 1936-2007.

and so that excess potential energy in the ocean continues to drive the changes in the observed peak velocity and tidal prism.

2.4 Considering the Changing Ditches

While many studies have considered the causes and effects of the changing inlet geometry, none have considered the effect of *the Ditches* on the Indian River Inlet's tidal prism. For the past 60 years, since 1948, flow velocities through the Ditches have increased steadily along with the physical dimensions of the two channels comprising the area. When Keulegan applied his repletion coefficient method at Indian River Inlet [17] he assumed that the Ditches were closed, and considered the basin singularly as Indian River Bay — arguing that the volume of water passing through the Ditches and being stored in Rehoboth Bay was very small relative to the volume passing through the Inlet and being stored in Indian River Bay. The repletion coefficient in Equation 2.1, K, is a function tidal period T, tidal amplitude in the ocean H, the cross sectional area of the channel a, the surface area of the basin A, the channel hydraulic radius r, the channel friction coefficient λ which is related to Manning's n, length of the channel L, and a coefficient resulting from the velocity distribution in the channel m [17].

$$K = \frac{T}{2\pi H}\frac{a}{A}\sqrt{\frac{2grH}{\lambda L + mr}} \tag{2.1}$$

After his single basin assumption, Keulegan applied a correction factor to the original estimates of basin tidal amplitude, lag times between tidal maxima and minima in the ocean and basin, and maximum channel velocity using parameters derived from analysis of the Ditches. His correction factor dictates that an increase in cross sectional area of the Ditches would have an adverse effect on the repletion coefficient for the Inlet as

$$K' = K\left(1 - \frac{a_0 V'_{0m}}{aV_m}\right), \tag{2.2}$$

where K' is the adjusted repletion coefficient for the Inlet, K is the original repletion coefficient, from Equation 2.1, for the Inlet assuming The Ditches are closed, a_o is the cross sectional area of the Ditches, V'_{om} is the theoretical maximum velocity through the Ditches, a is the cross sectional area of the Inlet, and V_m is the theoretical maximum velocity through the Inlet.

If a_o is large, then $(1 - a_o)$ is small and the adjusted K' is smaller than if the Ditches were closed: $K' < K$. If the repletion coefficient is thought of as the channel's ability to fill the basin, then the adjustment factor in Equation 2.2 is like a sudden expansion of the basin. The same amount of water enters through the channel, but that volume is a smaller percent of the now larger basin.

A brief investigation of the historical hydraulics in the Ditches reveals that the area appears to act as a stable channel, reacting directly to the forcing provided by the change in tidal range in Indian River Bay. The only constant variable observed in 1948 and 1988 was the lag time between high tides in Indian River Bay and Rehoboth Bay, which was 2 hours. Rehoboth Bay tides were observed at the north of the bay, very far from the Ditches, while Indian River Bay tides were observed at the north of the bay, very close to the Ditches. Here the assumption that the each bay fills everywhere simultaneously must be used, this is a common assumption made to simplify tides in basins [17].

Considering the known lag time between high tide in Indian River Bay and Rehoboth Bay of 2 hours, applied to Equation 2.3:

$$\alpha = \frac{\pi}{2} - \tau, \tag{2.3}$$

where α is the lag in oscillation in the protected bay, here Rehoboth Bay, and is a known quantity of 2 hours. Then $\tau = 0.56 radians$, which can be applied to Equation 2.4:

$$h_{1m} = \sin\tau, \tag{2.4}$$

yielding $h_{1m} = 0.53$. h_{1m} is the dimensionless ratio of the tide level in the protected bay to the tidal amplitude of the outer bay. From this relationship it is apparent that the inner bay and outer bay tide levels are related by

$$H_{RehobothBay} = 0.53 H_{IndianRiverBay}. \tag{2.5}$$

All of the above has been calculated from the observation that the lag time in oscillations of the two bays was 2 hours in both 1948 and 1988; lag time of tidal maxima was the only characteristic common between the two studies. The observed tides during the two studies validate the relationship in Equation 2.5. In 1948 the tidal range in Indian River Bay was 0.28m, with Rehoboth Bay at 0.14m – a ratio of 0.505. In 1988 the Indian River Bay tide was measured at 0.90m, with Rehoboth Bay observed to be half that, at 0.45m - a ratio of 0.5 [5].

Keulegan's repletion coefficient lookup table provides K and C, which is a dimensionless number relating tidal prism to volumetric flow rate, corresponding to $\sin\tau$. Here $\sin\tau = 0.53$, so $K_{Ditches} = 0.494$ and $C_{Ditches} = 0.8182$ [17, p. 93].

These values, along with the physical characteristics of the Ditches, can be used to calculate the maximum mean current through the Ditches by Equation 2.6.

$$V_m = 2\pi C \frac{A}{a} \frac{H_{ocean}}{T} \sin\tau, \tag{2.6}$$

where Vm is the maximum mean current in the channel, defined as the mean flow rate derived from the maximum displacements of the bay waters. C is from the table lookup above, A is the area of the protected bay (Rehoboth Bay), a is the cross sectional area of the channel (Ditches), H is the tidal amplitude of the outer bay (Indian River Bay), T is the tidal period (12.42hours observed), and $\sin\tau$ is from Equation 2.4. In words, this equation relates the velocity in the channel with

the full tidal range $2H$, which corresponds to the volume of water comprising the tidal prism ($2HA$), that passes through the channel of cross section a [17].

The area of Rehoboth Bay is $33,700,000m^2$ and did not change between the 1948 and 1988 studies. The cross sectional area of the Ditches, however, did change from 1948 to 1988. No direct bathymetric measurements of the Ditches geometry have been performed since the 1936 USACE survey of the natural inlet and both bays. To quantify the change in cross sectional area, two aerial photographs from the United States Geological Survey (USGS) archive (Figures 2.8 and 2.9) were used in conjunction with recorded limiting depths to approximate the cross sectional area. The limiting depth in 1948 was $0.91m$ [17] and a conservative $1.52m$ was used for 1988, taken from National Oceanic and Atmospheric Administration (NOAA) nautical chart number 12216.

Since the Ditches are two separate channels separated by an island, it is useful to create one effective channel dimension that is a combination of the two [17]. The effective cross sectional areas were computed as $a_{1948} = 360m^2$ and $a_{1988} = 894m^2$. Plugging these two values into Equation 2.6 yields $V_{m1948} = 0.81m/s$ and $V_{m1988} = 1.05m/s$ — two remarkably close values given the dramatic change in the Ditches' geometry. Also note that they are very close to the $1.28m/s$ design peak velocity of the Indian River Inlet, which was designed to scour [9].

Although the dimensions of the Ditches and the tidal prism of Rehoboth Bay have grown, it appears that the peak velocity through the area is relatively constant. There is considerable bottom friction in the Ditches area thanks to the intervening island and natural shorelines; although both of these are diminishing, visibly apparent in the two photographs in Figures 2.8 and 2.9, as the channels continue to grow. As the repletion coefficient of the Ditches approaches unity, the correction factor applied to the Indian River Inlet's repletion coefficient will also grow, adjusting the Indian River Inlet's K lower. There is a feedback loop linking

Figure 2.8: 1953 aerial photograph of the Indian River Inlet that also shows the Ditches. The known $152m$ wide inlet is used to scale the photograph.

the cross sectional areas of the Inlet and the Ditches, though the Inlet has historically proven to change at a much faster rate than the Ditches.

Keulegan's method can also be used to create a channel cross sectional area versus velocity curve, which can provide an indication of inlet stability. This method, when applied to the Indian River Inlet by the Committee on Tidal Hydraulics was deemed inadequate for its lack of consideration of Rehoboth Bay (because of the

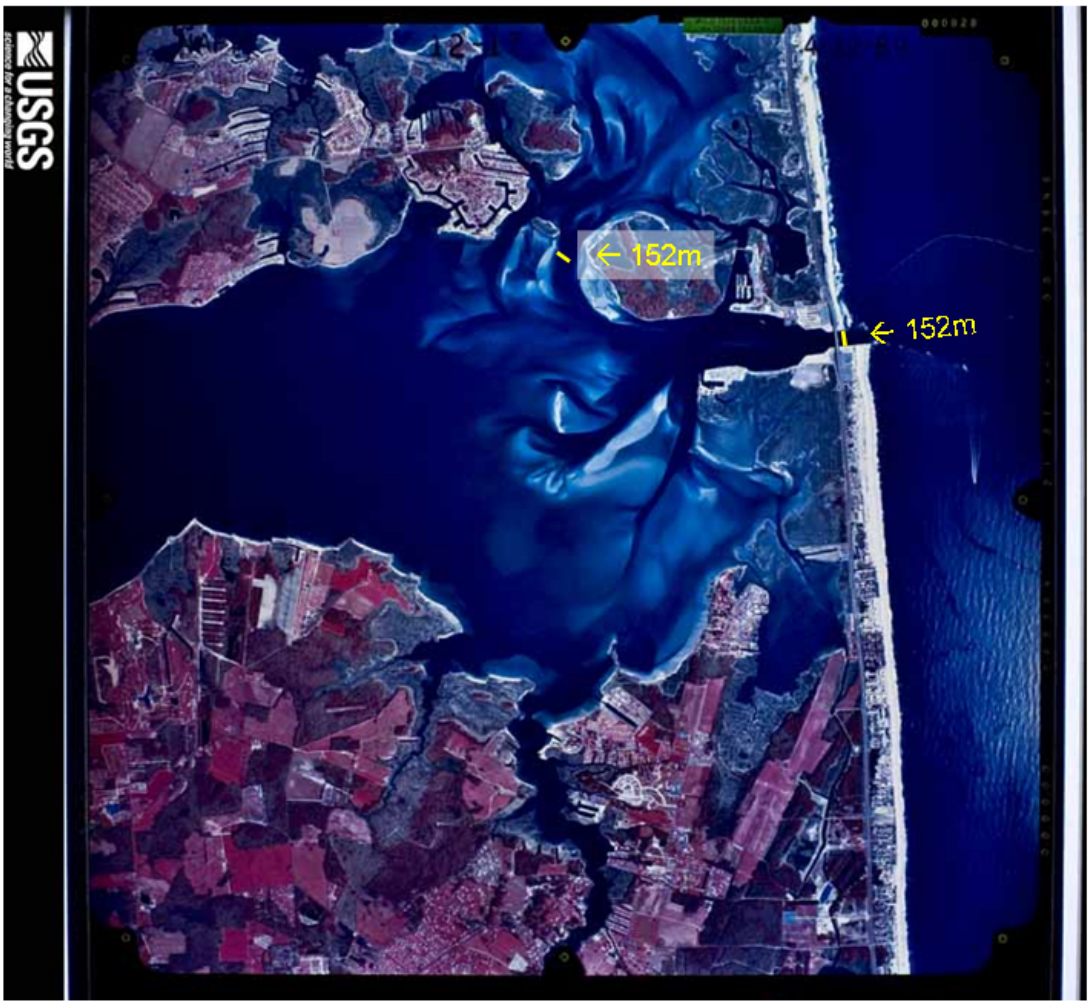

Figure 2.9: 1989 satellite photograph of the inlet area, scale comparison shown.

initial assumption about the Ditches) [5, p. 19].

2.5 Macro-turbulence

One likely culprit in the ongoing scour is high gradients in along-bed shear stress caused by macro-turbulence shed by the bathymetric rise collocated with the constricting channel and the bridge. Just considering the centerline of the inlet, comparison can be made between the undulating bathymetry and a periodic dune

field. In this case, the crest of the dune is roughened with riprap and bridge foundations.

A tidal current field study was undertaken in August 2007 to investigate the characteristics of inlet flow. A Workhorse Sentinel ADCP was mounted to a small vessel looking straight down, and data were collected over most of one 12-hour tidal cycle. Since the maximum depth in the scour holes approaches 35m, the maximum range of the instrument was set to $52.5m$ and broken into 105 bins each $0.5m$ long.

The vessel made systematic runs through the inlet, constantly collecting data at 1Hz. The highest observed velocities during the survey approached $3m/s$ both for flood and ebb tides. Operating in the relatively narrow inlet, and considering the high number of recreational boat traffic in the inlet during the survey, tracks perpendicular to the flow were not feasible. Instead, survey lines were run from about $200m$ west of the bridge to $150m$ east of the bridge repeatedly, as illustrated in the sketch in Figure 2.10. While tracks perpendicular to the mean flow would have been preferred to capture the three dimensional turbulence shed by the bridge piers, the parallel tracks that were used enabled the visualization of the wake flow in the lee of bathymetric features.

Because of the pattern of collection, data points were spread over time and space. The continuous data were first discretized in the time domain by considering twenty minute segments of data to be instantaneously collected, all adopting the median time tag. Then, analysis of the flow along the centerline of the channel was performed by considering all data points within $20m$ of the centerline to be on the centerline.

Limiting the analysis to two dimensions at a time simplifies the real world flow conditions but gives insight into the possible mechanism of scour, and scour hole propagation. The along-channel direction is considered the x-axis, with flow along this axis, u, being positive during ebb tide; and the vertical direction is the

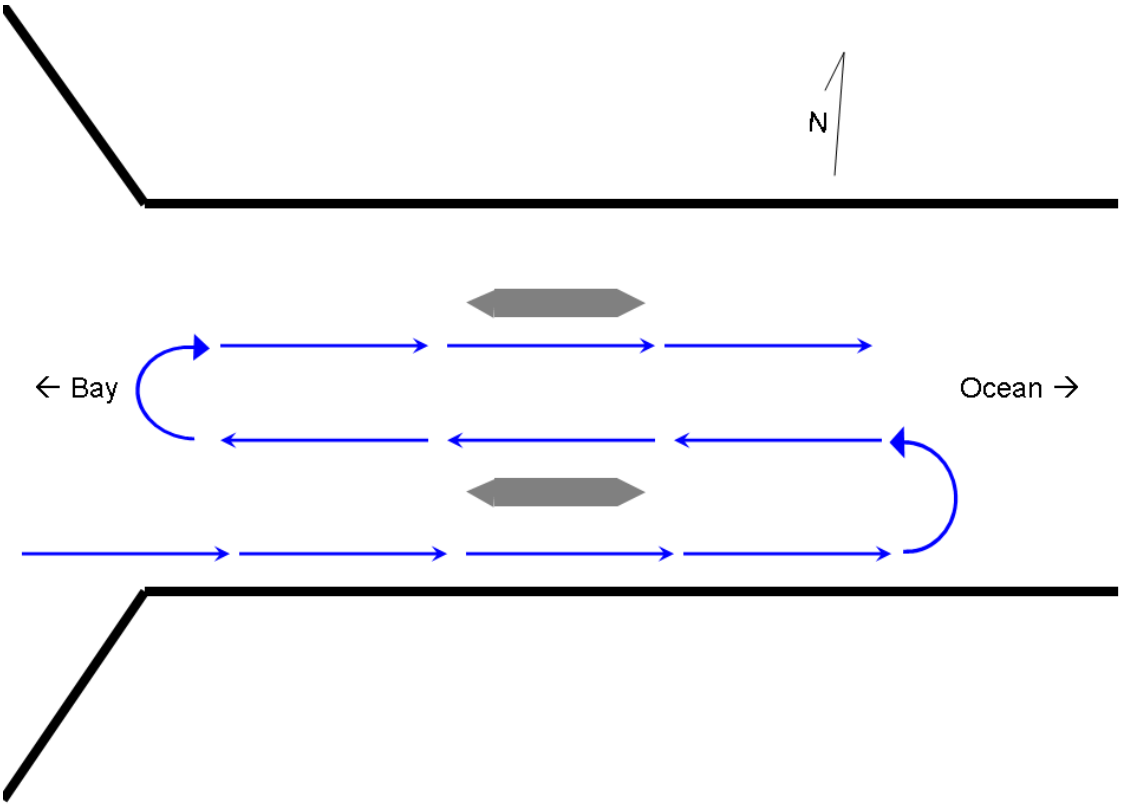

Figure 2.10: Sketch of the orientation of survey lines for the 2007 ADCP survey. Drawing not to scale.

z-axis, with positive flow, w, being up. Taking the vorticity, ω_y about the y-axis, which is the across channel axis and perpendicular to the centerline data slice,

$$\omega_y = \frac{\partial u}{\partial z} - \frac{\partial w}{\partial x}, \tag{2.7}$$

revealed coherent eddies being shed from the crest of the bathymetry coincident with the bridge foundations and armor riprap. The vorticity calculated from flow near peak ebb is plotted along the centerline slice in Figure 2.11 with concentrations of warm colors being coherent clockwise spinning eddies, and concentrations of cool colors spinning counter-clockwise.

From sequential time segments of the same centerline slice, these eddies

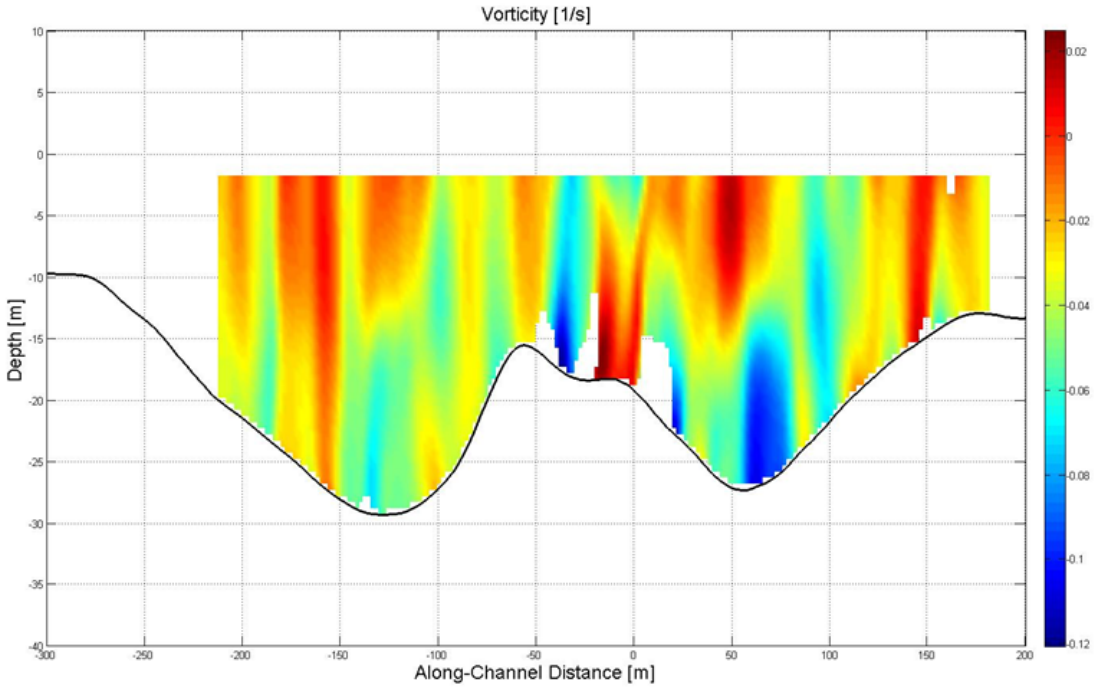

Figure 2.11: Vorticity plot from 2007 ADCP data, red eddies spin clockwise and blue counterclockwise. Colorbar represents vorticity with units 1/s.

appeared at different spatial locations, leading to the assumption that they were forming like eddies in the wake of a dune and being carried downstream by the background current.

When the permanent BBSMS ADCP's were installed, one of each instruments' beams was aimed approximately in the along channel direction. During the pilot *in situ* current profile collections similar eddy structures were observed. This deployment's instrument configuration allowed for time series analysis that proved these eddies were indeed separate from the background flow, and are advected downstream by the underlying ebb tidal current. Figure 2.12 is created by plotting the velocity returns along the entire profile versus time. The abscissa describes the distance along the profiler beam, and the ordinate contains the count of seconds elapsed from the start of data collection. The striping in Figure 2.12 represents

flow anomalies attributed to macro-eddies. The slope of the stripes is approximately $0.8m/s$, the same as the mean flow for the duration of this time stack.

The significance of this determination is the illumination of the wake structure that occupies the water column in the lee of the rise. The flow behind a dune is known to follow a characteristic pattern (Figure 2.13) which focuses high stresses on certain areas of the channel bed. The eddies seen in the two ADCP data sets are in the wake zone in Figure 2.13, below that sits a flow reversal zone while a high-shear boundary exists between them. The boundary follows a curve from the crest of a dune back to the bed, where flow is said to *reattach*. This reattachment zone flaps much like a flag in the wind. Reattachment variability coupled with the periodic impacts of eddies makes this area prone to sediment suspension.

The figure from Walker (2002) is based on aeolian dune research, but Best (2005) gives evidence that the same patterns of flow and sediment suspension appear for sub-aqueous dunes. Once suspended, the sediment in the inlet is carried away from its suspension point by the upwelling portion of the eddies, then transported out of the system. Paarlberg [27] states that the distance of reattachment, L, is a function of the height of the bathymetric feature, H_b and the ejection angle, α_s in the simplest parameterization, seen in Equation 2.8.

$$L = H_b(6.48 \tan \alpha_s + 5.17) \tag{2.8}$$

Equation 2.8 was evaluated using H_b as the relative distance between various bathymetric troughs and crests encountered by ebbing or flooding current; the ejection angle, α_s, was always null since the bathymetry was assumed to change smoothly. The results, plotted in Figure 2.14, reveal that one particular ebb tide reattachment point falls on the face of the scour hole currently experiencing enhanced local scour.

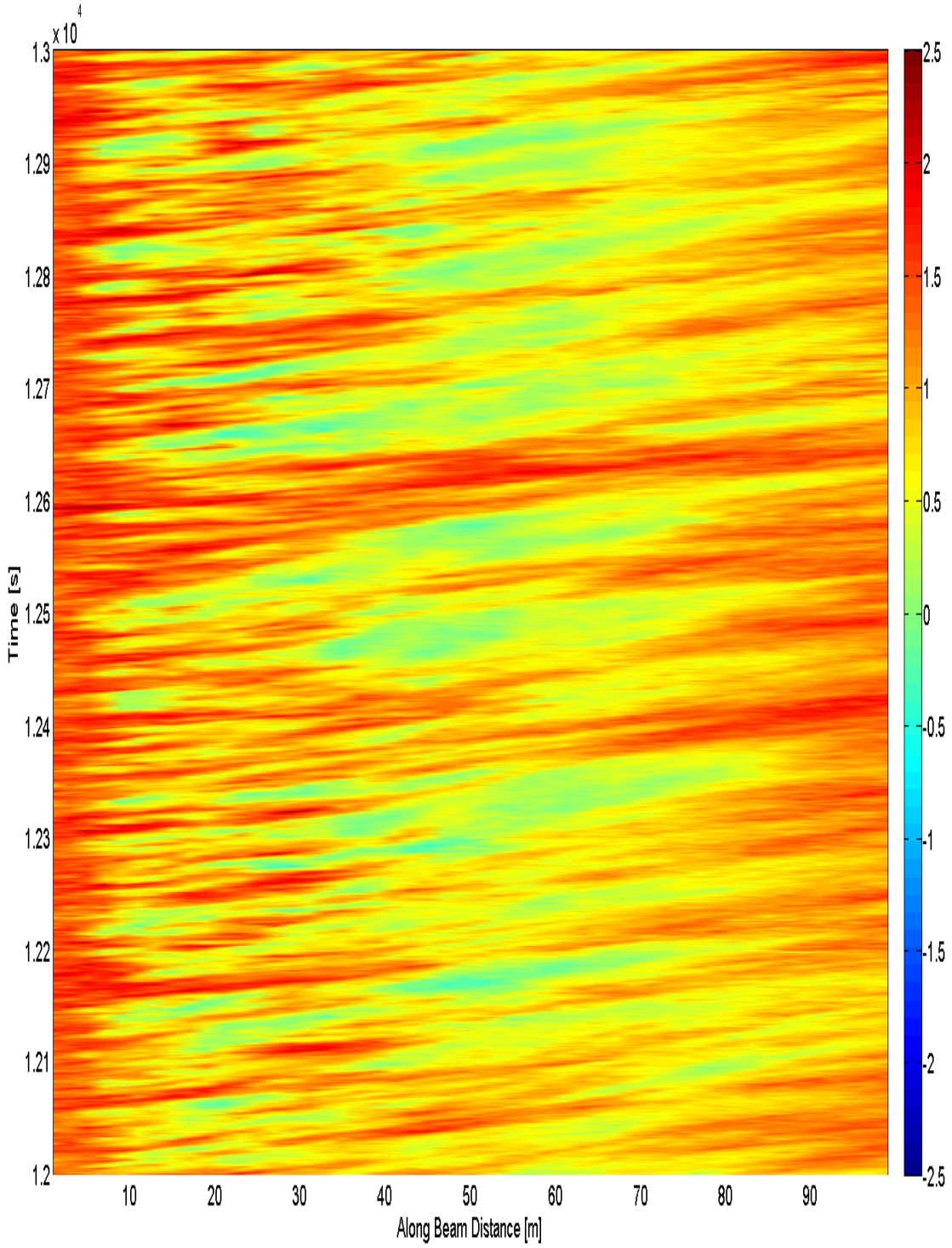

Figure 2.12: Time stack of velocity profiles from north pier beam 3, colorbar represents velocity in m/s.

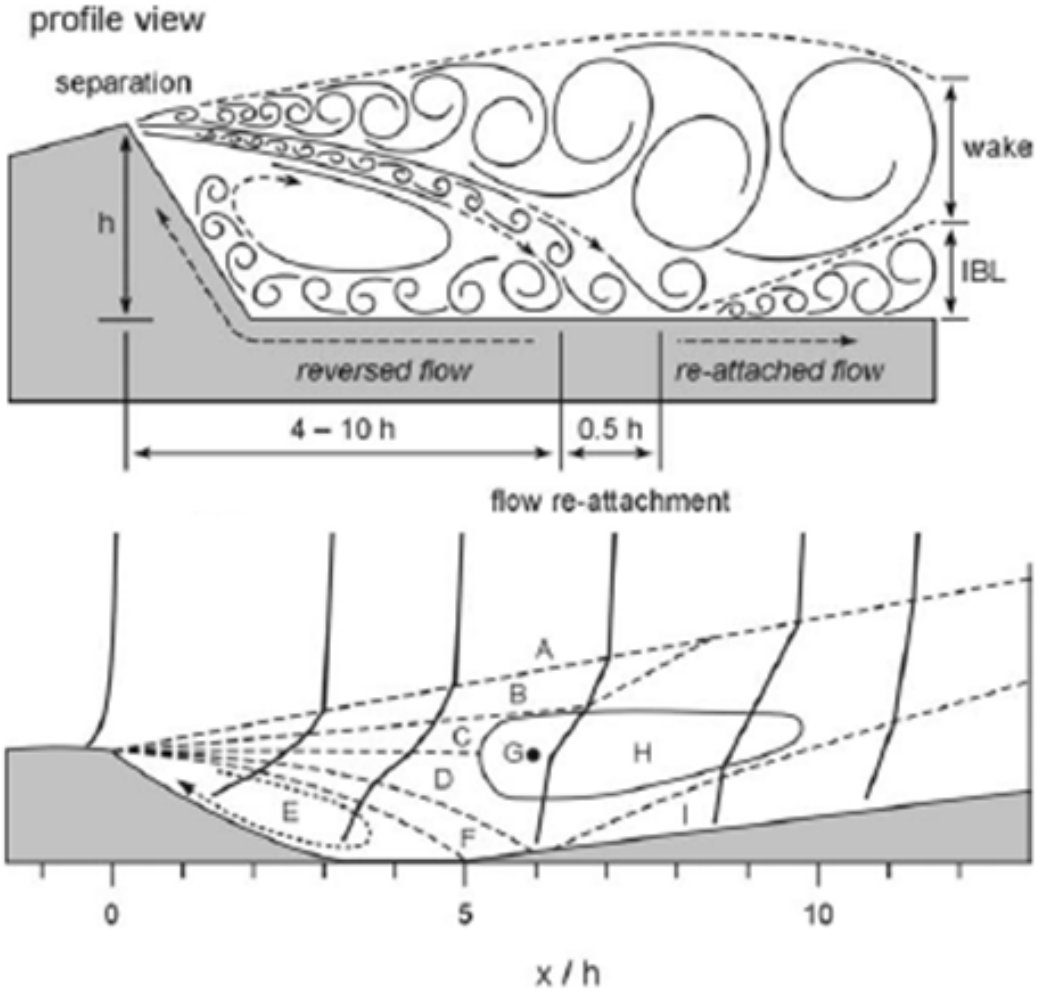

Figure 2.13: Figure from Walker (2002) showing the patterns of turbulence expected behind a dune crest.

The riprap roughened crest of the bathymetric rise undoubtedly alters the flow from the simple dune model, however this parameterization is still a useful tool in understanding one mechanism of scour hole propagation. If the face adjacent to the bridge is subjected to this reattachment, in addition to the interface between the riprap and the natural bed, then intuitively there should be more scour here.

Is it valid to consider this bathymetric rise a dune-like feature? Even if it is

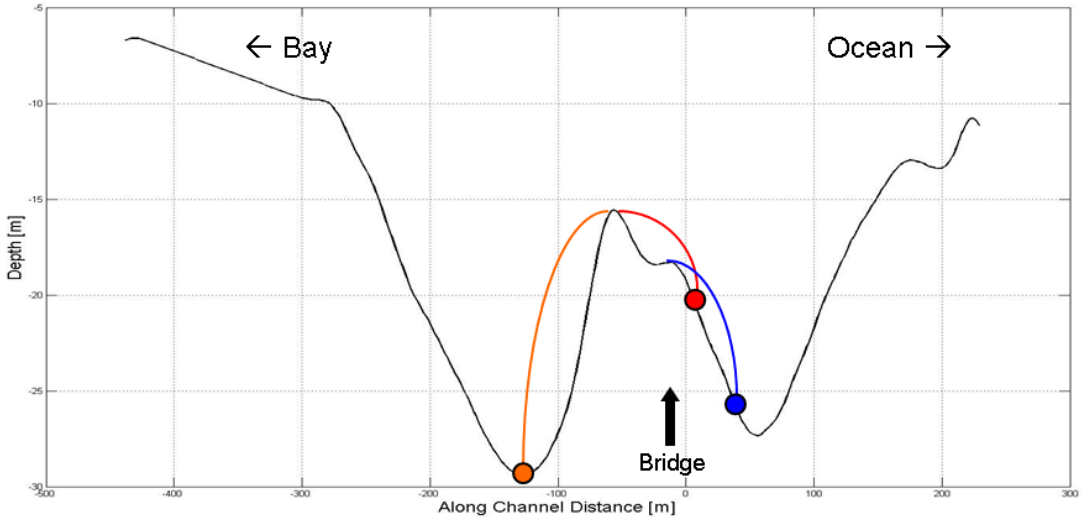

Figure 2.14: The results of the Paarlberg reattachment parameterization. Colors associate reattachment points with appropriate ejection points; orange for flood tide, red and blue for ebb tide.

not a dune *per se*, Best (2005) suggests that bedforms – regardless of classification – all exhibit similar wake shedding traits. Strict classification as a dune requires consideration of the depth of flow, grain size, and average cross sectional velocity. The Froude number, Equation 2.9, is used to classify the flow conditions as sub- or supercritical by comparing. $F_r < 1$ is subcritical and $F_r > 1$ is supercritical.

$$F_r = \frac{U}{\sqrt{gh}}, \tag{2.9}$$

where U is the mean flow through the effective cross section, and h is the depth of the effective cross section. Then for the Indian River Inlet (denoted IRI)

$$F_{rIRI} = \frac{3m/s}{\sqrt{9.81m/s^2 * 15m}} \tag{2.10}$$

$$F_{rIRI} = 0.25. \tag{2.11}$$

This satisfies the condition set by Kennedy [16; 8] that for dunes to occur $F_r^2 < \frac{1}{k}\tanh k$ where $k = \frac{2\pi h}{\lambda}$ and λ is the bedform wavelength. The Indian River Inlet

centerline feature has a wavelength of approximately 150m (k=0.628), so then

$$F_r^2 < \frac{1}{k}\tanh k \tag{2.12}$$

$$F_r^2 < 0.886. \tag{2.13}$$

For this particular bathymetry, the conditional statement classifies the feature as a dune or dune-like. The dune-like rise is sustained under tidally oscillating flow, so it lacks the asymmetry normally associated with dunes, but the classification allows the analogous flow patterns of dune fields to be compared with the flow in the inlet.

Further bedform classification is achieved by computing the *Ripple Index*, RI. RI is the ratio of bedform wavelength to bedform height, where the height is measured from crest to trough.

$$RI = \frac{\lambda}{h} = \frac{wavelength}{height} \tag{2.14}$$

Values of RI in the range 10-30 are classified as steep dunes [29]. The RI of the Inlet centerline rise is in the range of 9.75-11, putting it on the steep side of the dune spectrum. Keep in mind though that this steepness is only along this centerline slice, the bedforms are three dimensional and the slope moderates with distance from the center of the inlet. Regardless, the steep dune association allows for the relation between flow conditions in the lee of dunes and the flow conditions observed during field tests at the inlet.

Evidence that the upwelling boils, and thus entire eddies, carry sediment was collected during a thermal camera investigation of the boils that were visually observed breeching the surface during the first ADCP survey. The FLIR Systems ThermaCam P45HSV camera measures thermal infrared energy in the $7.5\mu m$ to $13\mu m$ wavelength range. It uses an uncooled microbolometer sensor array of $320x240$ pixels, and has a thermal sensitivity of $50mK$ at $30°C$. For this field study, the

camera was not tripod mounted in order to give the operator the freedom to track surface boils while the video stream was captured by a remote media recorder. This video stream was then used to reference the snapshot images taken by the P45HSV, some of which are presented here. The study was conducted pre-sunrise to avoid interference from the sun on May 8, 2008 during peak ebb flow. There was substantial cloud cover with gusty wind up to $6.5m/s$, and the air temperature was $21°C$ with 70% humidity, which holds significance that will be discussed later.

Originally, the thermal camera was used because of an assumption that the upwelling water should be a different temperature than the calm surface water. Intuitively, water suddenly lifted from deeper sources in the inlet would be cooler than the surface layer and thus should appear so in thermal infrared images. The thermal camera was able to pick up distinct boils instantly (Figure 2.15), although they appeared warmer than the surrounding water. The temperature difference assumption was invalid because during peak ebb flow, all of the water rushing through the inlet originated in the bays, where temperature distribution is relatively constant.

The reason the boils appear warmer than the surrounding water is that the emissivity, ϵ, of turbid water is lower than the emissivity of clear sea water [21]. The camera observes the world assuming a constant emissivity for everything in the field of view, so an object with a different ϵ value appears at a different apparent temperature—even if the real temperature is identical.

Emissivity is a ratio of the brightness of an object to the brightness of a perfect blackbody at the same temperature, and since brightness is related to the fourth power of the temperature by the Stefan-Boltzman equation, emissivity can be described as the ratio of the object's actual temperature to the assumed blackbody temperature [35].

$$\epsilon \propto B/B_{blackbody} \propto T/T_{blackbody} \tag{2.15}$$

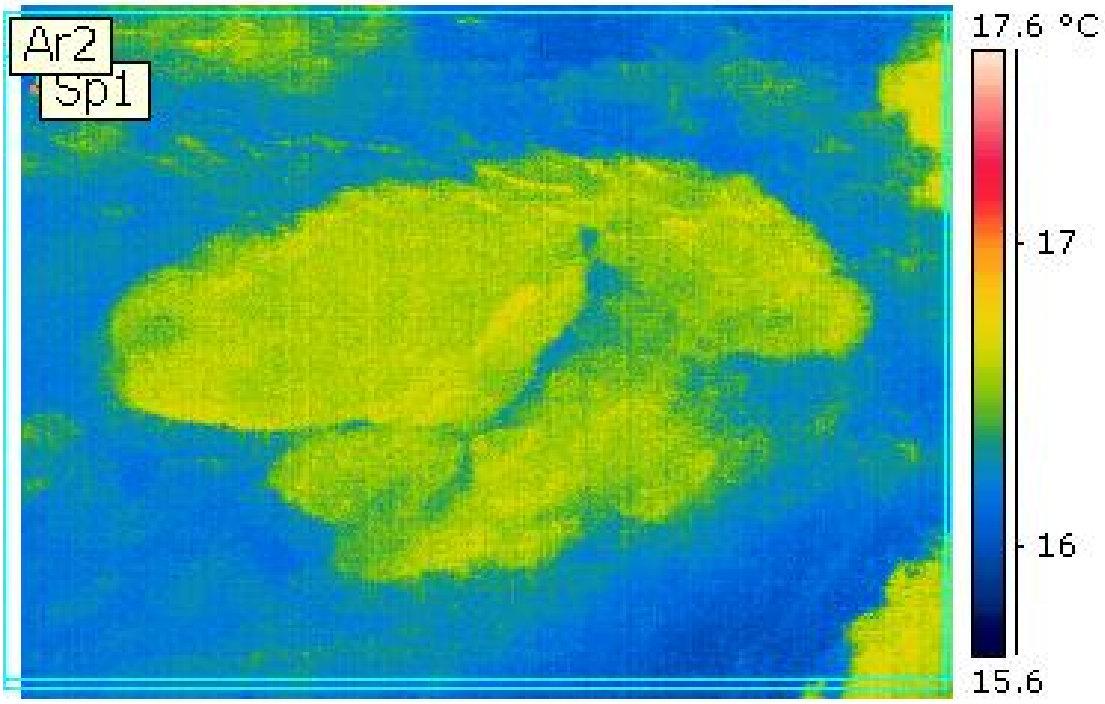

Figure 2.15: A surface boil appears warmer in thermal infrared images.

Assuming no emitters in the atmosphere influencing the signal to the sensor, Kirchoff's law states that the surface spectral emissivity is related to the spectral reflectance such that they always sum to 1, such that $\epsilon + \rho = 1$, where ρ is the spectral reflectance . Therefore, as the emissivity of the turbid water drops, its reflectance must increase to maintain the equality above. This increase in reflectance causes the turbid water to appear more like the atmosphere in terms of temperature, and since on the day of the experiment the atmosphere was quite warm relative to the water, the turbid surface boils appear warmer than the surrounding water [21].

The evidence presented here supports that scour is maintained by macroturbulence, probably in conjunction with a number of other factors. The original cause of local scour could have been turbulence generated by flow around the timber piles of the Cullen Bridge. Though data do not exist to support this hypothesis, modeling of the historical flow conditions and channel geometry could provide evidence.

Chapter 3

MONITORING METHODS

This section sets the framework for understanding the data that are presented in the following chapter. The work done in designing and implementing the BB-SMS is presented here, including descriptions of each instrument. Data processing techniques are presented in the respective instrument sections of Chapter 4.

3.1 Inlet Coordinates

It is difficult to process plots of data when the axes are given in the Delaware State Plane coordinate system because the area of interest is very small relative to the state of Delaware. In reaction to this difficulty, a local coordinate system was created with its origin approximately at mid-width of the channel and on the easternmost edge of the bridge. This "Inlet Coordinate" system is rotated from true easting and northing such that the x-axis is parallel to the axis of the channel. This makes it easy to refer to plots where features are presented relative to the bridge and channel walls rather than an obscure coordinate system.

Transformation between DE state plane and Inlet coordinates first involves a rotation of 5° in the clockwise direction. The axis of the channel runs slightly from southwest to northeast, and this 5° rotation aligns the x-axis with the channel axis. Next comes a translation to adjust the origin from the DE state plane origin to the local Inlet origin. The origin used for Inlet Coordinates was computed with a hand held GPS unit on a walking survey of the inlet boundaries performed August 13, 2007. The walking survey included the walkways that border the inlet walls and the

eastern walkway over the bridge and its purpose was to log the general boundaries of the inlet. It also gave the opportunity to standardize the local coordinate system by providing an origin and the alignment of the channel, which have been used in the transformation universally. Table 3.1 shows the inlet origin according to various datums and units—important since historical data are not consistent and thus need special processing.

Table 3.1: The Inlet Origin in DE State Plane coordinates with respect to different datums, in both feet and meters.

Inlet Origin		
Datum/Units	Easting	Northing
NAD27/feet	600929.7	221623.8
NAD27/meters	183163.4	67550.9
NAD83/feet	757201.1	221669.6
NAD83/meters	230794.9	67564.9

Note that the elevation or depth does not change in the transformation from DE state plane coordinates to Inlet coordinates. Care should be taken in referring all data to the same vertical datum, but once set–the elevation data will not change. Here is an example calculation showing the transformation into Inlet coordinates:

> Inlet Coordinate transformation Example: Point A is given in DESP, meters, and relative to NAD83: Northing, 67599.65 and Easting, 230792.133
>
> The appropriate Inlet Origin (Io) is Easting, 230794.9 and Northing, 67564.9. It is important not to forget rotating Io first. Io' (rotated) is Easting, 235805.33 and Northing, 47192.7.

$$
\begin{aligned}
A'_{Easting} &= [\ A_{Easting}\cos\theta + A_{Northing}\sin\theta\ ] - Io'_{Easting} \\
A'_{Easting} &= [\ 230792.133 * \cos(5) + 67599.65 * \sin(5)\ ] - 235805.33 \\
&= 0.27 \\
A'_{Northing} &= [\ -A_{Easting}\sin\theta + A_{Northing}\cos\theta\ ] - Io'_{Northing} \\
A'_{Northing} &= [\ -230792.133 * \sin(5) + 67599.65 * \cos(5)\ ] - 47192.7
\end{aligned}
$$

$$= 34.85$$

As illustrated by this example, in addition to adjusting the axes, the transformation reduces the size of coordinate values. Now it is easy to see that Point A sits less than one meter east of the bridge, and about 35m north of the inlet centerline—information that the raw data did not readily relay.

3.2 Instrumentation

The crux of the BBSMS are the three pair of instruments that collect the data about the bridge health. The tilt sensors were the only off-the-shelf products; the sonars and acoustic current profilers were custom made because of requirements regarding sonic frequency and instrument orientation, respectively. The underwater instruments were coated with *E-Paint*, an anti-fouling paint on their bodies; and *Bio-Grease*, an experimental anti-fouling coating made up of menthol in a petroleum based gel on their transducers. The instruments are controlled by computers housed in an aluminum enclosure, called the Traffic Box, that sits next to the northern land-based pier (See Appendix B for more on the Traffic Box).

3.2.1 Marine Electronics 250kHz 3D Profiling Sonar

First, it is worth noting that throughout this document the terms *profiling sonar* and *scanning sonar* and sometimes simply *sonar* are used interchangeably to refer to this instrument. Though both the current profilers and the profiling sonars use sonic pulses to gather information about the environment, this is the only instrument referred to as any type of *sonar*.

The stock version of this sonar employs a much higher frequency transducer, which would have been inadequate for penetrating the murky water in the inlet to sufficient distances. In order to achieve the desired penetration while preserving a

narrow 3° conical beam, the size of the transducer was increased — and thus the size of the environmental enclosure grew relative to the stock model. The dimensions can be seen on the drawing provided by Marine Electronics in Figure 3.1. The dome portion of the unit is made of uPVC while the cylindrical body portion is anodized aluminum.

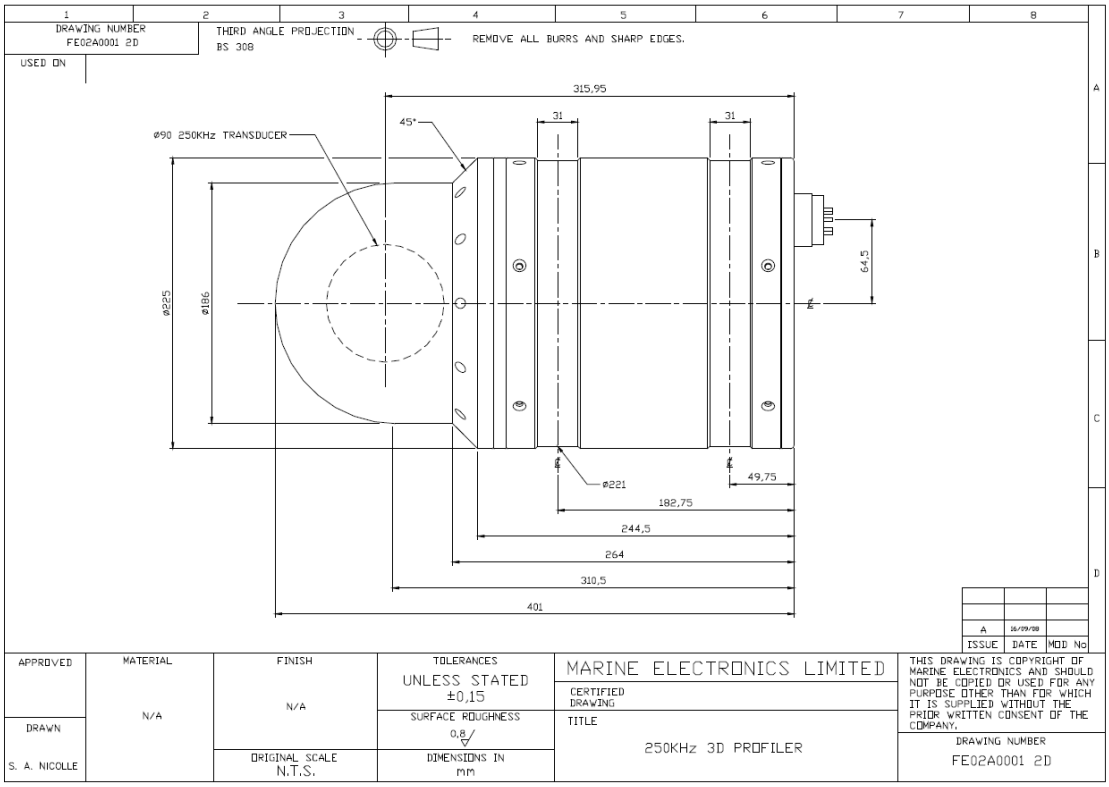

Figure 3.1: Technical drawing showing demensions of the body of the M-E 3D Profiling Sonar used in the IRIBBSMS [units: millimeters]. This drawing is the property of Marine Electronics.

The instrument achieves a full hemisphere of scans using only a single transducer and two axes of precision step motors that allow it to change pitch and azimuth. Scans always start and end at the same point, as indicated by an arrow on the flat back end of the instrument body. First a 180° *swath* is scanned, in increments chosen through a GUI. Then the transducer is rotated one step in azimuth,

and the second swath is scanned. Swath and rotation step sizes can be chosen as multiples of 0.9°.

In order to protect the instrument from the environment, and to securely fasten the instrument to the underwater frame, a block housing was cut out of Delrin plastic. The interior dimension of the Delrin block fits exactly the exterior dimension of the anodized aluminum cylinder, and two nylon set screws bite into one of the grooves in the sonar to keep it in place. The angles cut in the Delrin, visible in the photograph in Figure 3.2, allow the instrument to be positioned as close to the nose of the frame as possible.

Power and communications are sent to the sonar via custom molded Falmat cables. A 40m short cable connects to each instrument via a SubConn 8-pin female circular connector with threaded sleeve and to the long cable via another circular 8-pin SubConn connector with threaded sleeve. The long cables run from the Traffic Box to the cable tray above each pier and run 80m to the north pier and 160m to the south pier. Excess from the short 40m cable is coiled and stored on top of the cable tray and conduit under the bridge deck to provide the necessary slack should the instruments need to be brought above the water.

A schematic of the Falmat cable used for the sonar appears in Figure 3.3. The Falmat cables are marked either *SONAR* or *ADCP* at 1m intervals along their entire length for easy identification in the field.

3.2.2 Nortek Continental 470kHz Acoustic Doppler Current Profiler

Each Nortek Continental ADCP uses three separate 470kHz transducers which can act independently or in unison to collect current profile time series. Each transducer collects current profiles along the axis of its sonic cone, and the three signals can be processed together by the instrument to transform each 1D profile into one 3D profile. Because of the proximity of our instruments to the steel in the bridge pier and the underwater frame, a compass was not included and thus

Figure 3.2: Photograph of one Sonar dry fit in its Delrin block, white E-Paint has been applied, photo taken just before Bio-Grease application on dome.

the instruments lost their ability to rectify data into the common East-North-Up coordinate system.

The transducers are equally spaced around a circle, each angled 25° away from the center of the instrument as shown in Figure 3.4 taken from the Nortek user manual. The indicator arrow on the Delrin plastic body of the instrument points toward beam 1, and beams 2 and 3 are numbered ascending in the clockwise direction. The ADCP's were configured to collect data at 1Hz from 50 discrete

Figure 3.3: Diagram of the Falmat cable used for Sonar communication and power, including pinouts for the SubConn cable interfacing with the sonar and wiring scheme for the M-E control box.

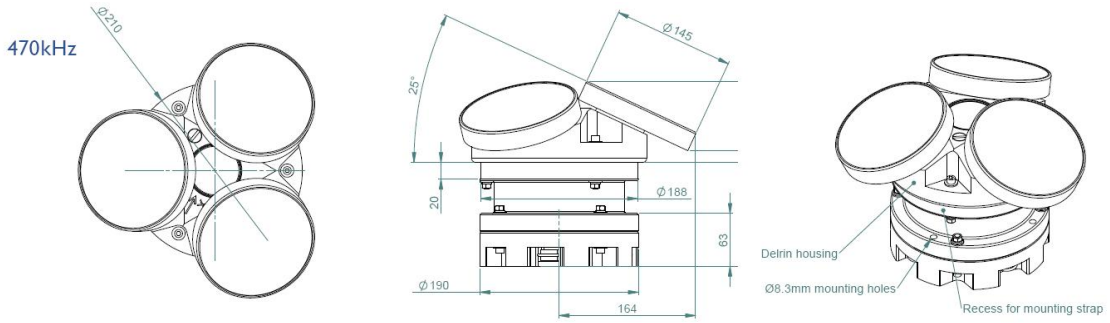

Figure 3.4: Nortek Continental ADCP 470 kHz physical specifications, from Nortek [units: millimeters].

bins each 2m long, for a total profile length of 100m. The shallow deployment depth limited the BBSMS current profilers to two usable beams, as the remaining beam signal intersects the channel floor within a few meters — the beam spatial configuration is shown in Figures 3.16 and 3.17.

A mounting block of Delrin plastic was used to securely fasten each ADCP to its underwater frame, similar to the sonar mounting method. The insides of the two part block match the recess in the instrument body, and two pass-through holes allow the block to be bolted into the underwater frame. Figure 3.5 shows the south pier's ADCP ready for installation.

Power and communications are sent to the ADCP via custom molded Falmat cables. A 40m short cable connects to each instrument via an Impulse 8-pin male rectangular connector and to the long cable via a circular 8-pin SubConn connector with locking sleeve. The long cables run from the Traffic Box to the cable tray above each pier and run 80m to the north pier and 160m to the south pier. Excess from the short 40m cable is coiled and stored on top of the cable tray and conduit under the bridge deck to provide the necessary slack should the instruments need to be brought above the water. The wiring scheme for the ADCP cables can be seen in Figure 3.6.

Inside the Traffic Box, the ADCP cable is stripped and the conductors are

Figure 3.5: Photograph of one ADCP ready for deployment, white E-Paint and Bio-Grease has been applied.

situated in their appropriate terminals on the *incoming terminal block*. This block was constructed to receive the raw incoming conductors from the instruments, and provide the necessary power and data links in an organized format. The block is configured as shown in Figure 3.7. The block has the capacity to receive the incoming sonar conductors as well, however since Marine Electronics supplied a separate control box that receives raw conductors, this feature is not used.

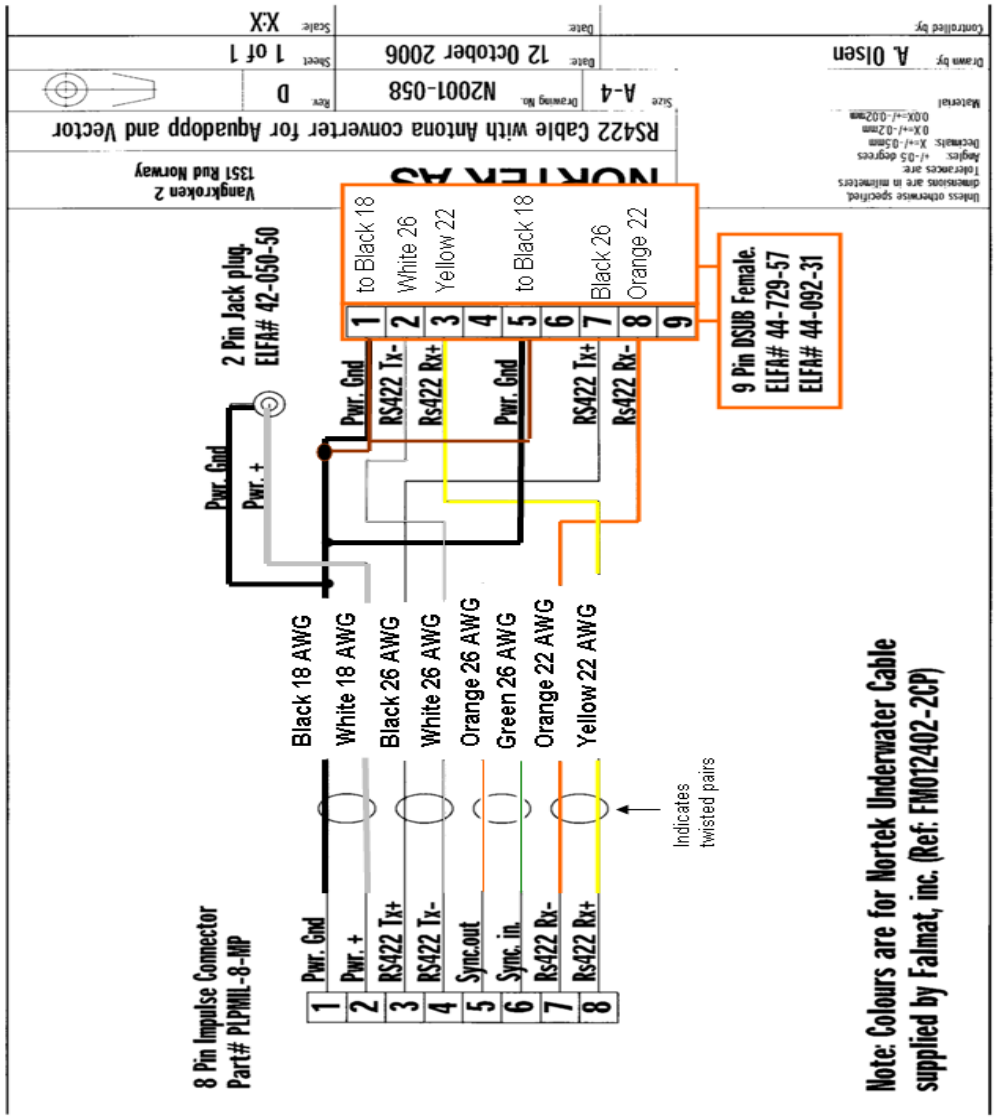

Figure 3.6: Wiring diagram color coded for Falmat cable and showing how the lead end should interface with the incoming terminal depicted in Figure 3.7.

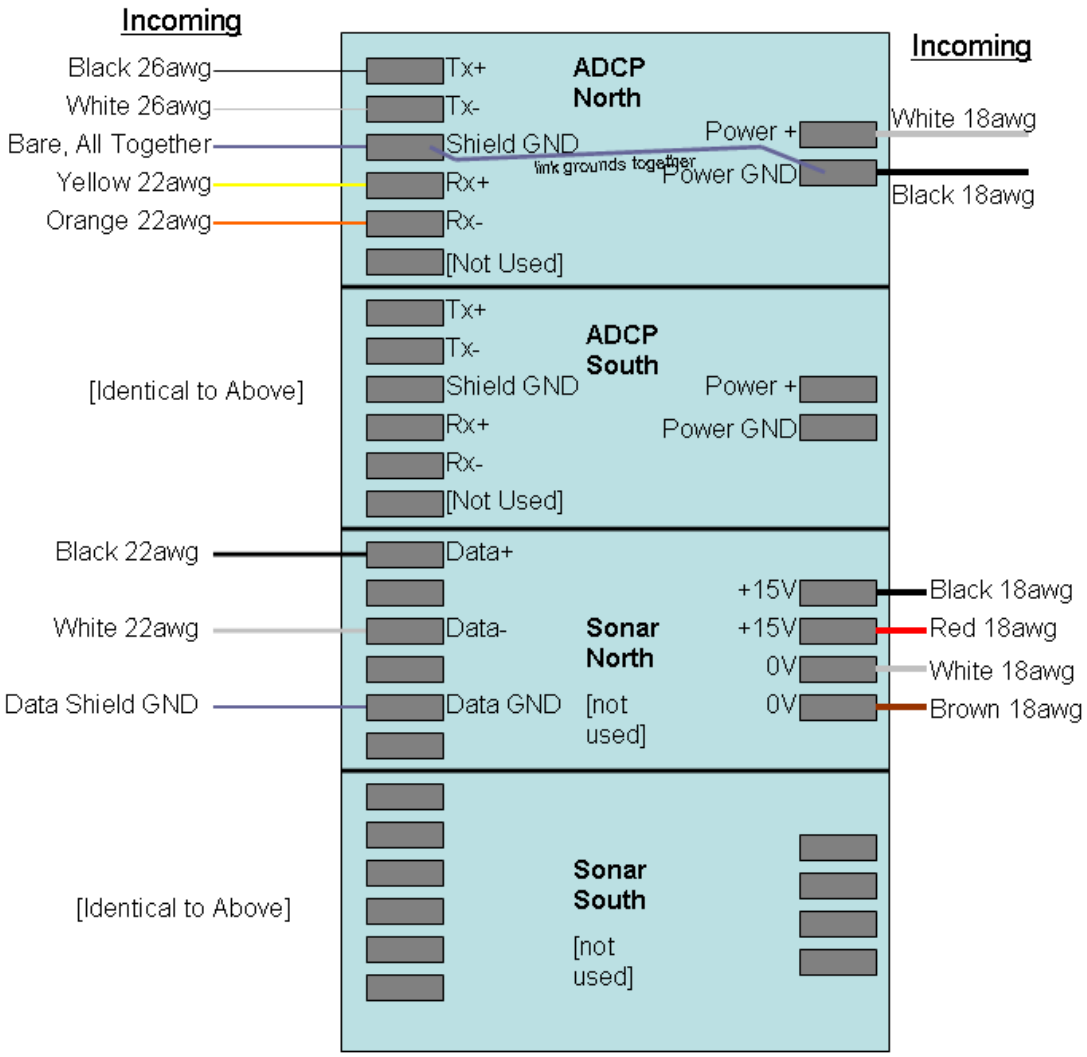

Figure 3.7: The Incoming Terminal Block that is found on the second shelf of the Traffic Box (see Appendix B).

3.2.3 HL Planar D-Series dual axis Inclinometer

A pair of dual axis tilt sensors were installed, one on the top of each pier supporting the northbound lanes of the bridge. Measurement Specialties, an American company based in Virginia purchased the rights to sell the D-Series from the German HL Planar Technik company that makes the sensors. The HL Planar D-Series is designed to operate in high vibration environments, and is built with a rugged IP67 aluminum enclosure which can resist the salty air under the bridge. The units used in the BBSMS have serial numbers #0546622 and #0642126.

These instruments exploit the level free surface of an electrolytic fluid with constant conductivity inside a closed vessel to calculate tilt. The fluid surface bounds the forced electric field (see Figure 3.8), and platinum electrodes measure the change in resistance to compute the relative deviation from horizontal along a particular axis. The dual axis inclinometers use two such domes, one designated for each direction of measurement.

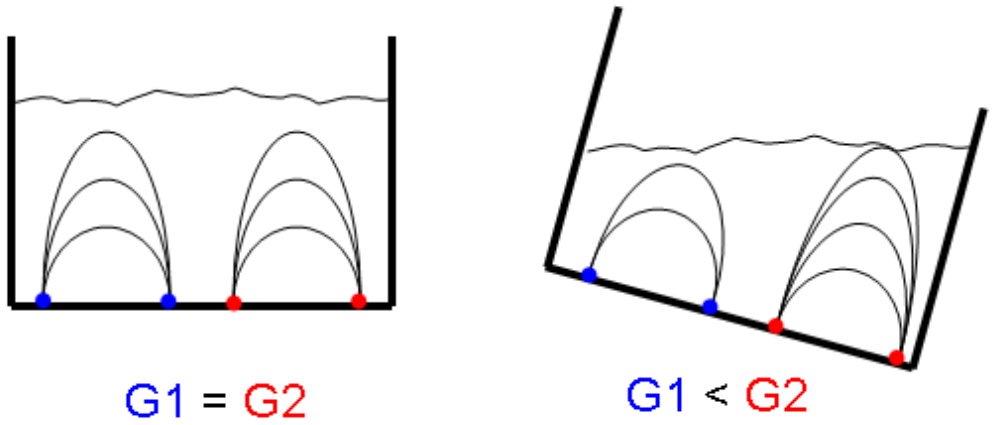

Figure 3.8: A schematic of how the electrolytic fluid tilt sensor operates with twin pairs of electrodes reading the difference in resistance due to their respective orientation relative to the free surface of the fluid. Reproduced from manual.

The D-Series inclinometers selected for this application output current from $4 - 20mA$ which scales linearly with its $\pm 5^{\circ}$ tilt measurement range. The current output model was selected over a voltage output model after consulting with HL Planar representatives because of the need for a robust signal over long stretches of cable. The analogue current signal is changed to voltage at the data logger through the use of precision 100ohm shunt resistors, and raw voltage is recorded. Later, during processing, the logged voltage data are converted to tilt.

Custom wired waterproof connectors link the shielded 8-conductor 24AWG power/data cable to the instrument; the connectors were ordered from Binder USA by the manufacturer and cables were purchased from Digi-Key in one 500 foot and one 1000 foot spools. Power was originally supplied by an Omega DC power supply while data were logged on a DataQ logger which required periodic manual downloads. After DelDOT expressed interest in converting the tilt sensors to near-real-time, a Campbell Scientific data logger with the capability to supply power, log data, and ftp data was installed.

The Campbell logger collects a data point every 2 seconds, then stores the average of 30 of these signal points. This acts to filter some of the high frequency vibration and noise that plagued the tilt signal under the original configuration with the DataQ logger. Once per hour, the collection of these 60s averaged signals are sent via secure network to the University of Delaware servers.

The sensors were installed using threaded rod anchored in concrete in the top of the pier, a mock-up of this method can be found in Figure 3.9. The x-axes of the sensors are aligned in the along channel direction, roughly east-west. The y-axes are perpendicular to these, in the across channel or roughly north-south direction. This means that if the top of the pier tilts either east or west, the x-axis will register the change. A visual representation of the signal outputs related to tilt directions is in Figure 3.10.

Figure 3.9: Mockup of the tilt sensor install technique using threaded rod anchored into concrete.

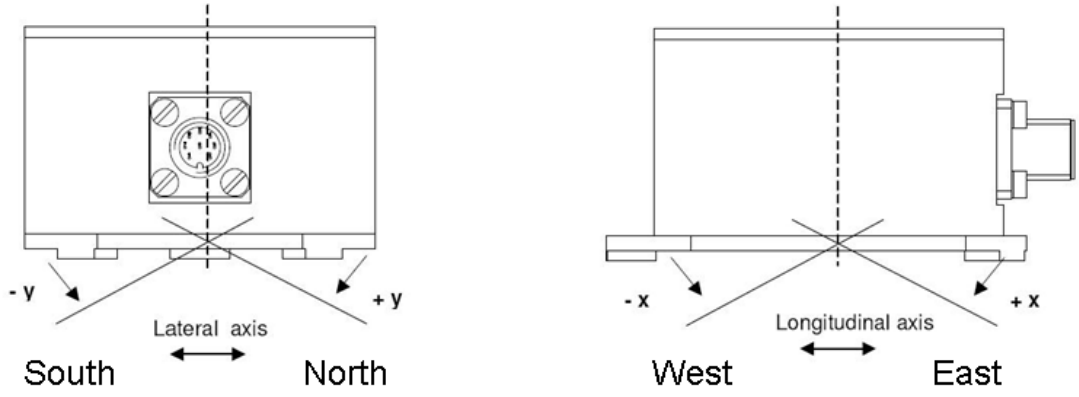

Figure 3.10: Visual representation of current outputs associated with tilt in the approximate compass directions associated with the BBSMS installation. Reproduced from manual.

The conductors in the Digi-Key cable do not match the colors specified in the HL Planar manual exactly, which is of no consequence as long as the wiring scheme is documented. Table 3.2 contains the function of each pin of the tilt sensor connector and the associated color code of the Digi-Key cable.

Table 3.2: Wiring color code and pin outputs for the tilt sensors.

Pin	Name	Description	Color
1	$+U_b$	Positive power supply	White
2	RxD	Rx serial signal RS232	Brown
3	TxD	Tx serial signal RS232	Green
4	GND	Ground	Yellow
5	XOut	X-axis output	Black
6	SGND	Signal Ground	Orange
7	YOut	Y-axis output	Blue
8	NC	Not Used	(Red)

The RS232 send and receive capabilities of the tilt sensors are not used in daily operation. During bench tests, these connections were used to interface the instrument with a computer to obtain operation characteristics.

3.2.4 Mount Design

In order to survive the treacherous currents, structures intended for installation in the inlet must be capable of withstanding significant forces. In 1988, DelDOT used a design velocity of 15 ft/s when considering the placement of riprap around the bridge piers. Observations of typical peak velocities in the inlet during data collection in August 2007 revealed similar values, and so a design velocity of $u = 15ft/s = 4.57m/s$ was used as a baseline to design the steel frames that would be used to fix and protect the underwater instruments.

In order to achieve the desired durability, the frame shape was designed first with unspecified members - later structural analysis was used to determine the necessary member type. This design can be seen in Figure 3.11. The approach

to designing the instrument frame focused on long term performance, and gave immense weight to the unknown. Many factors of safety were added throughout the design process, as the comparative cost between building a robust frame or losing a custom built instrument heavily favored building a very strong frame.

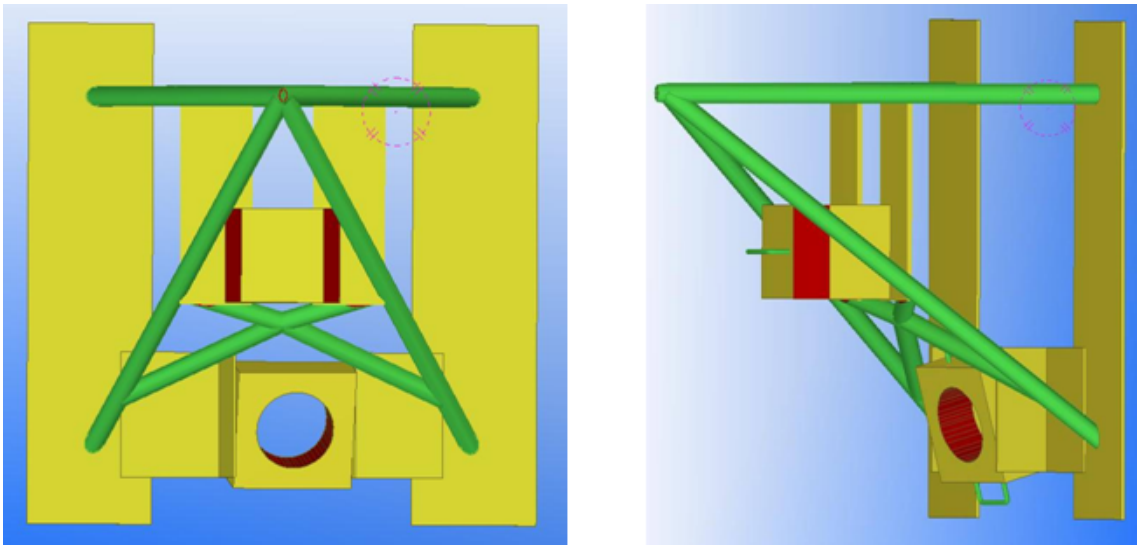

Figure 3.11: As built technical drawing of structural members of the frame. These drawings also show the rough instrument locations by showing the instrument mounting blocks.

The force per unit inch of frame exposed to the flow is a combination of forces from the steady currents and turbulence. Shown below, the Morison equation considers both the drag force applied by a steady component of flow and the force due to fluid acceleration, and was used to approximate a design force range. Since the unsteady portion of the flow near the bridge piers is due to unpredictable eddies, only the drag force was calculated directly.

$$\begin{aligned} F &= F_d + F_i \\ F_d &= \frac{1}{2}\,\rho\, C_d\, A_p\, |u|\, u \\ F_i &= \rho\, C_m\, V\, \frac{du}{dt}, \end{aligned} \tag{3.1}$$

where in Equation 3.1 F_d is the drag force on the member in the direction of the flow, $\rho = 1028\frac{kg}{m^3}$ is the density of sea water, C_d is the drag coefficient and depends on the cross section shape of the member, A_p is the area of the member perpendicular to the flow, and u is the flow velocity that imparts the force. If $A_p = d_p * h$ where d_p is the diameter or width of the member perpendicular to the flow and $h = 1$ then the formula outputs force per unit length of the member, and so was the formula treated for this calculation. Plugging in design values of $C_d = 1, A_p = 0.0013\frac{m^2}{m}, u = 4.57\frac{m}{s}$ the drag force per unit length of member is approximately $14\frac{N}{m}$.

Since the lift force and inertia force were both ignored in the above calculation, and also since the final shape of the frame will include bulky instruments that will augment the reaction to the fluid forces, a design force of about $450\frac{N}{m}$ was used to select the type of member used to build the frame. Four different common member types were analyzed using STAAD structural analysis software: $2in$ x $2in$ angle stock $0.25in$ and $0.1875in$ thick and $2in$ diameter round structural tube with either $0.25in$ or $0.1875in$ thick walls. The material analyzed was universally 316 Stainless Steel, selected for its resistance to corrosion in salt water environments. 316 stainless steel has a tensile strength of $515MPa$, compression strength of $170MPa$, and a modulus of elasticity of $193GPa$. Deflections were computed at the nose of the frame and at two nodes on the site trusses. Under forcing from various angles, the nose of the frame deflected more than the side truss nodes, but the maximum deflections were all less than $3.2 * 10^{-3}m$. Generally the round structural tube performed better than the angle stock, and given the relatively small difference in deflections between the $0.25in$ and $0.1875in$ wall thicknesses, the thinner walled tube was selected in consideration of weight and cost.

Two identical frames were built (photograph in Figure 3.12), and feet were

stamped out of $0.375in$ thick 316 stainless steel plate.

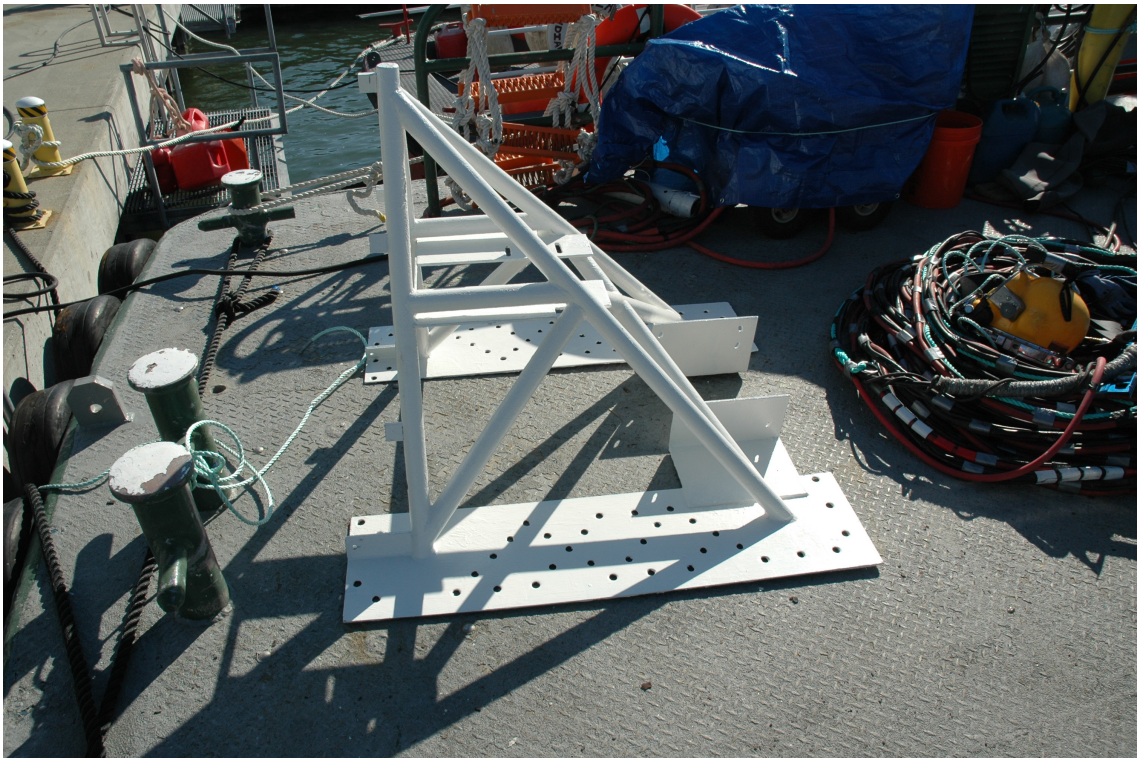

Figure 3.12: One of the two identical underwater frames, sitting on the deck of the dive boat ready for installation.

The final foot design used two parallel skis welded to the frame that would be bolted onto the pier using Hilti concrete anchors. The anchor holes were spaced and aligned such that adjacent holes met the minimum distance required by the anchor specifications, while avoiding the reinforcing steel under the concrete skin of the pier. Refer to Figure 3.13 for the hole pattern on the foot plates.

The pattern reflects the need for avoidance of two separate rebar patterns, as Pier 2 and Pier 3 contained different gages and alignment of rebar in the respective areas of instrument frame installation. Again adding a comfortable factor of safety, the designers required the dive contractor to use 24 concrete anchors per frame, ensuring that the frames would remain in place for the remainder of the life of the bridge. The frame feet were designed sufficiently well that a last minute change in

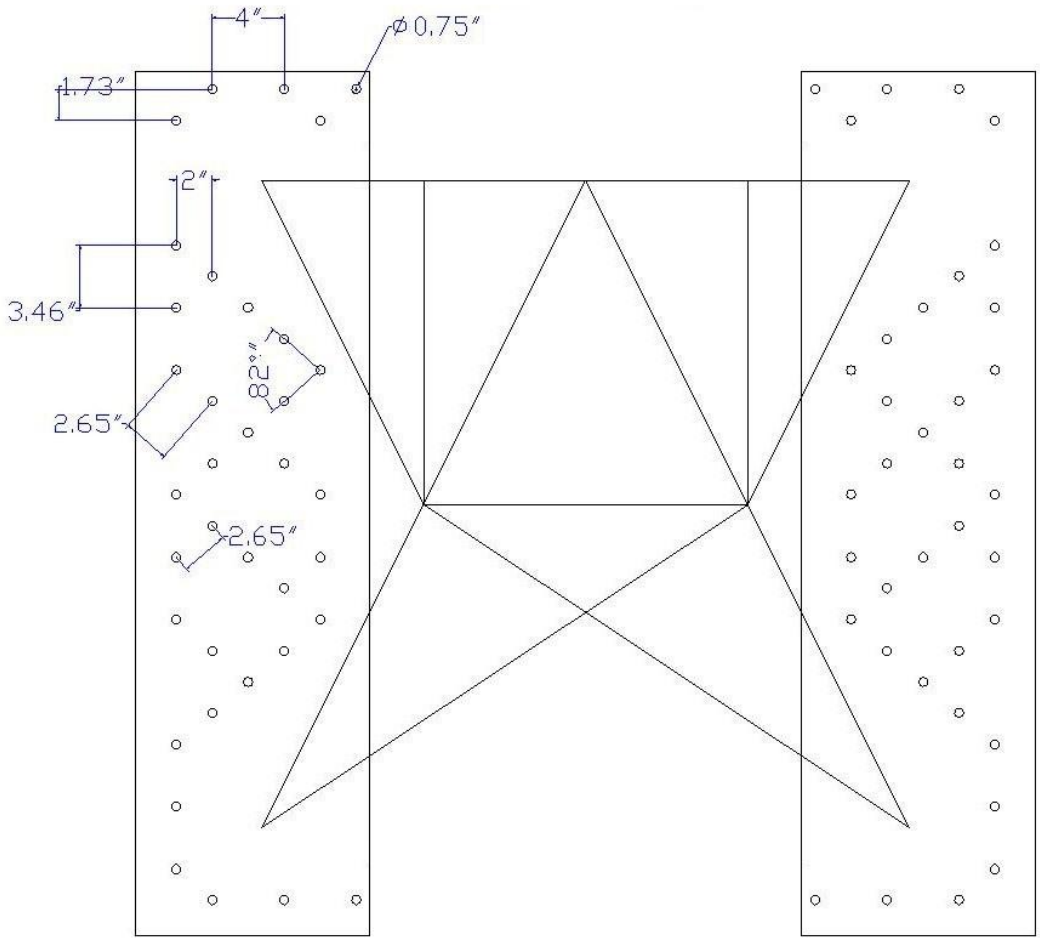

Figure 3.13: Technical drawing of the hole layout stamped into the stainless steel feet. The orientation of the frame members also appears in this drawing.

the size of the anchor used, from $0.5in$ to $0.625in$, provided no need for foot design change, though given the increased capacity of the larger anchors only 20 were used per frame.

A stainless steel mesh lid sits atop the frame to protect the instruments from the barrage of fishing weights and other potentially damaging debris. Above the water, a galvanized steel fender was welded to each pier's steel skirt to prevent drifting boats from colliding with the submarine frame. The fender was designed as

a sacrificial element

3.2.5 Instrument Location

Due to foul weather during the final week of the installation phase, the contracted divers ran short on underwater time and so the exact locations of the instruments could not be surveyed directly. Instead of using the underwater man to position the survey prism, another member of the dive team positioned the prism atop the nose of the above-water fender so the survey team could record its position. Subsequent measurements of the distances between the fender nose and the pier, and the fender to the top of the instrument frame provided enough information to calculate the positions of the instruments.

Figure 3.14 shows a schematic of distances measured in meters between various points on the fender and frame. Since we need to know the vertical position of the instruments relative to a standard datum, all of the relative measurements need to be referred to the location of a known point. The divers measured the top of the instrument frame at 0.2m below the bottom of the steel skirt, which was known to be 1.53m below MLW in 1965. To correct a measurement made relative to MLW in 1965, add 0.57m to refer the measurement to NAVD88. Since the sonar dome is approximately 0.73m below the top of the frame, and the top of the frame is 0.2m below the bottom of the steel skirt, then the sonar instrument is considered 3.03m below NAVD88.

The horizontal positions of the sonar domes can be calculated relative to the measured horizontal position of the nose of the fender. Since each sonar is mounted on an identical frame, and at the same vertical position, the calculation will be shown only once, even though the offsets are different in direction for the north and south piers. Figure 3.15 shows a schematic of the relative locations of the sonar dome and the fender nose, with dimensions given as distance from the pier face. The distance from the pier face is not directly the offset between the

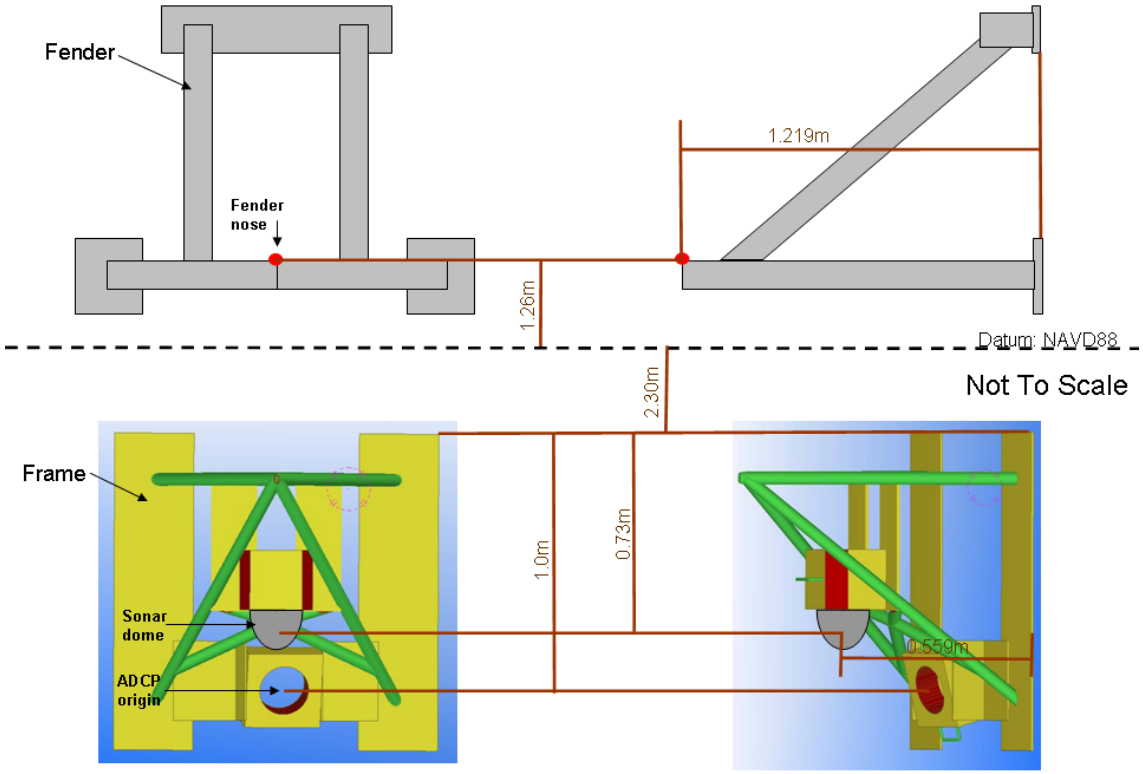

Figure 3.14: Schematic of relationships between the fender, pier, waterline, steel skirt bottom, frame, and instrument

two points however, because the pier face is not vertical. The position of the nose of the north pier fender (the red dot in Figure 3.15) is 230792.133 meters easting and 67599.650 meters northing in Delaware State Plane coordinates. The divers measured this point as 1.219m perpendicular from the pier face, and from drawings the sonar dome is 0.559m perpendicular from the pier face. These measurements are applicable to both the north and south setups. The normal line to the north pier face is 40° below due east, and the normal line to the south pier face is 50° above due east — due to the shape of the piers and the attitude of the axes of the piers. Adjusting the perpendicular offsets according to these angles, the north pier easting and northing measured at the nose of the fender should be

$$E_{dome} = E_{fender} - 0.506m - 0.07m_{pier\ slope} \tag{3.2}$$

and

$$N_{dome} = N_{fender} + .424m + 0.06m_{pier\ slope} \tag{3.3}$$

yielding

$$E_{dome\ North} = 230791.557m \tag{3.4}$$

and

$$N_{dome\ North} = 67600.134m \tag{3.5}$$

in DE state plane coordinates. Accordingly, for the south pier

$$E_{dome\ South} = 230798.839m \tag{3.6}$$

and

$$N_{dome\ South} = 67525.628m. \tag{3.7}$$

The vertical positions of the two ADCP's can be approximated using similar relative measurements. The center of each ADCP sits 1m below the top of the frame, and thus 3.33m below the NAVD88 datum. The origin of each ADCP can

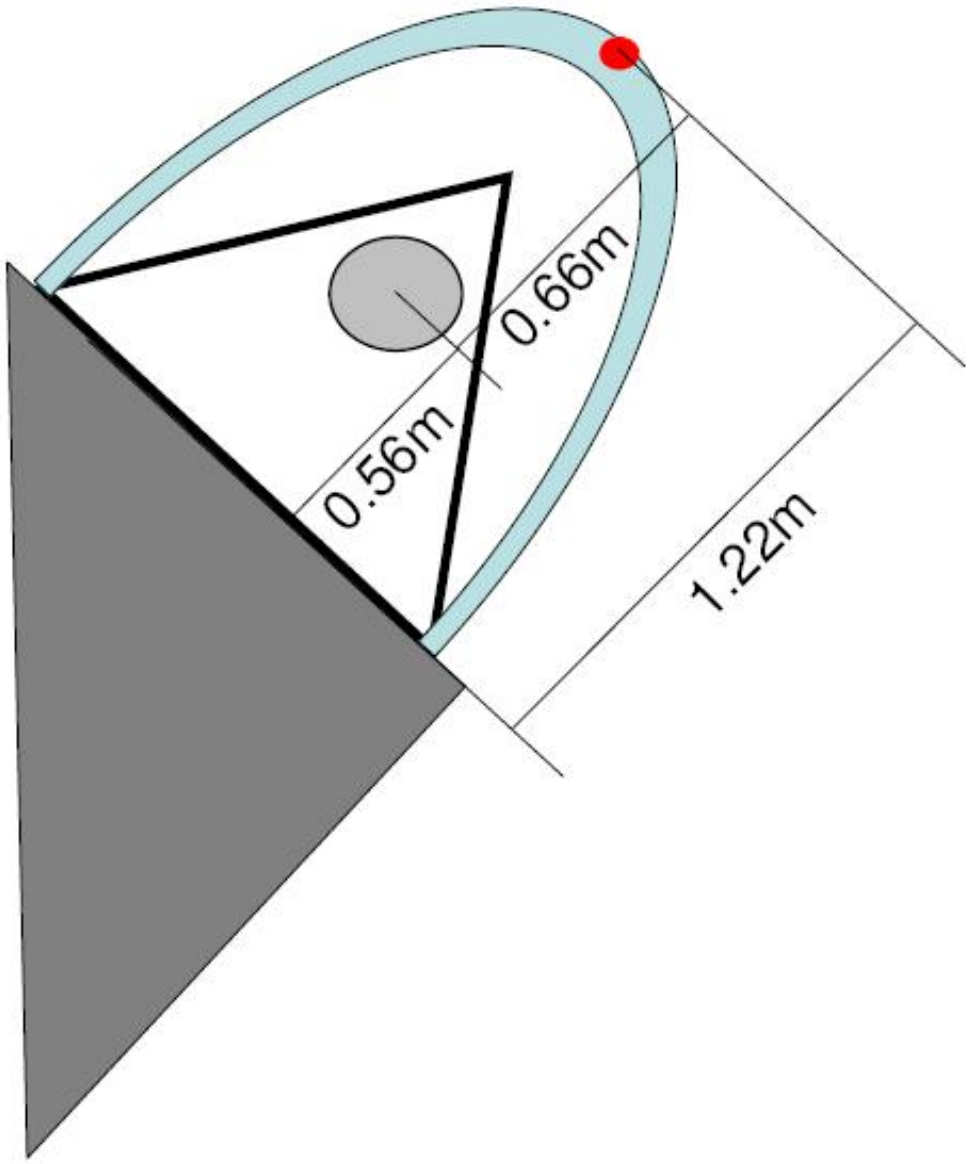

Figure 3.15: Plan view of the locations of the fender nose (red dot) and the sonar dome, relative to the pier face

be computed in the same manner as the sonar dome locations above. The origin of each ADCP is considered a point on the pier face at the elevation of the instrument. This approximation is valid because the instrument is located very close to the pier face and because the individual beams do not originate at exactly the same location. Again recalling that the slope of the pier face adds an adjustment term, the north pier ADCP horizontal location is found by

$$E_{ADCP} = E_{fender} - 0.934m + 0.07m_{pier\ slope} \tag{3.8}$$

and

$$N_{ADCP} = N_{fender} + 0.784m - 0.06m_{pier\ slope}. \tag{3.9}$$

Then the horizontal location of the north pier ADCP origin is

$$E_{ADCP\ North} = 230791.269m \tag{3.10}$$

and

$$N_{ADCP\ North} = 67600.374m \tag{3.11}$$

and the horizontal location of the south pier ADCP origin is

$$E_{ADCP\ South} = 230798.599m \tag{3.12}$$

and

$$N_{ADCP\ South} = 67525.34m \tag{3.13}$$

in DE state plane coordinates.

In addition to locating the instrument, the orientation of each of the 3 beams of the ADCP needs to be considered. ADCP data are gathered in beam coordinates, meaning data from one beam contains only velocities towards or away from the sensor along that beam axis and not in a standard orthogonal coordinate system. In beam coordinates, positive velocities are away from the sensor and negative velocities are toward the sensor.

The orientation of respective beams is best illustrated by giving their endpoints, which can be found in Table 3.3.

Table 3.3: Endpoints of individual ADCP beams originating from either the north or south pier, as noted. Projection is DE state plane, meters; vertical reference is NAVD88. Note that Beam 1 on both piers ends below the channel bed.

	Easting	Northing	Depth
North Pier			
Beam 1	230857.6	67562.1	-67.6
Beam 2	230852.8	67521.6	-6.8
Beam 3	230890.2	67586.5	-6.8
South Pier			
Beam 1	230857.3	67574.6	-67.6
Beam 2	230893.6	67556.2	-6.8
Beam 3	230845.5	67613.6	-6.8

The following two figures illustrate the beam orientations in relation to the bathymetry, two figures are used to give depth perspective that is not apparent in one figure alone.

3.3 Collection Scheme

The sampling pattern of all of the instruments of the BBSMS is choreographed and automated. A computer program called *Advanced Task Scheduler* (ATS) controls the operations of opening instrument software and running surveys. The 12-hour cycle described in Table 3.4 is repeated twice per day, though each computer is restarted only once per day at midnight GMT. No two underwater instruments may operate simultaneously due to possible sonic interference. Sonar scans take the most time to perform, so a 4.5 hour time slot is allotted for each complete sonar survey.

Advanced Task Scheduler software is not associated with Microsoft Windows Task Scheduler, though it can perform the same tasks it also gives the ability to send specific keystrokes and sequences of commands. This power is necessary for BBSMS

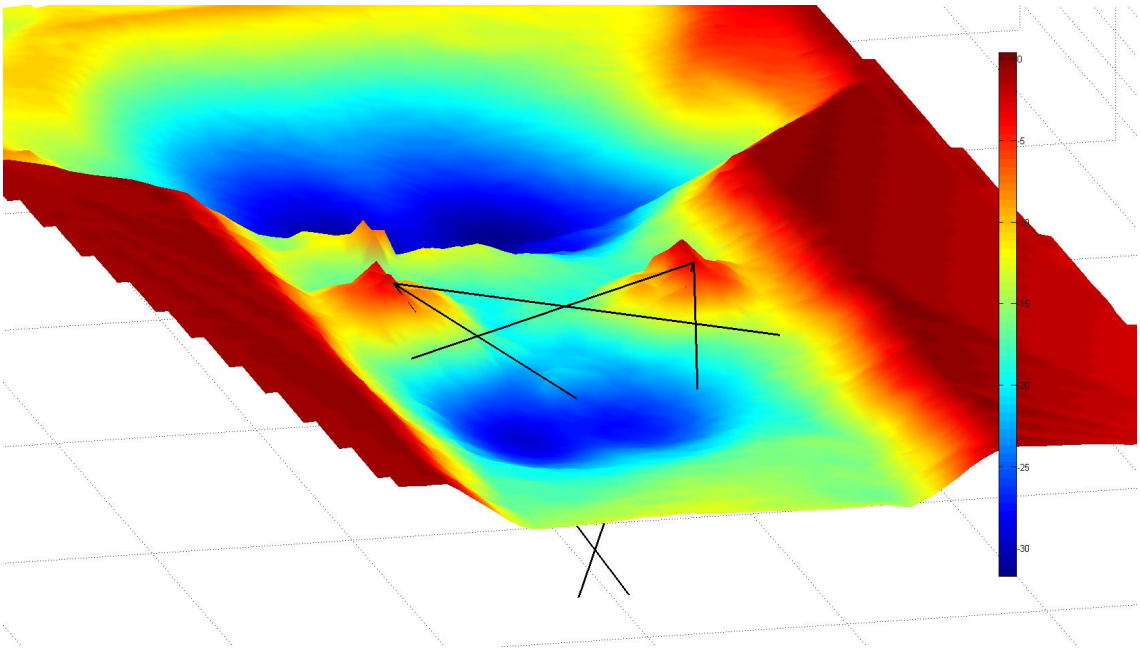

Figure 3.16: Oblique angle view of ADCP beams generated from instruments on both piers. Beams are numbered such that 1 is down, 2 is the next clockwise beam, and 3 is next clockwise from 2.

operation since the individual instrument software is not designed to be run on a recurring schedule. Support for the ATS software is limited, and some commands have periodically disappeared from one of the BBSMS computers resulting in inferior system operation. Text files containing the proper sequence and content of all commands are saved on each respective computer in the Traffic Box.

3.4 Data Link

The Traffic Box under the bridge is linked via a radio modem with the DelDOT field office which gives network access to the computers and instruments in the BBSMS; the radio modem was installed March 14, 2008 by DelDOT IT personnel. The radio signal is frequently blocked by cranes and other apparatus involved in the construction of the new bridge, and thus a reliable connection remains elusive. While the data link operates, data are transferred twice per day by the underwater

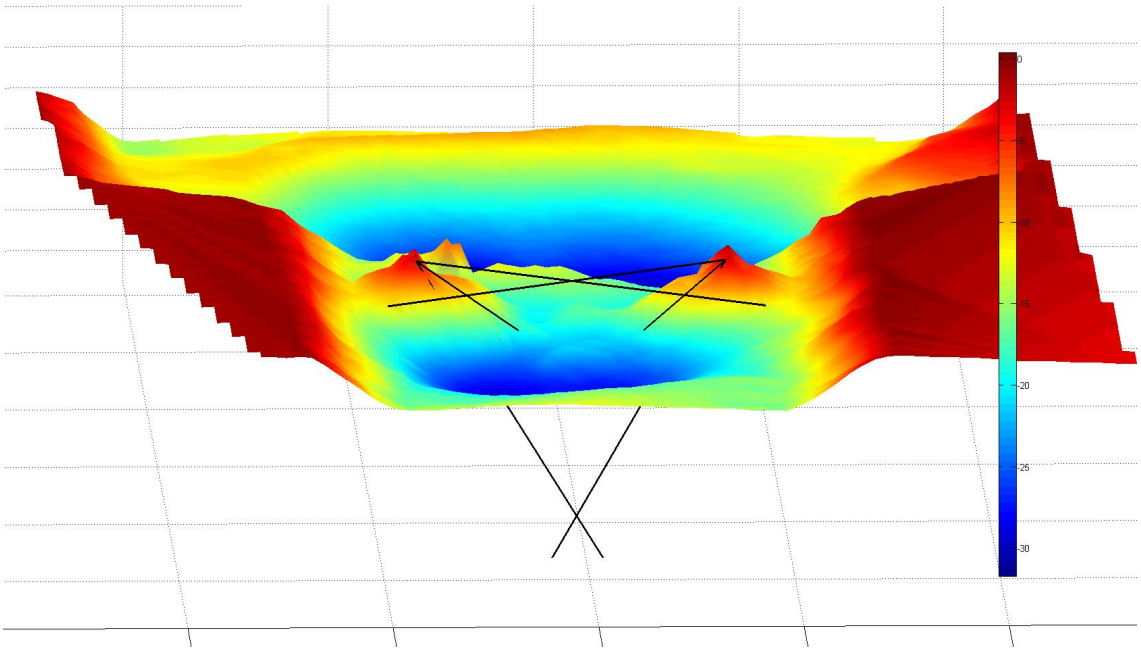

Figure 3.17: Along channel view of ADCP beams, looking west from the ocean. Note that beam 1 goes below the bed very quickly on both the north and south piers.

Table 3.4: The 12 hour automated BBSMS collection schedule, repeated twice per day. Times are GMT. *tilt data are collected and transfered hourly, see Section 3.2.3.

Time	North Pier		South Pier	
00:00	CPU Reboot	tilt*	CPU Reboot	tilt*
00:04	Collect 10min ADCP	tilt*		tilt*
00:15		tilt*	Collect 10min ADCP	tilt*
00:30	Collect 1 sonar scan	tilt*		tilt*
5:00	Collect 10min ADCP	tilt*		tilt*
5:15		tilt*	Collect 10min ADCP	tilt*
5:30		tilt*	Collect 1 sonar scan	tilt*
10:04	Collect 10min ADCP	tilt*		tilt*
10:15		tilt*	Collect 10min ADCP	tilt*
11:00	FTP data to University	tilt*	FTP data to University	tilt*
12:00	Repeat Cycle		Repeat Cycle	

equipment and once per hour by the tilt system datalogger.

This link also allows communication from remote locations. Through the

State of Delaware's secure network the laptop computer can be accessed directly, and the other two computers can be accessed through the laptop. Windows' *Remote Desktop Connection* program, found under *Start – Programs – Accessories – Remote Desktop Connection*, is used to log on to the field laptop. The program *Virtual Network Connection* or *VNC* is then used to control the individual north and south computers via the laptop.

While radio communication is viable, remote access allows troubleshooting both of the instruments and of the automated control program that dictates scan times and data transfer. Remote troubleshooting is valuable because it saves the time and money that is needed for the 200 mile round trip between the University and the field site.

3.5 BBSMS Installation

The Bridge and Bathymetry Scour Monitoring System was installed in two phases over the course of about one and a half years. Phase I began in August 2007 and included the installation of the tilt sensors, associated cables, the Traffic Box, and cable tray and conduit. Phase II began in earnest in October 2008 and included the installation of the underwater sonar and ADCP components, along with their support components.

Phase I was executed by CACR and the DelDOT bridge inspection team, using the DelDOT Under Bridge Inspection Vehicle (UBIV) on two dates in the summer of 2007. Significant preparation work allowed the installation of the tilt sensors, custom cable tray, and power/data cables to be completed in a timely fashion. The method of securing the tilt sensors is described in Section 3.2.3. The cable tray was made by CACR by ripping $6in$ diameter thin-walled PVC in half, then sanding and covering the edges to prevent damage to cables. In the field, these 10 foot sections were installed atop existing conduit under the west side bridge deck (the angle steel on this side appeared more robust), between the east and west spans

of the bridge. Sections were overlapped such that dragging cables from the north would not cause damage, and are held in place with many hundred weather and UV resistant zip ties.

Along with the cable tray, the Traffic Box and incoming cable conduit were installed during Phase I in anticipation of their need during Phase II. The configuration of the Traffic Box is detailed in Appendix B. Twin runs of $3in$ diamter PVC are used as conduit to run the cable from the cable tray under the bridge deck down the vertical face of the pier and into the Traffic Box. This conduit is held to the pier by plastic conduit clamps fastened with concrete anchors and construction adhesive. Each run of conduit contains cables from either the north or south pier's instruments, markings show their designation. Drain holes and a U-trap prevent condensation or runoff from entering the Traffic Box through these conduits.

Figure 3.18: Photograph taken during Phase II that best shows the UBIV, Traffic Box, and vertical white PVC conduit on the face of the nearest pier.

Phase II of installation work involved much more coordination as teams from CACR, DelDOT, and Boswell Underwater Engineering worked during October and November 2008. Boswell managed the underwater operations, with support from CACR. While underwater mounts and above water fenders were being installed by Boswell, the CACR and DelDOT UBIV teams worked to shore up the vertical PVC conduit above the Traffic Box, drag the proper sonar and ADCP cables to staging zones above their designated piers, and install new vertical conduit on the piers being instrumented. Figure 3.19 shows a composite of photographs taken after the installation of the components on the south pier.

The gray conduit visible in Figure 3.19 is an open channel with a locking lid, zip ties were used to secure the lid after installation, but access to the cables should be easy in the event repairs to the system are needed. Similarly, the stainless channel conduit that guides the cables from the top of the steel pier skirt to the underwater instrument mount also employ a removable lid to allow access.

It is worth repeating here that short runs of both sonar and ADCP cables run from the instruments to the staging zone in the cable tray above or nearly above each instrumented pier. Excess from these short runs is coiled and chained to the angle steel that holds the cable tray. If, for some reason, the instruments need to be removed from the mount, this excess cable should be uncoiled first to provide the needed slack so that the instruments can be brought to the surface *before* any connectors are removed. The connectors are not wet-mateable and should not be exposed to salt water for any reason.

The sacrificial fender is visible in Figure 3.19, as well as a cautionary sign—both intended to prevent boaters from approaching the pier where the sensitive and valuable equipment resides out of sight below the surface.

Figure 3.19: Composite of photographs taken from the UBIV of the fender and conduits ready to receive cables.

Chapter 4

DATA

This section presents raw data, processing methods, processed data, and discussion of notable features for each type of data used in the Indian River Inlet BBSMS.

4.1 Sonar Data

The raw sonar data collected by the system is processed at the University with a program that filters false returns and merges data from the north and south sonar by interpolating to fill in a grid covering the area of interest. Examples of the quality of returns of the raw data from each sonar can be found in Figures 4.1 and 4.2; they reveal that the channel bed in the area of interest is sufficiently observed by at least one sonar unit and that false returns must be filtered for accurate bathymetry output. Each sonar appears adept at returning reliable signals from the opposite side of the inlet, while errors plague nearby returns. A scale controlled interpolation technique [30] was used in favor of a linear interpolation to accommodate the changing spatial scale present in the raw data. Since the sonar collects points in concentric circles, adjacent points become farther apart with distance away from the sonar. The interpolation code considers this phenomenon as well as the growing "cone size" of the sonic pulse as the distance from the sensor increases, see Figure 4.3 for a plot showing how the lx term varies with distance away from each sonar.

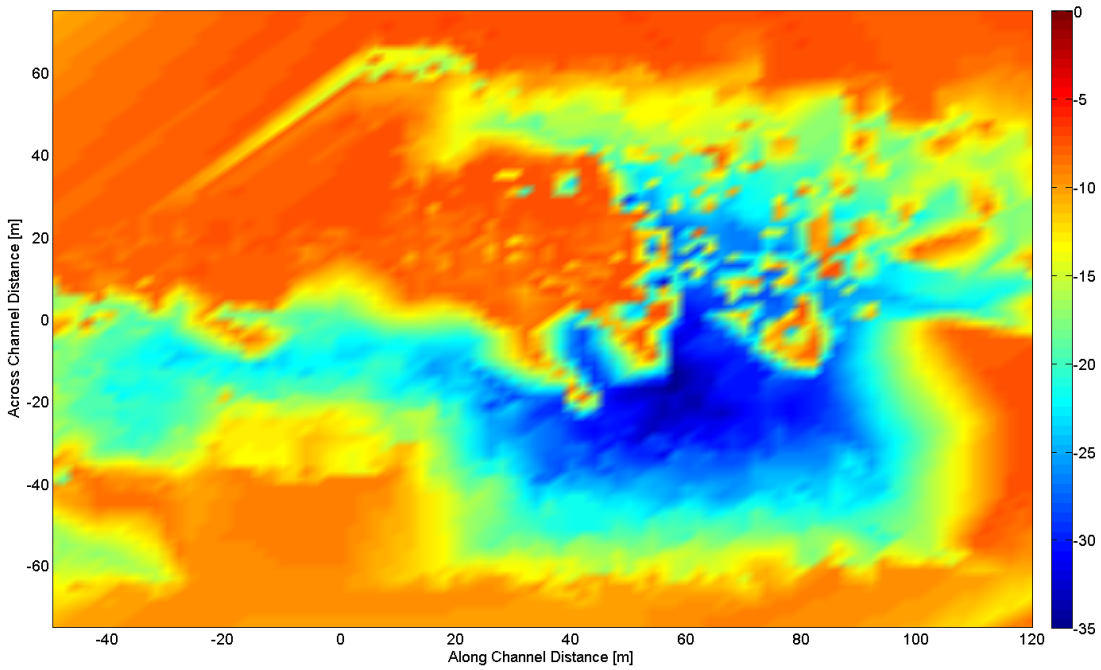

Figure 4.1: A surface representation of the raw returns from one scan of the north pier sonar. Filtered only for data density.

The lx term can be thought of as an allowance value that caps the distance inside which observations surrounding an output point influence that point. Assigning different lx terms for each output grid point allows a smooth looking surface to be generated even though the distribution of observations changes, as seen in Figure 4.4.

Since the bathymetry is collected from two remote points, with significant overlapping data points of varying accuracy, processing is considerably complicated. Measurement error can be estimated by assuming that accuracy degrades with distance from the transducer. During the merging process, each raw data point is weighted with the inverse of its resultant vector so that the system favors data that are collected from the nearer sonar. The problem with this approach is that while it allows the interpolator to choose more accurate data near the instruments, it has the opposite effect on data far from the instrument — where false spikes may have

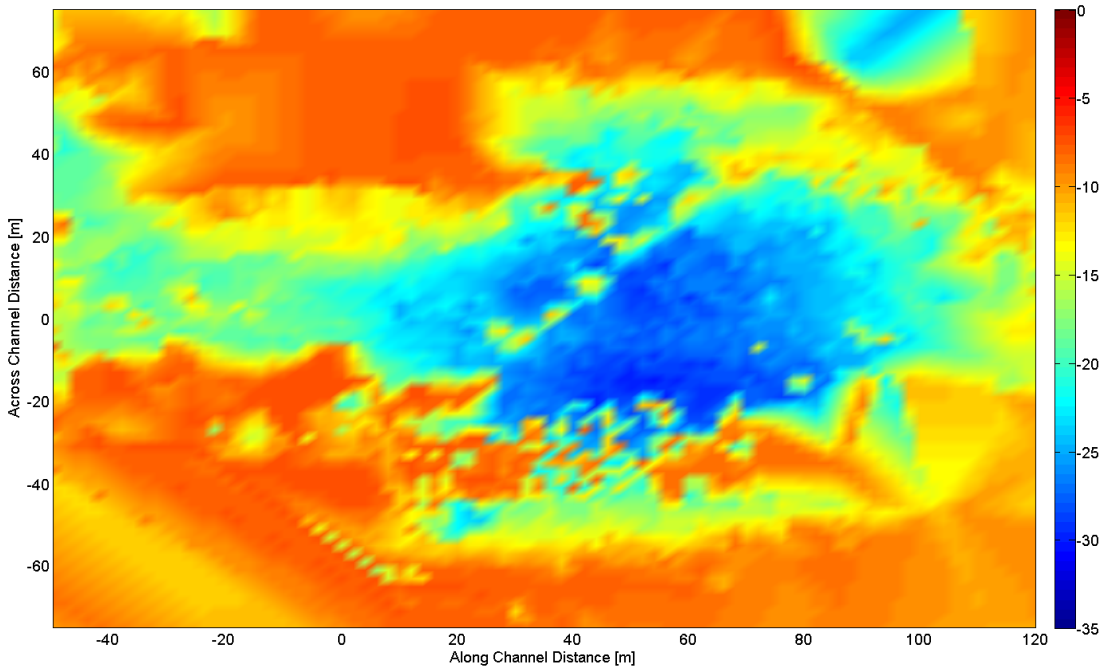

Figure 4.2: A surface representation of the raw returns from one scan of the south pier sonar. Filtered only for data density.

shorter resultants than real returns from the bottom of the scour hole. However, the pass requirements of the filter window are such that singular anomalous points do not influence the output. Since the data points are distributed randomly in space, as illustrated in Figure 4.4, a square output grid can be used without enhancing interpolation errors normally associated with forcing polar data on to a rectangular grid.

The goal of the sonar monitors is not to observe transient bedforms, but rather to observe the general elevation of the bed at each collection time. By removing the limit on bedform frequency, the interpolation length scale can be exploited to minimize error and to create a full, expressive bathymetry map as a final product. In locations where there is sparse distribution of observations, the code allows the interpolation length scale to double until the sampling error falls below a specified

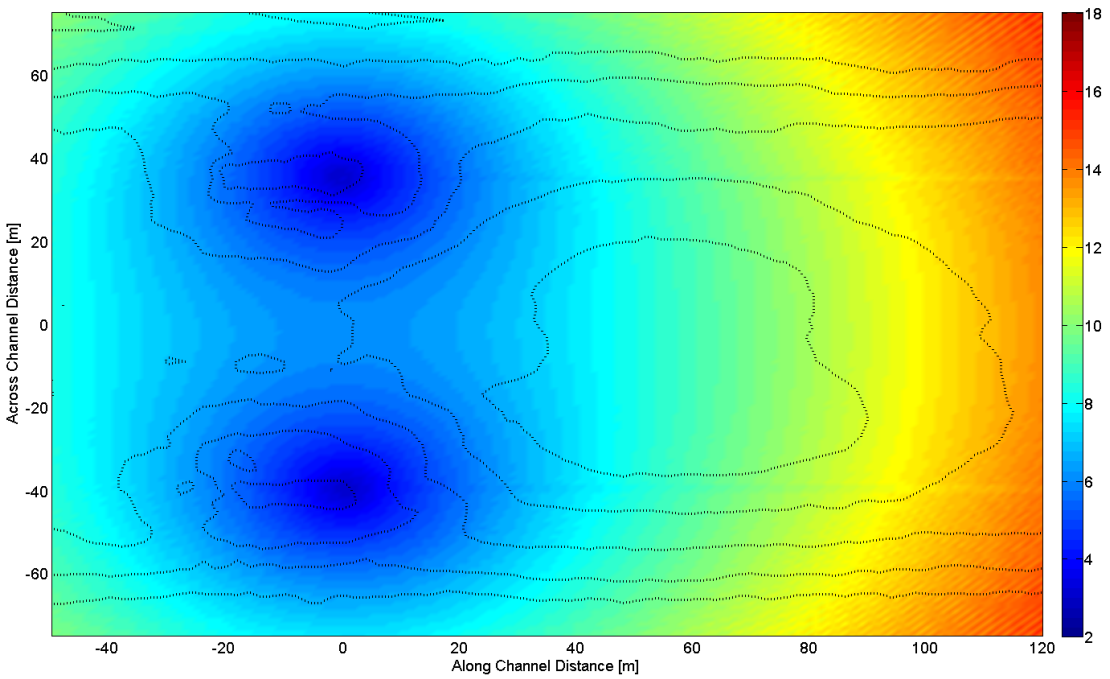

Figure 4.3: The combined interpolation length scale, which varies with distance from both sonars. Bathymetry contours included for reference.

threshold. Additionally, the 2m by 2m square output grid provides the best output resolution versus interpolation error reduction. This optimization considered all of the residuals as symptoms of measurement error and thus sought to reduce the interpolation error [30].

Comparisons between the BBSMS output and an accepted US Army Corps multibeam data set from 2007 are shown in Figures 4.5 and 4.6. Note the accuracy of the BBSMS sonar in Figure 4.5, those areas that appear blank did not contain enough observations to produce reliable output. Figure 4.6 compares contours of the same elevations between the two data sets. The two ellipses highlight areas that contain anomalous features in the BBSMS data, the bumps in the more recent contour lines suggest slumping of material from above that has settled downslope.

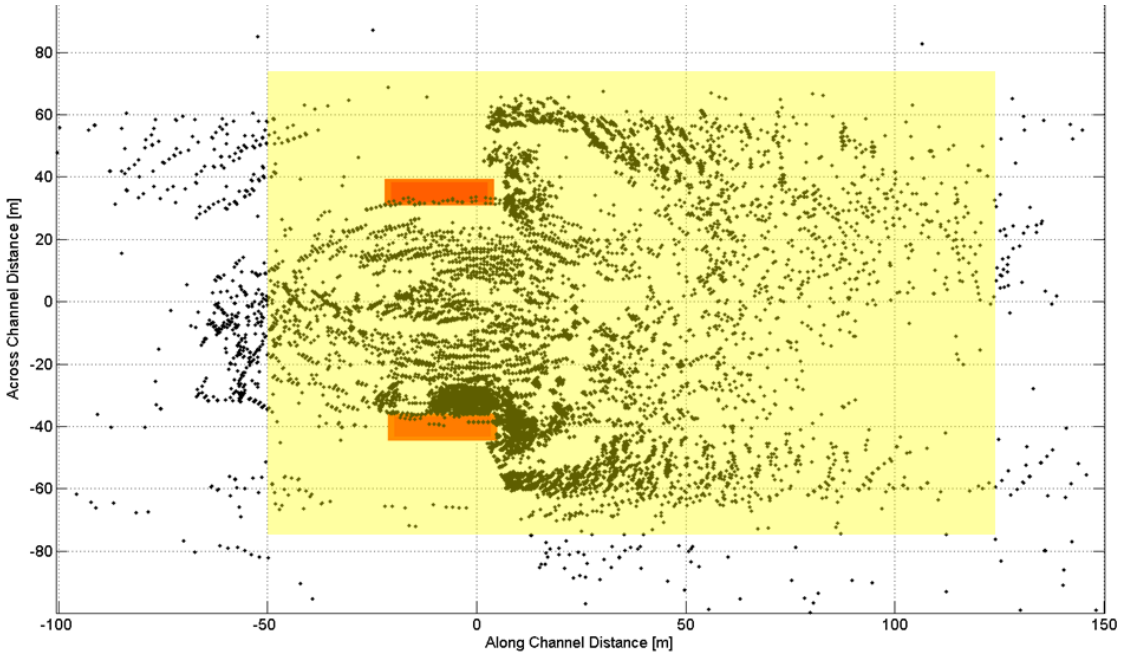

Figure 4.4: The distribution of combined observations from the north and south sonar, pier footings have been included for spatial reference. This represents typical coverage of a combined scan. The interpolation grid area is highlighted.

The bathymetry output is the most interesting, and approachable, to DelDOT engineers, and so considerable effort was spent developing a meaningful presentation method. Google Earth software allows users to display data in geographic space, allowing easy visualization of the Indian River Inlet scour holes and their proximity to the bridge. The automatic processing code creates pictures of the most recent bathymetry, and of any recent changes in bathymetry, that DelDOT officials can view using Google Earth—samples of these Google Earth overlays are shown in Figures 4.7 and 4.8. This code can readily be updated in the future to accommodate additional output maps, should the need arise.

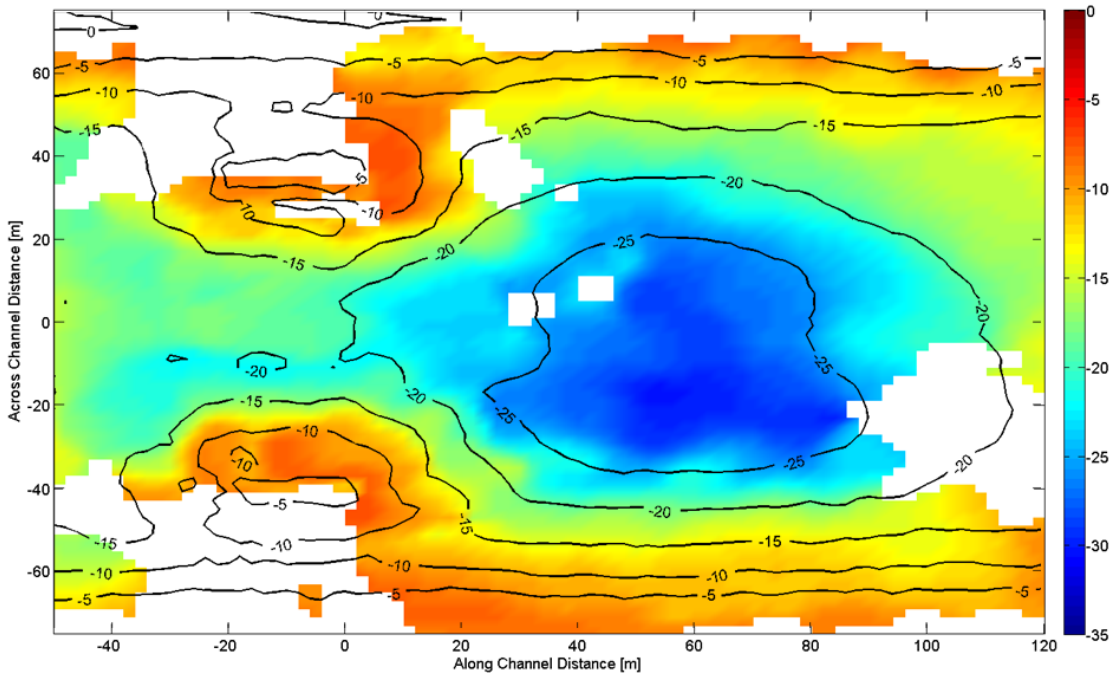

Figure 4.5: Final result of merging, filtering, and interpolating BBSMS sonar data (colorbar is meters of depth). US Army Corps bathymetry data in contour for comparison.

4.2 ADCP Data

Analysis of pilot current profile data suggests the presence of coherent eddies propagating in the direction of mean flow. The Fast Fourier Transform (FFT) of a 1.5hour data set reveals the presence of a significant fraction of energy at a frequency of about 1/25Hz in most of the bins. Mean flow along the channel during this data set was 0.9m/s, suggesting that some of the eddies could be as large as 22.5m. Similar macro-turbulence was observed during an August 2007 survey using a boat mounted ADCP, though the spatial scale was not so large, evidence suggests that these flow structures are real and occur regularly under normal tidal conditions.

A subset of typical velocity data from the pilot study was selected for in depth analysis. Visual inspection of the raw data plots show trends which appear to be the advection of cohesive flow structures. In time series of individual bins, they

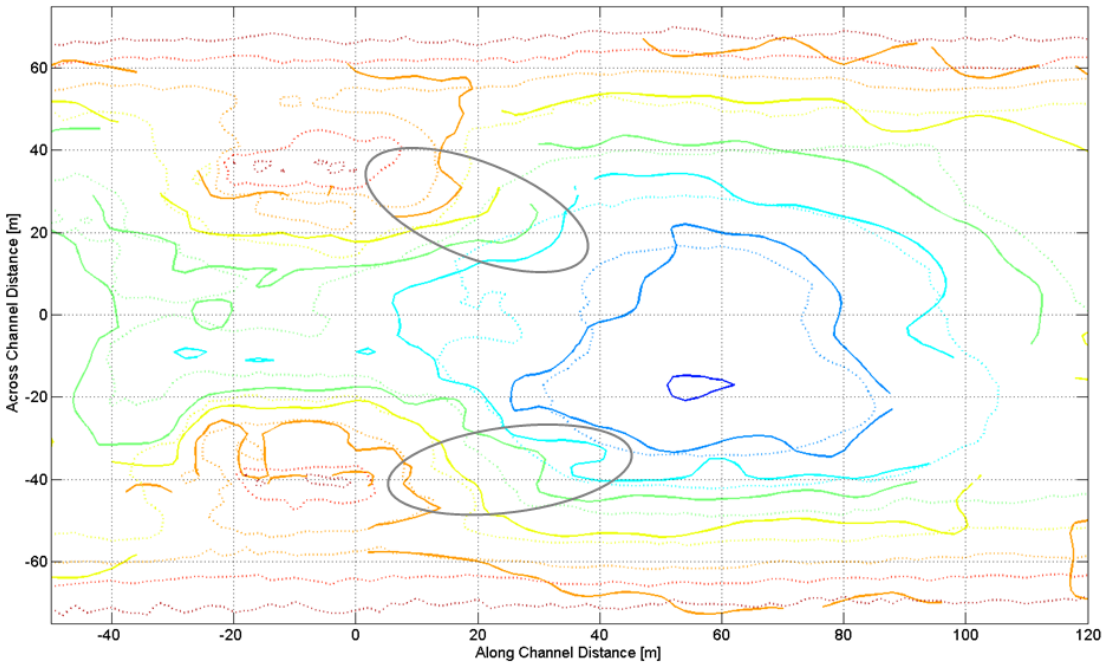

Figure 4.6: Comparison of similar contours from USACE 2007 data and BBSMS November 2008 data. Two circled areas highlight zones where slumping may have occurred.

appear as periodic oscillations above and below the mean stream flow which can be seen in Figure 4.9. In plots of time versus distance (see Figure 2.12), distinct striations follow a consistent slope of about 0.8m/s, which compares well with the mean stream velocity during the data subset of 0.84m/s.

The data in this $1000s$ subset does not possess the dominant $25s$ signal that is exhibited in the data when it is considered as a whole. Rather there are two spikes in energy at $100s$ and $160s$ approximately equal in amplitude. This suggests that at $70m$ along the beam, the eddies initially shed by the bathymetric rise have significantly expanded in size. This pattern of turbulence transferring to lower frequencies is visible in the time series in Figure 4.10.

If positive velocity values are assumed to represent right-hand spinning eddies, and negative velocity values represent left-hand spinning eddies when the mean

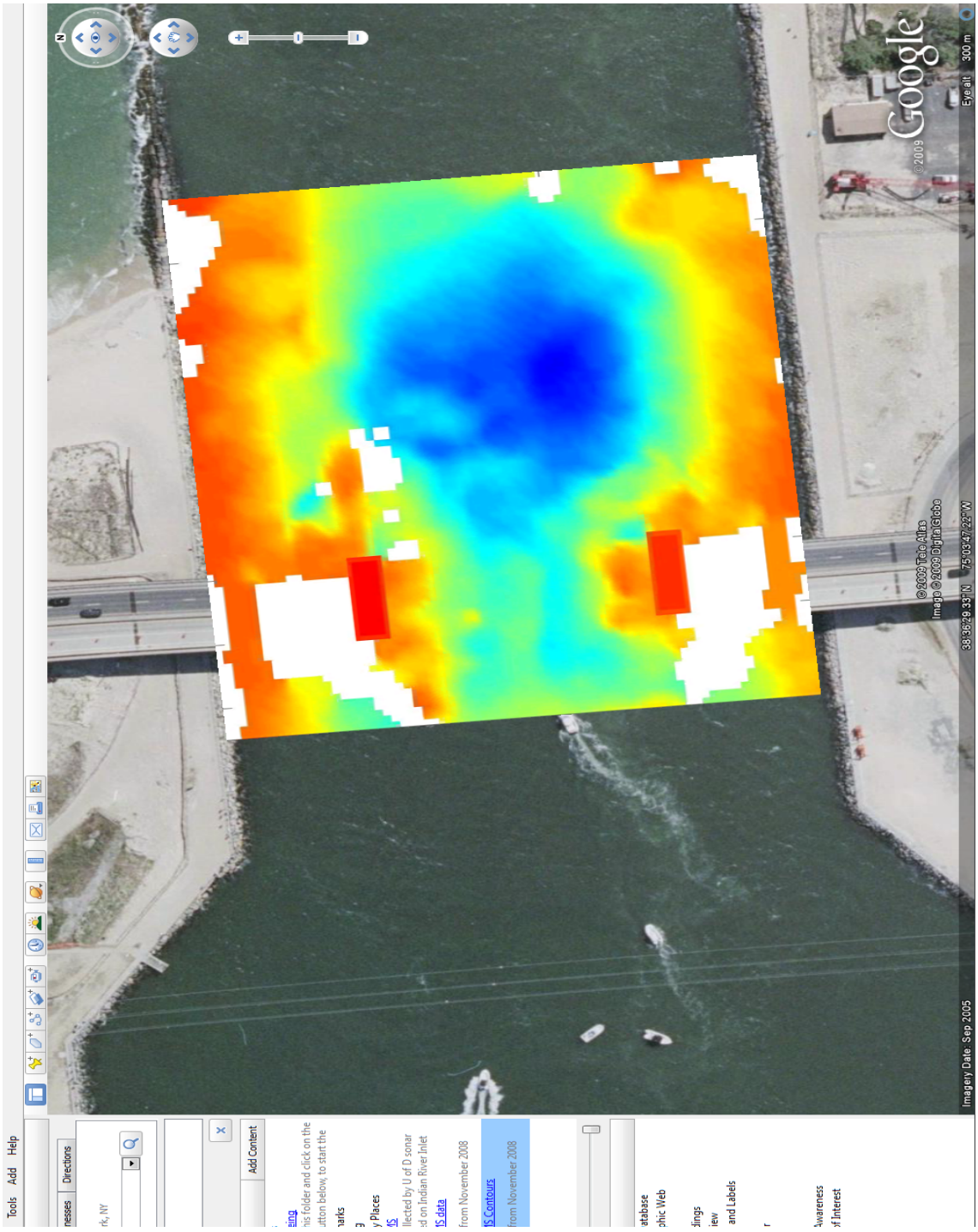

Figure 4.7: A screenshot of BBSMS data represented as a surface geo-referenced in Google Earth.

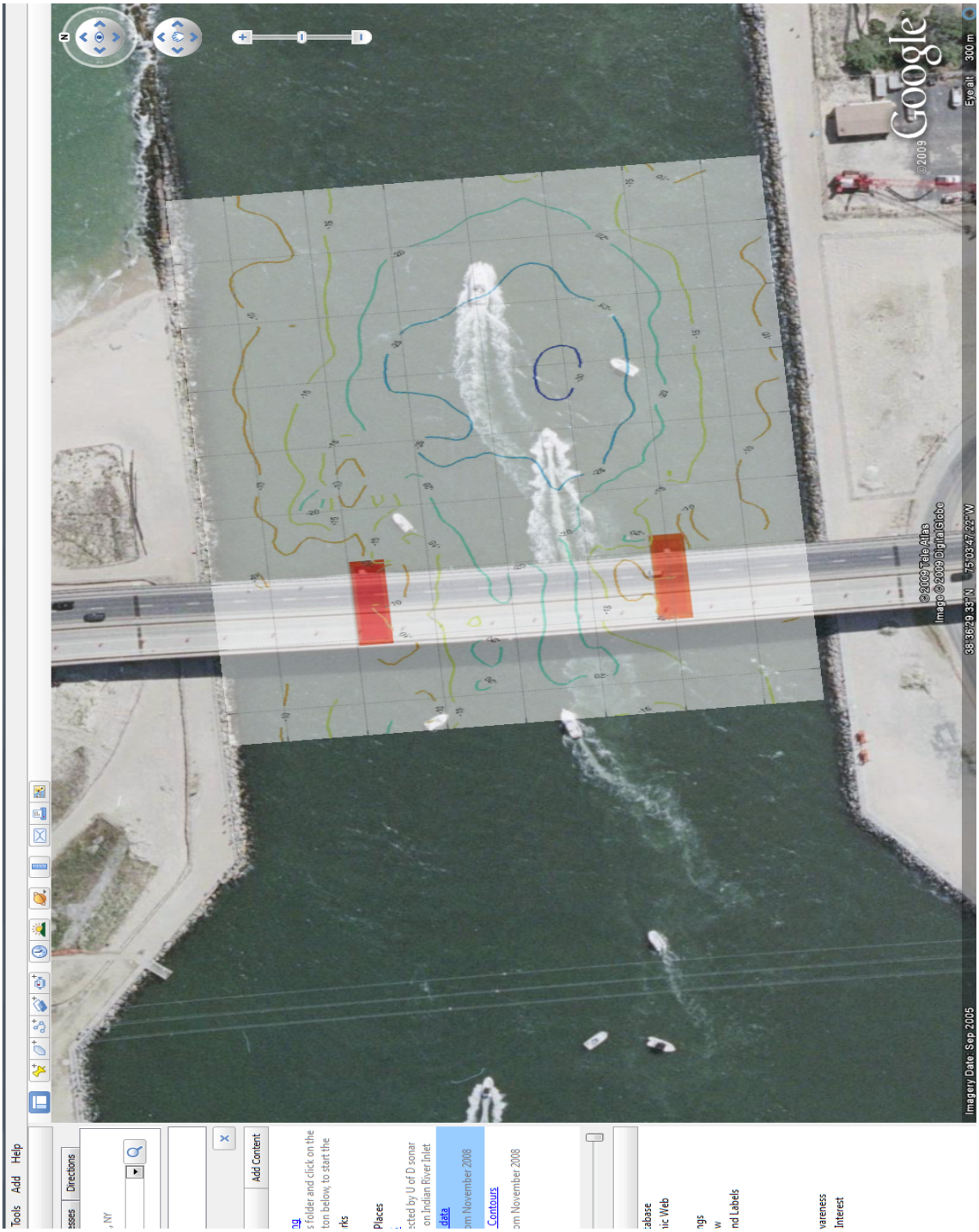

Figure 4.8: A screenshot of BBSMS contours geo-referenced in Google Earth.

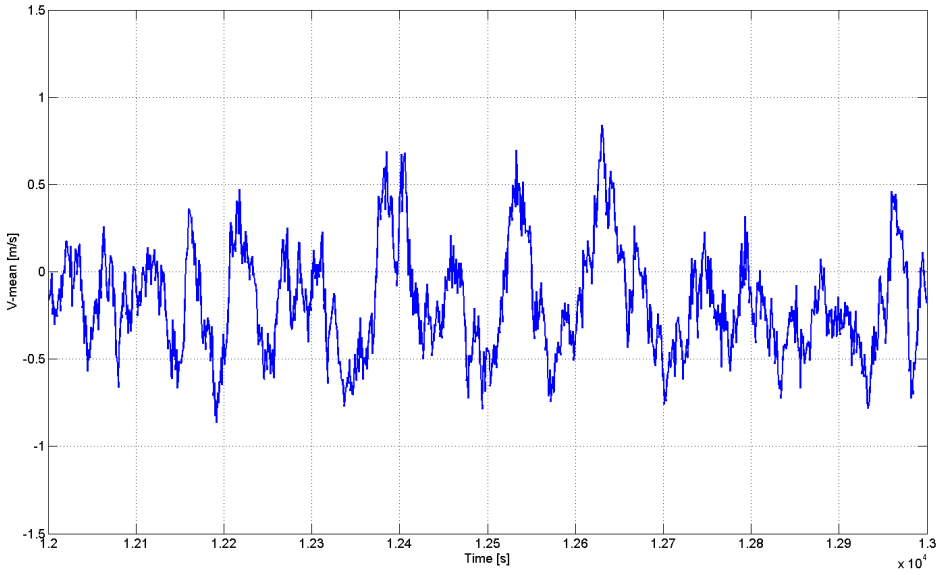

Figure 4.9: Time series of velocity data, with mean removed, in the 70m bin from beam 3.

is removed, then the duration for which the velocity is positive can be used to approximate the size of a right-hand eddy. Figure 4.11 shows a schematic of how positive and negative velocity values can be used to approximate the size of eddies. Since the mean stream flow is approximately along the beam, the eddies are carried along in the direction of flow, while their interaction with the stream flow causes them to expand in volume.

Since the initial focus was on the $70m$ bin during the $12000s$ to $13000s$ time segment, and the mean stream flow was $0.84m/s$, then the same features should first encounter the $30m$ bin about $36s$ sooner. The same routine of FFT analysis of the $30m$ bin time series reveals a concentration of energy in the range from $80s$ to $100s$—further evidence that the eddies grow in size as they are advected downstream.

Noting that the dominant energy changes in favor of a longer period while the magnitude of the signal between the $30m$ and $70m$ bins decreases, it is likely this is due to energy being conserved within the eddy. Keep in mind that this

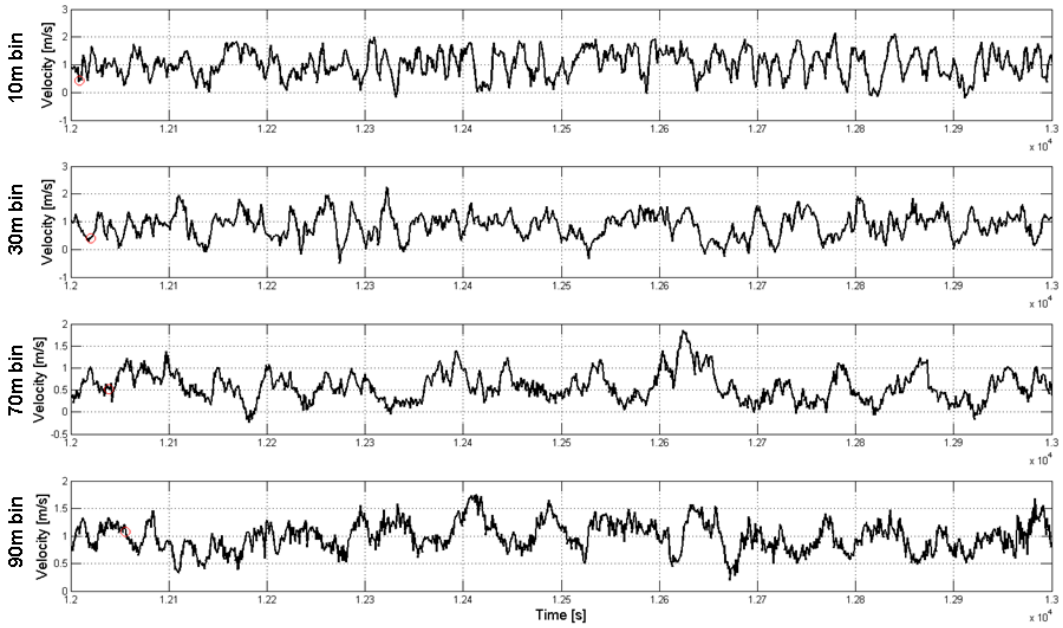

Figure 4.10: Comparable time series of velocity data at 10m, 30m, 70m, and 90m bins. Red circles follow the same 'plug' of water through time at the mean velocity.

rough analysis was performed on data that are assumed to be parallel to the mean flow, when in fact there is a difference of a few degrees. Also there are interactions between the fluid and the bathymetry which results in phenomena that affect the results of the above analysis while remaining computationally elusive themselves. One example of such a feature is the vertical flow through the water column; the ADCP cannot measure this flow because it intersects the beam at near a right angle. Refer to Figure 2.12 for visual evidence in the $30m$ to $75m$ range that some external force changes the flow pattern.

During flood tide the currents appear more organized, lacking much of the chaotic turbulence visible in the time stack of the ebb tide (Figure 2.12). While not perfectly smooth, the flood velocities in the time stack seen in Figure 4.14 do not oscillate with as high an amplitude as the velocity profiles observed during

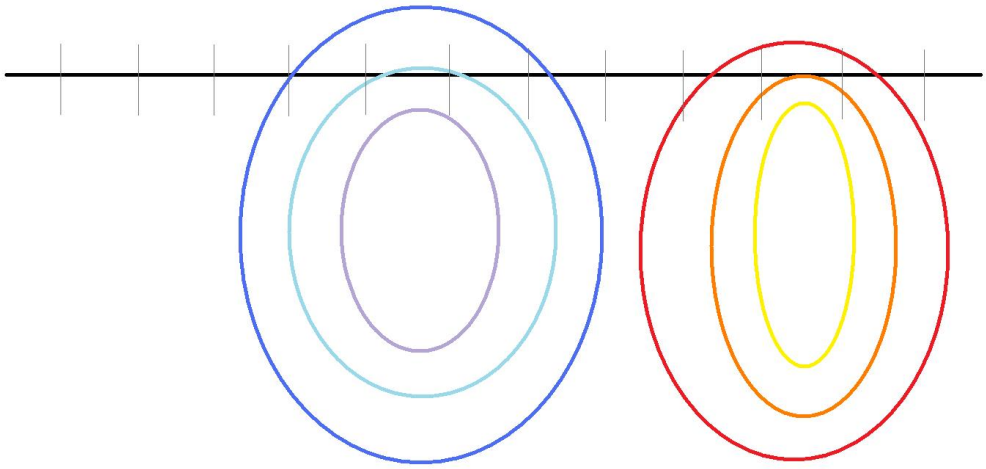

Figure 4.11: Schematic of how beams interact with a velocity profiler beam. The black line represents the beam, broken up into bins, and the red or blue represent right-hand and left-hand eddies respectively.

ebb tide. The mean standard deviation of velocities in each bin over the 1000s ebb data set is $0.35m/s$ with a mean flow of $0.84m/s$; and the mean standard deviation of velocities in each bin during the 1000s flood data set is $0.16m/s$ with a mean flow of $-1.22m/s$. This disparity in flow characteristics justifies the assertion that macroturbulence shed from the bathymetry during ebb tide is unique and significant in the scour process.

Daily processing of the ADCP data will not include the above FFT analysis, rather the system will use multiple short-duration observations to note the mean flow conditions at various times throughout the day. The mean flow data can then be coupled with observed tide data to give reliable characteristic flow conditions for different tidal elevations. Once a sufficient database has been compiled, DelDOT engineers will be able to approximate expected velocity values given the predicted tide. Knowledge of the typical flow characteristics are important for two reasons,

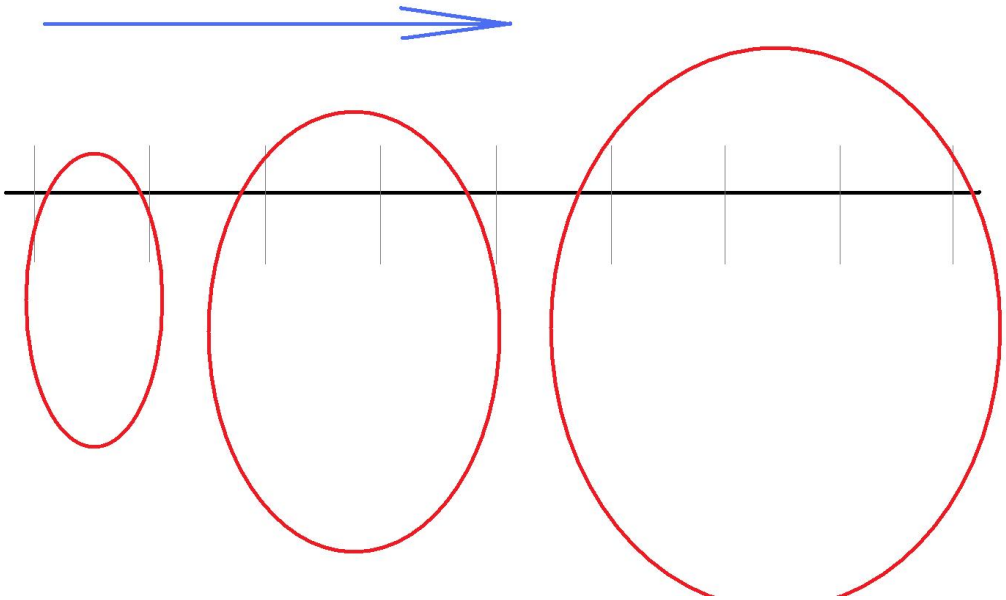

Figure 4.12: Schematic of an eddy growing in volume with advection downstream (along a profiler beam)

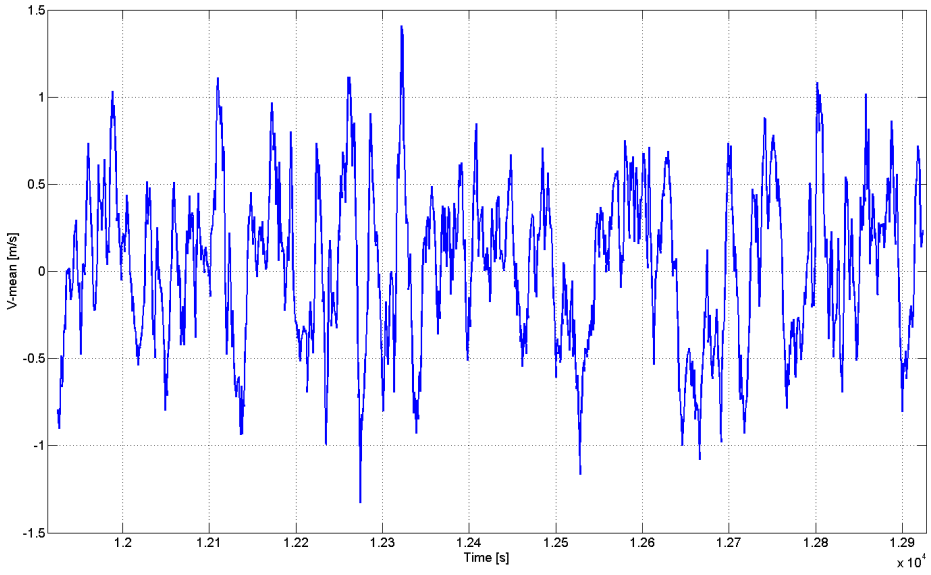

Figure 4.13: The time series of data from the 30m bin appears to oscillate about the mean at a higher frequency than the data from the 70m bin.

first the information can be used to estimate sediment transport, and second it can be used to calculate the fluid forces interacting with the bridge piers.

4.3 Tilt Data

For the first 6 months of deployment, the tilt data were collected with a DataQ brand logger that stored the information on an SD memory card. The data had to be periodically downloaded, which meant long periods where the latest data sat idle in storage, and long drives to the field site to download small packets of data. At the request of DelDOT engineers, the data logger was upgraded so that the latest information could be transferred via the Internet for real time viewing. A Campbell Scientific datalogger with FTP capability replaced the DataQ model.

The Campbell logger collects a data point every 2 seconds, then averages these every minute — thus eliminating much of the noise that was present in the signal collected by the first logger. Once per hour, the Campbell logger sends the data to the University for processing and storage. Though the new logger drastically improved the signal to noise ratio of the tilt observations, the apparent trend of pier tilt prevailed. During Phase II of the installation of the BBSMS, the respective conditions of both tilt sensors were visually and manually observed to be normal, and thus it is believed that the tilt signals returned by these instruments is the result of a physical change.

Under the first data logging scheme, individual points were collected at short intervals and stored directly on the logger card. This method resulted in large deviations of data points around a mean that seemed to be slowly changing with time. These data were filtered in such a way as to preserve the trend while eliminating outliers and variations that were presumably due to noise. Figures 4.15 and 4.16 show the composite results from many datasets downloaded from the DataQ logger in blue and the refined Campbell data sets in black. Note the large deviation in the

blue portion of the signal and the trend in the along channel data from the north pier, which represents tilt toward the west.

Even though the tilt data is collected with the finest temporal resolution of the system, it is best for recording long term trends in bridge attitude. Engineers expect no movement of the piers, though during the first year of deployment BBSMS tilt sensors appear to have measured a gradual shift that equals $\frac{1}{2}$ inch of displacement at the top of the northern pier based on point of fixity calculations (M. Cann and J. McConnell, *pers. comm.*). Armed with this data, DelDOT performed a series of follow-up surveys to conclude that the bridge remains safe for public use. Incoming tilt data provides DelDOT engineers an independent means of monitoring, as pier attitude changes can occur even in the absence of bathymetry changes or anomalous flow conditions.

4.4 Tides

The xTide program for Matlab is used to generate tidal information in the inlet. Nearby tidal stations exist at the Coast Guard station just inside the main channel of Indian River Inlet, and at the Lewes Ferry Terminal. Using the Lewes tide as the ocean and the Coast Guard tide as the bay, the head loss along the inlet can be calculated directly. In his 1967 paper, Keulegan used Atlantic City, NJ tidal data corrected for time as the approximation for ocean tide; comparison of data from the Lewes Ferry Terminal tide station with the time-corrected Atlantic City tide station reveals a mean difference of 1cm (maximum difference is 13cm, standard deviation is 6cm). See Figure 4.17 for an example of how well these two tidal signals agree.

From the time series of head difference between the ocean and the bay, a number of characteristics of the tidal flow can be calculated. For instance, the times of slack tides were of particular interest during the installation of the underwater components, and can be found when the head difference in between the ocean and

the bay is zero. Of course this method is an approximation, and does not account for inertial or frictional forces, rather it only considers the head difference as the dominant factor in fluid velocity in the inlet. In practice, this method of estimating slack tide times has proven more successful than alternate methods of adding an empirical time offset to high or low ocean tides.

The time of bay filling and emptying can also be approximated from the ocean-bay difference, thus giving information on tidal prism and the effect of freshwater induced super-elevation of the bays. During this three-day example tidal period, average filling time was 6 hours 3 minutes and average emptying time was 6 hours 10 minutes. Brown's design method uses a filling time of 17050 seconds (4.74 hours), but recall that duration is associated with maximum channel velocity.

4.5 UDoo Bathymetry Surveys

Data from the University of Delaware's personal watercraft hydrographic survey vessel, named the UDoo, will augment the automated output products of the BBSMS. Surveys will be conducted to target particular areas of the inlet, and performed prior to and immediately following storms to determine their significance in the inlet morphodynamics. The operation manual for the UDoo makes up Appendix A.

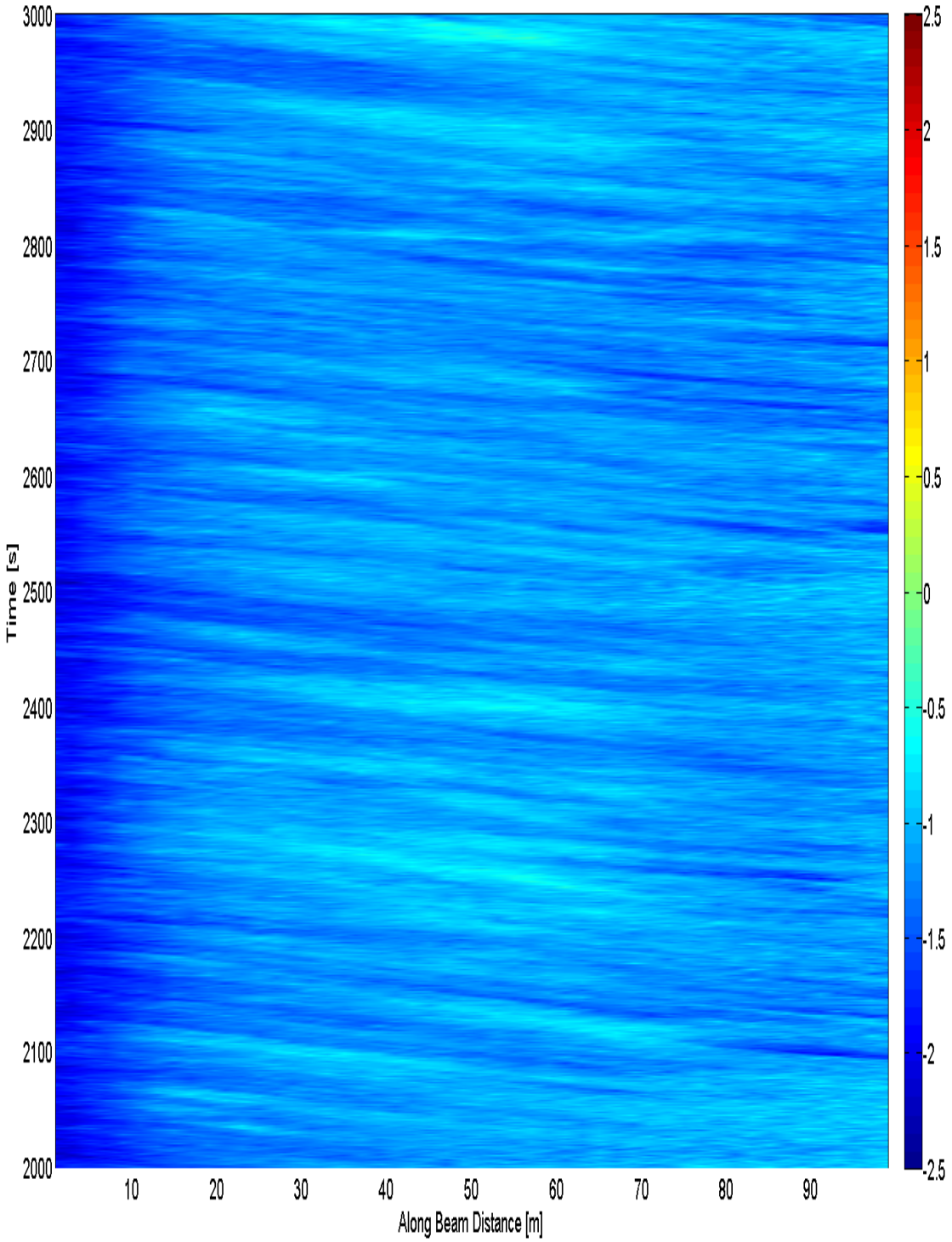

Figure 4.14: Time stack of flood tide velocities showing less chaotic behavior than the ebb velocities in Figure 2.12.

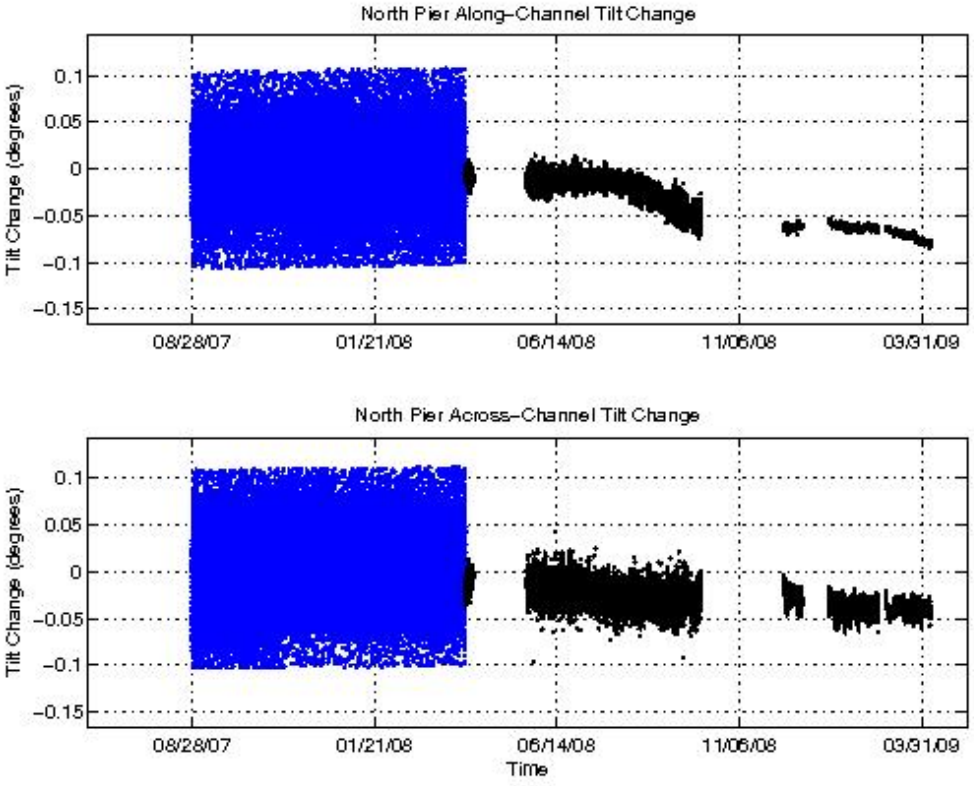

Figure 4.15: Compilation of tilt data from the north pier, DataQ data in blue, Campbell data in black.

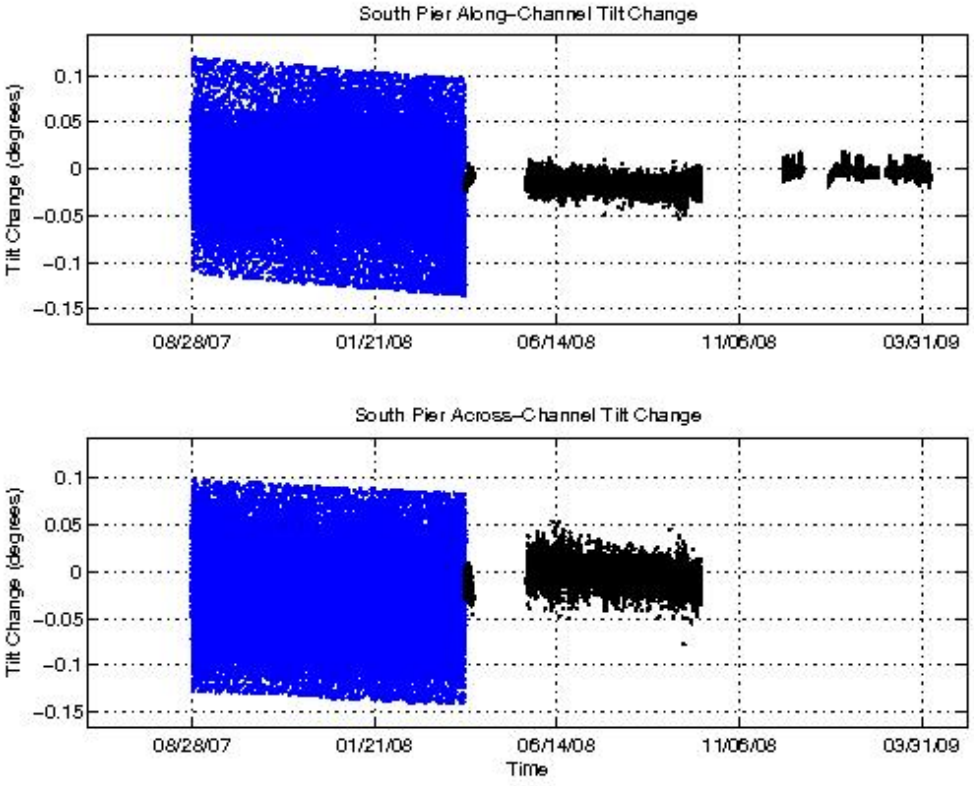

Figure 4.16: Compilation of tilt data from the south pier, DataQ data in blue, Campbell data in black.

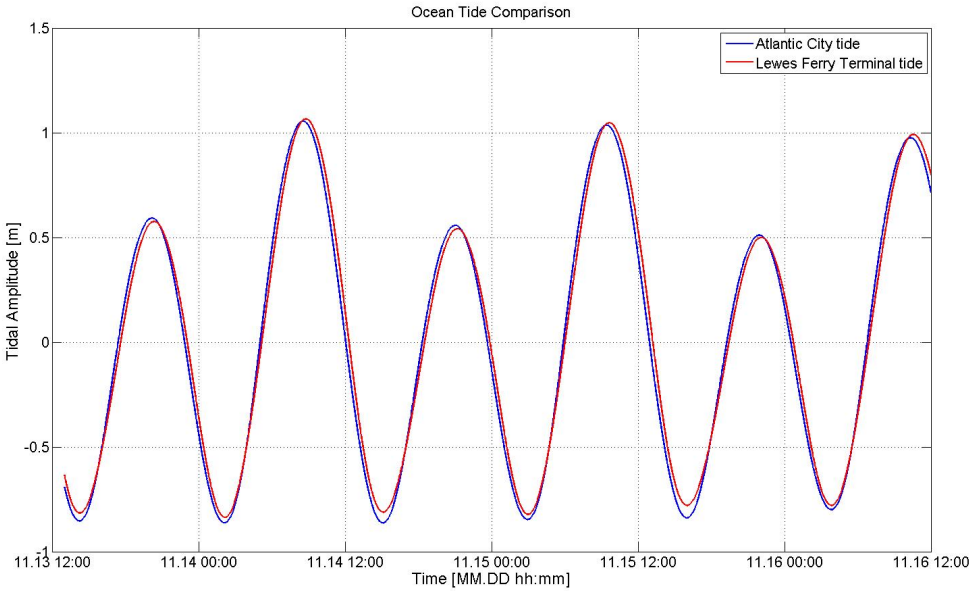

Figure 4.17: Atlantic City tide with a 0.5 hour offset (blue line), Lewes tide (red line).

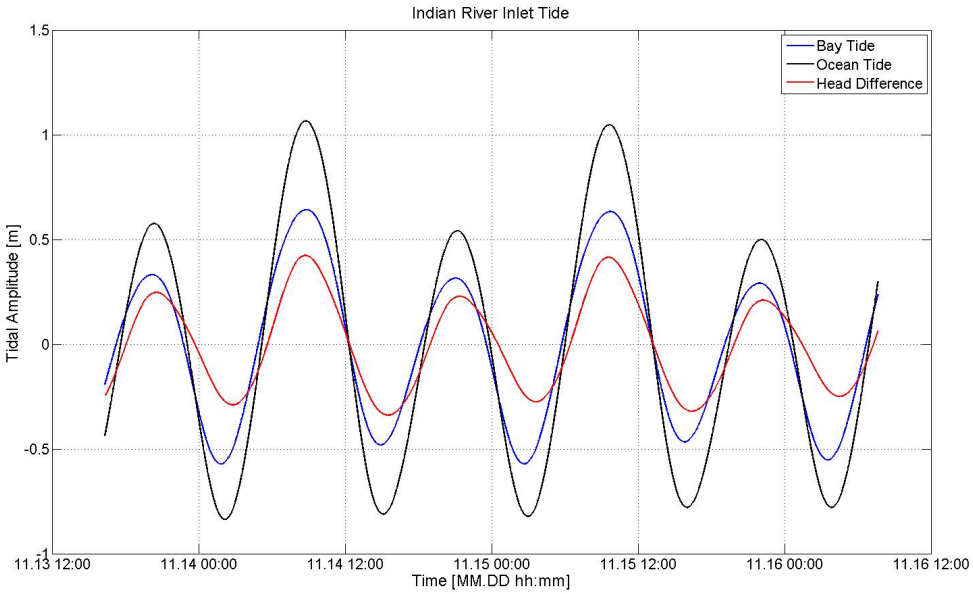

Figure 4.18: Head difference between the ocean tide and bay tide.

Chapter 5

CONCLUDING REMARKS

The BBSMS was specifically designed for the Indian River Inlet Bridge and the large menacing scour holes that threaten its stability. It will operate for the remainder of the life of the current bridge, providing DelDOT engineers and officials with information in near-real time. The primary function of the system is to arm DelDOT officials who ensure public safety on a daily basis, but the data collected on coupled bathymetric changes and tidal forcing also hold the potential to advance the understanding of the inlet morphodynamics.

Advanced scour monitoring systems are not feasible for every scour-prone bridge, as the BBSMS required a large capital investment. However when that cost considered over the life of the project and compared to the cost of the structure, the value of a near-real time decision making tool outweighs the expenditure. The automated system requires no daily operation by any technician or dedicated personnel, further saving cost, and the information output products are delivered directly to the end-user DelDOT engineers.

The power of the BBSMS is derived from the variety of data that are collected in near-real time. Independent parameters can be used to assess the health of the bridge, even if anomalies do not exist across all of the component data streams. For example, the sustained trend in pier attitude observed by the tilt sensors will not appear in either the current profiles nor in bathymetry surveys. DelDOT engineers were able to perform follow up tests and surveys to determine the safety of the

bridge in reaction to one set of data. Having eyes on these multiple parameters increases the value of the system.

Through future modeling, augmented by the accumulation of bathymetry and tidal current data, a more complete understanding of the inlet's morphodynamics will be achieved. The Indian River Inlet will continue to provide engineering challenges long after the current bridge is removed and the BBSMS project is terminated. Since its construction, state and federal engineers have been struggling to keep up with myriad new problems. Models assimilated with data collected by the BBSMS could provide engineers with valuable predictive capabilities, enabling engineers to maintain the Indian River Inlet long into the future.

References

[1] Best, J., 2005. "Kinematics, topology and significance of dune related macro-turbulence: some observations from the laboratory and field." *Spec. Publs. int. Ass. Sediment*, 35: 41-60.

[2] Chiew, Y., 1995. "Mechanics of Riprap Failure at Bridge Piers." *Journal of Hydraulic Engineering*. 121(9): 635-643.

[3] Chiew, Y., 2004. "Local Scour and Riprap Stability at Bridge Piers in a Degrading Channel." *Journal of Hydraulic Engineering*. 130(3): 218-226.

[4] Chiew, Y. and Lim, F., 2000. "Failure Behavior of Riprap Layer at Bridge Piers Under Live-Bed Conditions." *Journal of Hydraulic Engineering*. 126(1): 43-55.

[5] Committee on Tidal Hydraulics, 1994. "Indian River Inlet: An Evaluation by the Committee on Tidal Hydraulics." *USACOE Report*.

[6] Delaware Department of Transportation, 1988. "Condition Report on Indian River Inlet Bridge." *DelDOT Report*.

[7] Delaware Department of Transportation and Federal Highway Administration, 2004. "Final Environmental Assessment and Nationwide Section 4(f) Evaluation." `http://www.deldot.gov/information/projects/indian_river_bridge/why_new_bridge.shtml`.

[8] Garcia, H. M. (ed.), 2007. "Sedimentation Engineering: Processes, Measurements, Modeling, and Practice." *ASCE Publications*.

[9] Gebert, J. A.; Watson, K. D.; Rambo, A. T.; 1992. "57 Years of Coastal Engineering Practice at a Problem Inlet: Indian River Inlet, Delaware." *USACOE Report*.

[10] General Assembly of the State of Delaware, 1919. *Laws of the State of Delaware*.

[11] Greiner, Inc., 1989. "Scour Effects on Foundation Capacity." *unpublished*.

[12] Hu, C. H., 1989. "Scour at Indian River Inlet Bridge." *DelDOT Report*.

[13] Indian River Inlet Bridge Project Website. `http://www.deldot.gov/information/projects/indian_river_bridge/`.

[14] Indian River Inlet Commission, 1931. "Report of the Indian River Inlet Commission."

[15] Jarrett, J. T., 1976. "Tidal Prism - Inlet Area Relationships." *GITI Report 3*. US Army Corps of Engineers. Vicksburg, MS, USA.

[16] Kennedy, J. F., 1963. "The Mechanics of Dunes and Antidunes in Erodible-Bed Channels." *Journal of Fluid Mechanics*. 16(4): 521-544.

[17] Keulegan, G. H., 1967. "Tidal Flow in Entrances: Water-Level Fluctuations of Basins in Communication with Seas." *CTH Technical Bulletin No. 14*. Committee on Tidal Hydraulics, US Army Corps of Engineers. Washgington, DC, USA.

[18] Lagasse, P. F.; Clopper, P. E.; Zevenbergen, L. W.; Girard, L. G.; 2007. "Countermeasures to Protect Bridge Piers from Scour." *NCHRP Report 593*. Transportation Research Board. Washington, DC, USA.

[19] Lauchlan, C. S. and Melville, B. W., 2001. "Riprap Protection at Bridge Piers." *Journal of Hydraulic Engineering*. 127(5): 412-418.

[20] Lilycrop, W. J. and Hughes, S. A., 1993. "Scour Hole Problems Experienced by the Corps of Engineers; Data Presentation and Summary." *CERC Report*: 11-18.

[21] Liu, W., Field; R. T., Gantt; R. G., and Klemas, V.; 1987. "Measurement of Surface Emissivity of Turbid Waters." *Remote Sensing of the Environment*, 21: 97-109.

[22] McGehee, D. D. and Lilycrop, W. J., 1989. "Indian River Inlet Field Measurement Program." *CERC Report*.

[23] Melville, B. W. and Coleman, S. E., 2000. *Bridge Scour*. Water Resources Publications, LLC. Highlands Ranch, CO, USA.

[24] Morgan, M., 2005. *Pirates and Patriots: Tales from the Delaware Coast*. Algora Publishing. New York, NY, USA.

[25] O'Brien, M. P. and Dean, R. G., 1972. "Hydraulics and Sedimentary Stability of Coastal Inlets." *Proceedings of the* 13^{th} *Coastal Engineering Conference*. American Society of Civil Engineers. New York, NY, USA.

[26] O'Shea, D., 2006. "Why A New Bridge is Needed over the Indian River Inlet." *DelDOT Press Release*.

[27] Paarlberg, J. A., Dohmen-Janssen, C. M., Hulscher, S. J. M. H., 2007. "A Parameterization of Flow Separation Over Subaqueous Dunes." *Water Resources Research*, 43.

[28] Parola, A. C., 1993. "Stability of Riprap at Bridge Piers." *Journal of Hydraulic Engineering*. 119(10): 1080-1093.

[29] Perillo, G. M. E. (ed.), 1995. *Geomorphology and Sedimentology of Estuaries*. Elsevier. New York, NY, USA.

[30] Plant, N. G.; Holland, K. T.; Puleo, J. A.; 2002. "Analysis of the Scale of Errors in Nearshore Bathymetric Data." *Marine Geology*. 191:71-86.

[31] Richardson, E. V. and Lagasse, P. F. (eds.), 1999. *Stream Stability and Scour at Highway Bridges*: 551-556, 717-722. American Society of Civil Engineers. Reston, VA, USA.

[32] Schall, J. D.; Price, G. R.; Fisher, G. A.; Lagasse, P. F.; Richardson, E. V.; 1997. "Sonar Scour Monitor: Installation, Operation, and Fabrication Manual." *NCHRP Report 397A*. Transportation Research Board, National Academy Press. Washington, DC, USA.

[33] Schall, J. D. and Price, G. R., 2004. "Portable Scour Monitoring Equipment." *Transportation Research Board Report*.

[34] Simpson, C. O., 1956. *Beach Erosion: Delaware Bay and Atlantic Ocean, 1956 Report and Recommendations*. Delaware State Highway Department.

[35] Stewart, R., 1985. *Methods of Satellite Oceanography*. University of California Press. Berkeley, CA, USA.

Appendix A

UDOO MANUAL

The UDoo is the University of Delaware's personal watercraft hydrographic survey vessel, built in 2008 and 2009 after the system of MacMahan (2001). To summarize, the personal watercraft provides a low cost platform for performing hydrographic surveys in areas where vessel agility is crucial. One such example is the surf zone, where the shallow draft and responsive handling allow the surveyor to approach the beach in such a manner that would be impossible for larger boats, while retaining the ability to power out of dangerous situations such as the need to escape the bore of a breaking wave.

The UDoo was built under the guidance of Jamie H. MacMahan, with the unique distinction of targeting the Indian River Inlet for future surveys. There are two main differences between designing a system for the shallow surf zone and designing for the deep inlet: first, we installed an MRU or motion reference unit, and second, we designed the transducer arm such that a few different lengths can be swapped according to the needs of a particular survey. Intuitively, the surf zone surveys will benefit from the corrections provided by an MRU and from its ability to flag data points read under extreme tilt, but MacMahan (*pers. comm.*) has proven that since the water depth is shallow, the corrections are less than the survey accuracy. Though the system was initially designed for the inlet, this does not preclude it from being used for surf zone surveys, considerations were made during design that allowed the UDoo to retain its universal ability as a hydrographic survey vessel.

The design goal was to make the system modular, so that parts and pieces can be replaced or added as needed. There are three black waterproof Underwater Kinetics (UK) cases that sit on an aluminum frame at the back of the vessel, and one blue waterproof UK case with a clear lid that sits inside a sun screen on an aluminum mount at the helm. Below the handlebar there is a keypad, much like one you would find at the checkout of a fast food restaurant, in a clear waterproof box. At the extreme aft of the vessel, on the starboard side, there is one post extending up that holds the GPS and radio antennae, and one post extending down that holds the sonar transducer. All of these components, except for the aluminum bracket that holds the monitor and sun shade, are removable and so the UDoo can be used as a personal watercraft platform to support a range of field work.

A.1 Components

Some of the other literature I have written on the Udoo employs 3-letter abbreviations that roughly describe the function or association of that particular piece of equipment. Table A.1 shows what these abbreviations represent.

Table A.1: Abbreviations used in UDoo literature to describe components and parts associated with specific devices.

CPU	Computer found inside Big Box
GPS	Global positioning system, antenna and power
KVH	Brand name of the Udoo's MRU
MON	Monitor, box, and associated cables
PAD	Fast food style keypad programmed with hot keys for surveying
PWR	System power
RAD	The radio and antenna for the RTK GPS
SNR	Sonar Echosounder

This block diagram employs these abbreviations and can be used if new cables or bulkheads need to be ordered, or for a general illustration of the interrelated components of the UDoo.

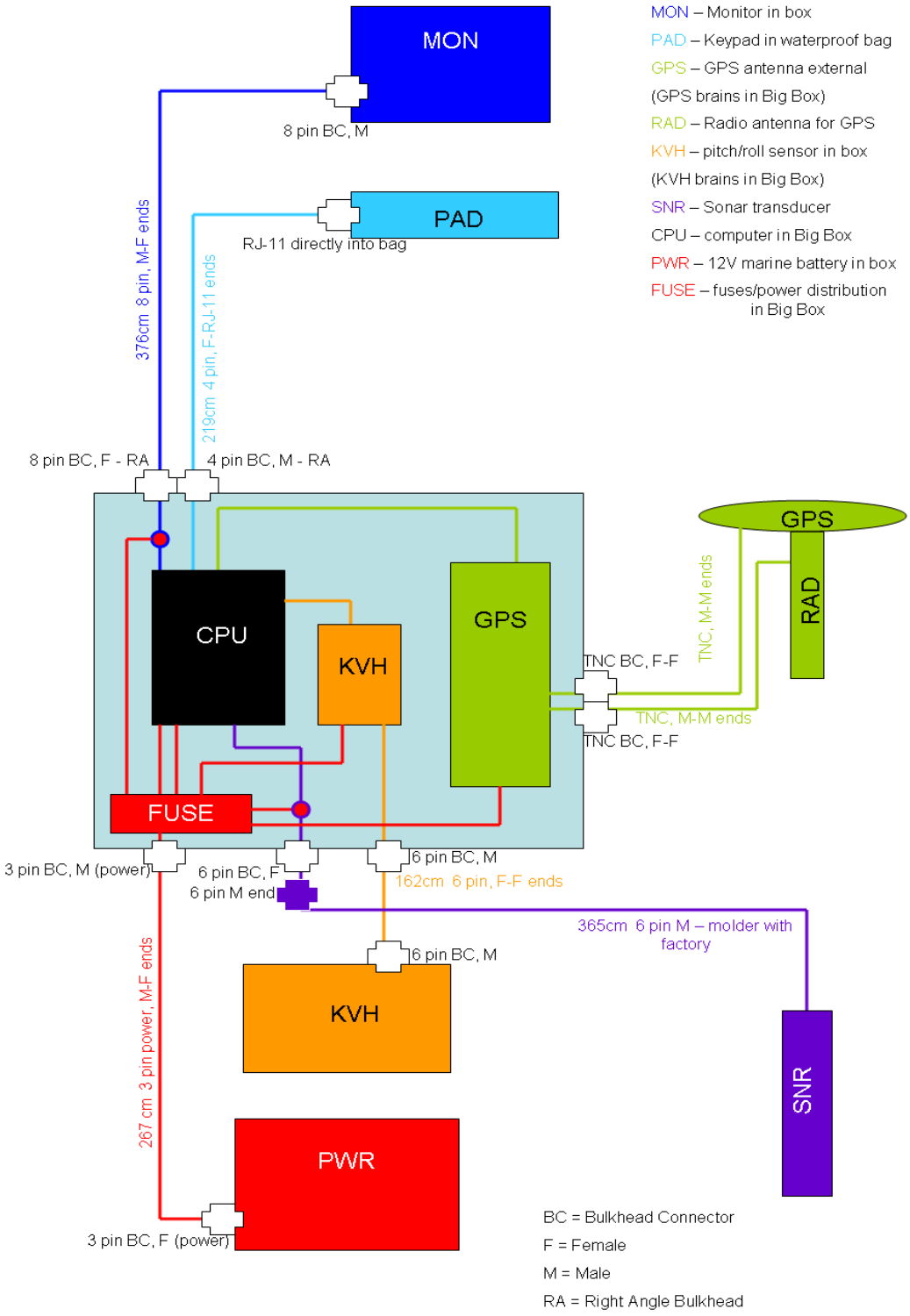

Figure A.1: Block diagram of UDoo components and connections, approximate lengths of cables are given.

The remainder of the diagrams in this appendix may use the above abbreviations, but for the most part I will use full names in the text. Aside from their use in other literature and diagrams, you will find the 3-letter abbreviations written in permanent marker on the bulkhead connectors associated with each respective piece of equipment. Since the UDoo system is modular, the description of components here will be broken down according to the boxes inside of which pieces are contained.

A.2 Aluminum frame

The aluminum frame is not a permanent fixture on the UDoo. It sits on the aft deck of the UDoo and is held in place by straps. The custom made side clips hold on to the rail and allow considerable tension in the straps that holds the frame and all of the components in place. Usually an additional safety strap is employed to link the frame to the D-ring just under the rear seat. The frame is made of up a number of components that can be adjusted or replaced should the need arise. For easy travel, the masts are removable as are their support arms.

The Big Box (Section A.3) rests on the fore portion of the frame, which looks like it would be cantilevered when the frame is not on the UDoo. When in place, though, the rear seat supports the weight of the Big Box through the angle bracket, which is adjustable for height.

The KVH box (Section A.5) rests just aft of the Big Box and slightly starboard of center. The nylon straps holding the aluminum frame onto the UDoo run underneath the KVH box and neither interferes with the other.

The battery box (Section A.6) rests on the aluminum plate that rests on the aft deck where the weight of the battery helps hold the frame in place. A safety bar is bolted across the rear opening of the frame after the battery is in place, and a 6 foot long nylon strap is stretched over the top of the battery box to hold it firmly in place.

There is one auxiliary mast on the port side of the aluminum frame; possibilities for its use include camera mounts, photovoltaic solar arrays, and pirate flags.

A.2.1 Monitor Mounting Plate

The monitor box (Section A.4) and shade combination get bolted onto an aluminum plate that is a permanent fixture on the UDoo. The flat aluminum plate sits just above the steering column and is unmistakable as the monitor mounting location. It is cut to fit onto the four bolts that hold the steering assembly to the hull (See Figure A.2), and is currently held in place with nuts glued with blue thread lock. The factory nuts holding the steering assembly were not removed, rather the excess bolt length was exploited to mount this aluminum plate. The blue thread lock is used to ensure that the extra nuts do not vibrate loose, it can be loosened with a wrench.

There are four $\frac{3}{8}in$ diameter holes in the mounting face, positioned to receive the bolts protruding from the back of the monitor box. The hole spacings are shown in Figure A.3.

Two resting arms support some of the weight of the monitor onto a flat portion of the steering assembly. These arms have been coated in blue rubber to avoid marring the plastic of the hull or the steering assembly. Additionally, the yellow hatch cover had to be modified to allow it to open and close in the presence of the monitor mounting plate. These modifications do not affect the operation of the vehicle.

A.3 Big Box

The Big Box is the black UK 827 Loadout waterproof case ($28.8''x20.1''x9.7''$), and it sits directly behind the operator when the UDoo is fully equipped. A total of seven bulkhead connectors are located on the front, right side, and back of the Big

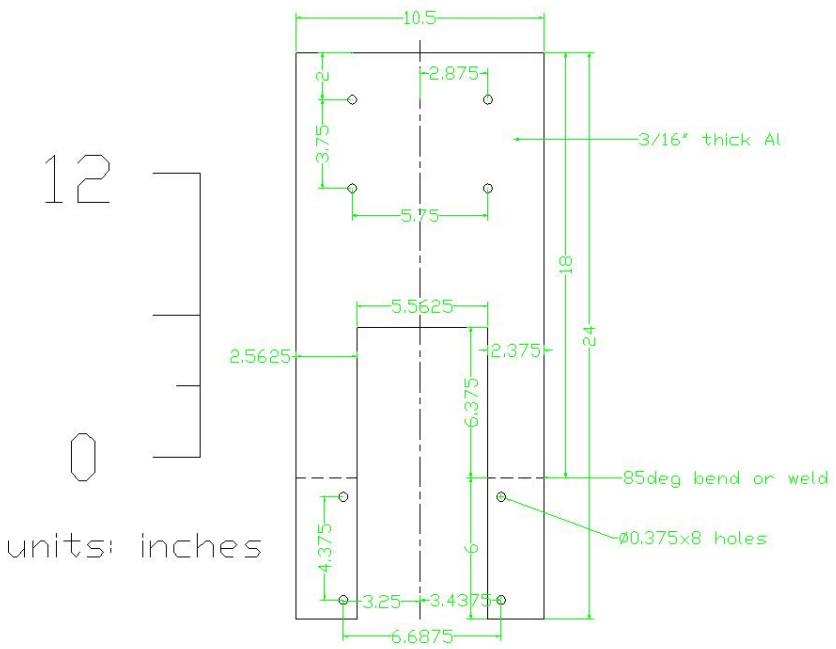

Figure A.2: Technical drawing of monitor mounting plate, cutouts for exact fit around steering column were added after fabrication.

Box. The Big Box can be thought of as the brains of the entire system, it houses the computer, the GPS rover receiver, and the KVH input/output device. Also inside the Big Box is the power distribution block, with fuses that will trip in the event of excess amperage. The fuse block was designed and built by Michael Davidson, Senior electronics Specialist for the CEIG department and questions or problems regarding this part should be directed to him. Auxiliary parts inside the black box are a rollable keyboard and small mouse for the computer, a clear plastic stick used to prop the lid open - stored in the lid, and various pieces of foam used to prevent the electronic components from shifting.

The fuse block is covered with a clear plastic sheet to prevent contact with live electric wires, CAUTION: DO NOT TOUCH THE WIRES WHEN THE BATTERY IS CONNECTED. 4 brass screws can be removed to lift the plastic cover and access

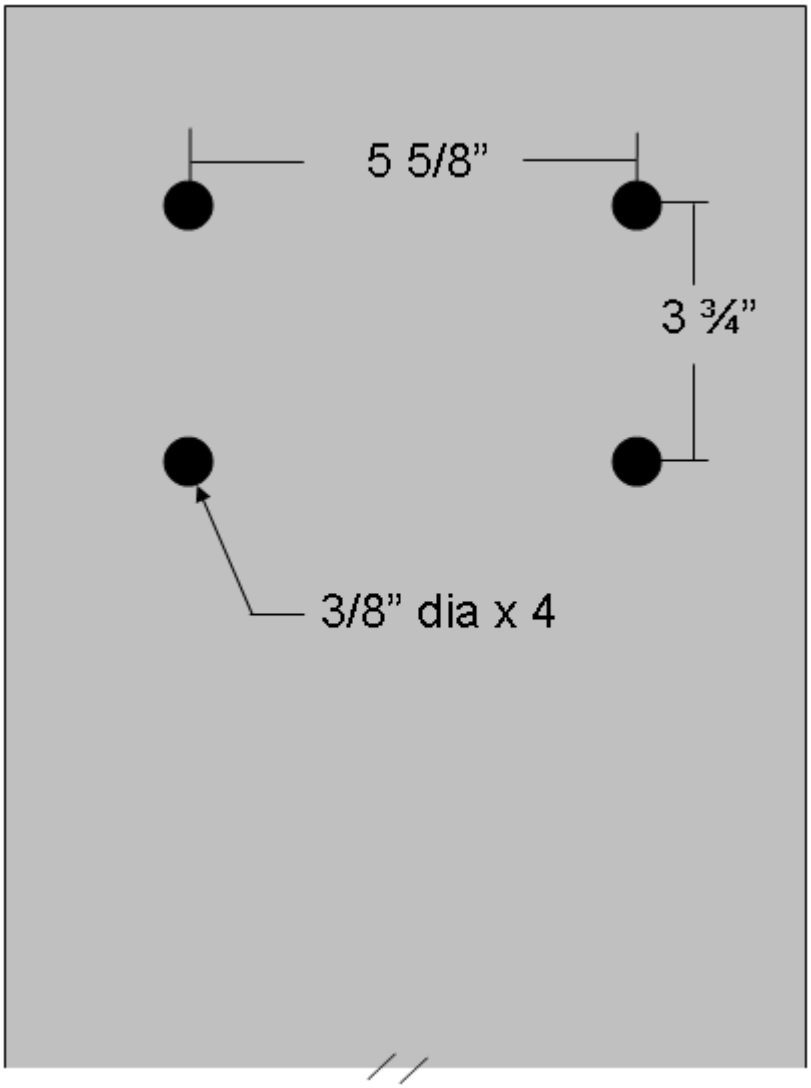

Figure A.3: Hole spacing on the monitor mounting plate that is affixed to the UDoo.

the terminals. Power is provided to the Big Box via the 3 - 10AWG wires that come through the bulkhead connector labeled PWR. One of these is +12V, one is 0V (ground), and the other is reserved (not currently used). The +12V wire is designated with red coloring, and connects to the red input terminal on the fuse block, the 0V is not colored red and it connects to the black input terminal on the

fuse block. See A.4 for reference on where these terminals are located on the fuse block.

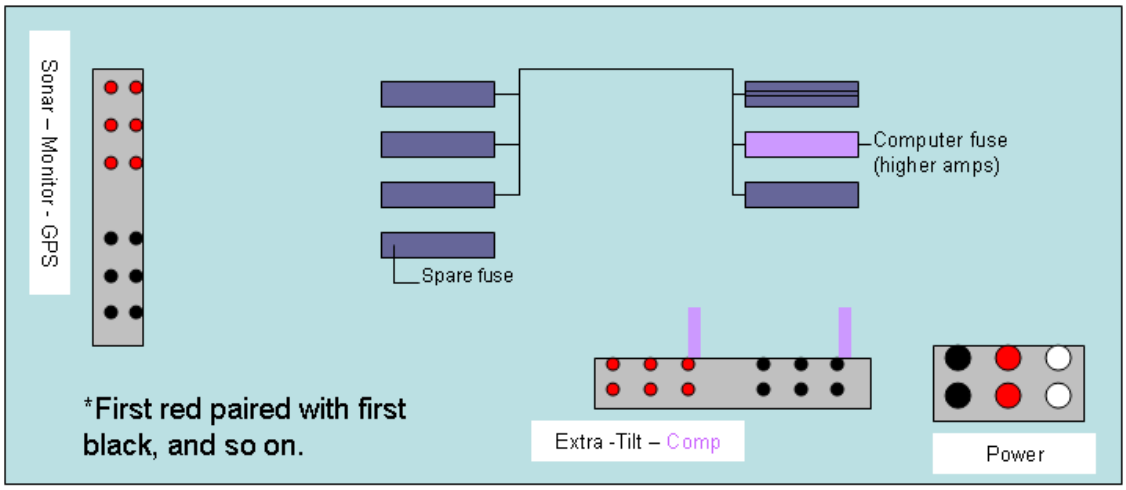

Figure A.4: Simplified schematic of the fuse block in the Big Box. This component takes in power and distributes it to other UDoo components.

Power is distributed to the various components from this common input. The amperage needs of each component dictate the size of the fuse linking the common input to the designated output terminals. These output terminals are labeled on the fuse block to prevent confusion, in addition to being described in A.4 above. The computer, KVH brains, sonar, GPS, 'BlackBox' brand serial data converter, and monitor all receive power through the fuse block, the GPS can run on its own internal battery but none of the other components have this capability.

The KVH brains box sits on the floor of the Big Box and is held in place with Velcro. It is wired and configured to output its proprietary string of stabilized pitch, roll, and yaw data. The data is output as differential RS422 signal from KVH-serial port #2 which comes out of the white colored terminal strip on the back of the brains box. Since the computer cannot recognize the differential signal through its serial ports, a converter is used to take in the differential signal and output an RS232 serial signal through a typical Dsub9 connector into the computer.

Note: the A/B and +/- designations in the KVH manual differ from standards found on the web. Through trial and error, the final configuration of the KVH output and BlackBox converter described here was discovered; the configuration documented here is correct and operates properly. Three wires come out of the KVH White terminal strip: black from terminal #28, white from terminal #29, and blue from terminal #30. These connect to the BlackBox terminals as follows: Black to the Ground terminal, white to the RD(+) terminal, blue to the RD(-) terminal. Additional terminals on the BlackBox terminal strip provide it power, with a red wire coming in from the Extra slot on the fuse block, and its associated black wire using the common Ground terminal on the BlackBox terminal. See photograph for reference. The Blue terminal strip receives the signal from the KVH instrument, this wiring plan can be found on page 17 of the KVH product manual. The wires entering the Blue terminal are factory wires, so their coloring is consistent with the coloring in the manual. This is the same cable that is found in the separate KVH box (Section A.5), and a portion remains as spare should repairs need to be made. The white wire with green stripe is the ground, connected to terminal 13; white wire with blue string is TX+, connected to terminal 14; blue wire with white stripe is TX-, connected to terminal 15; white wire with orange stripe is RX-, connected to terminal 16, orange wire with white stripe is RX+, connected to terminal 17, green wire with white stripe is +12VDC power input, connected to terminal 18.

Configuration of the KVH brains for proper output is done according to the KVH manual page 27, for KVH output type. Use the three buttons on the front of the KVH brains box to perform this series of steps, the manual is very helpful here. Page 29 of the KVH manual shows the output sentence structure which you will need when you are configuring Hypack to read the pitch, roll, and yaw signal - this procedure will be covered in the Hypack section.

On top of the KVH brains sits the UDoo computer, the brains of the entire

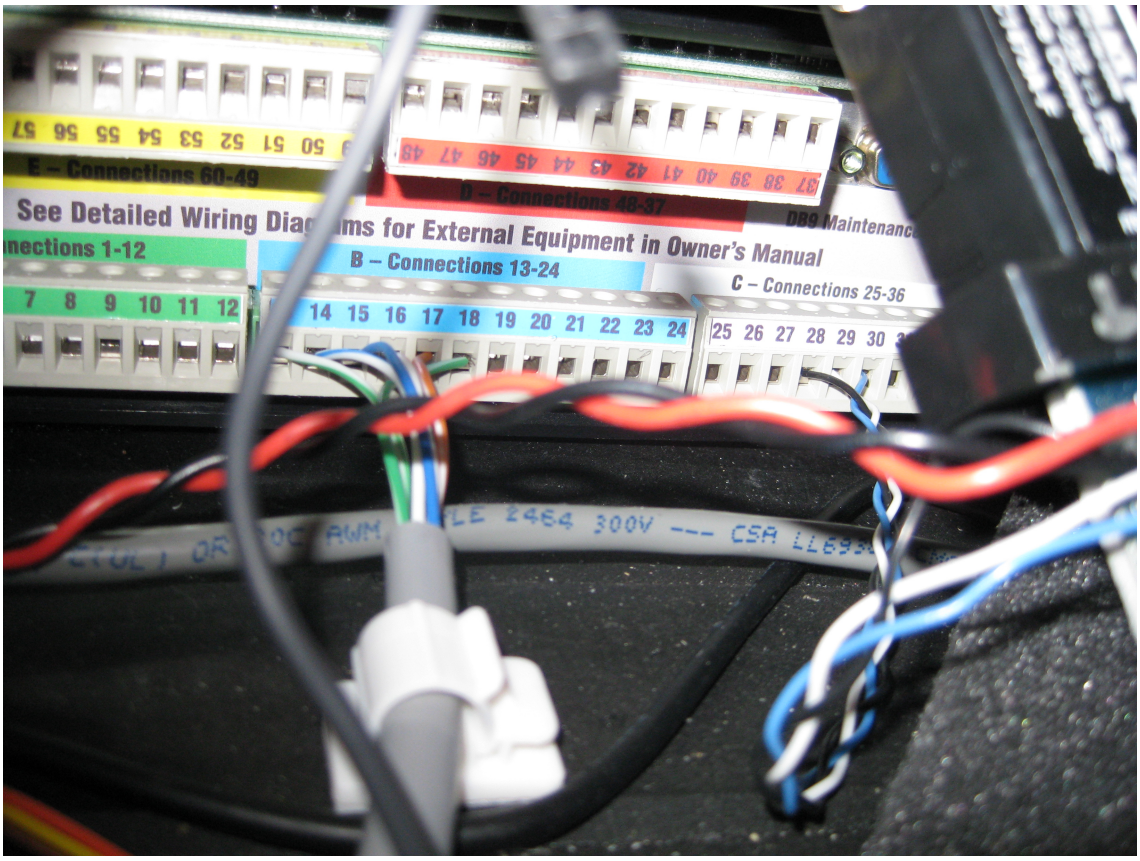

Figure A.5: Photograph of the wired terminal strips on the back of the KVH brains box.

system and the last permanent resident of the Big Box. Held to the KVH brains by Velcro, the computer receives all signal inputs from the instruments, interfaces with the monitor and keypad, and runs the survey software Hypack.

Three COM ports are used on the back of the computer, COM1 is where the computer interfaces with the GPS rover, COM5 is for the sonar, COM6 is for the KVH. Additionally there is one VGA connector for interfacing with the monitor, one PS/2 connector for interfacing with the keypad, one reserved USB port for the yellow Hypack key dongle, power input, and one USB port that can interface with the rollable keyboard or the mini-mouse (a port-powered USB hub may be added so all of the USB devices can be used at once). Additional USB ports on the front of the

computer are unusable while it is in the Big Box due to spatial limitations. There are two unused COM ports on the back of the computer that allow for expansion of the system. Note in the photograph in Figure A.6 that the GPS rover is not connected to COM1.

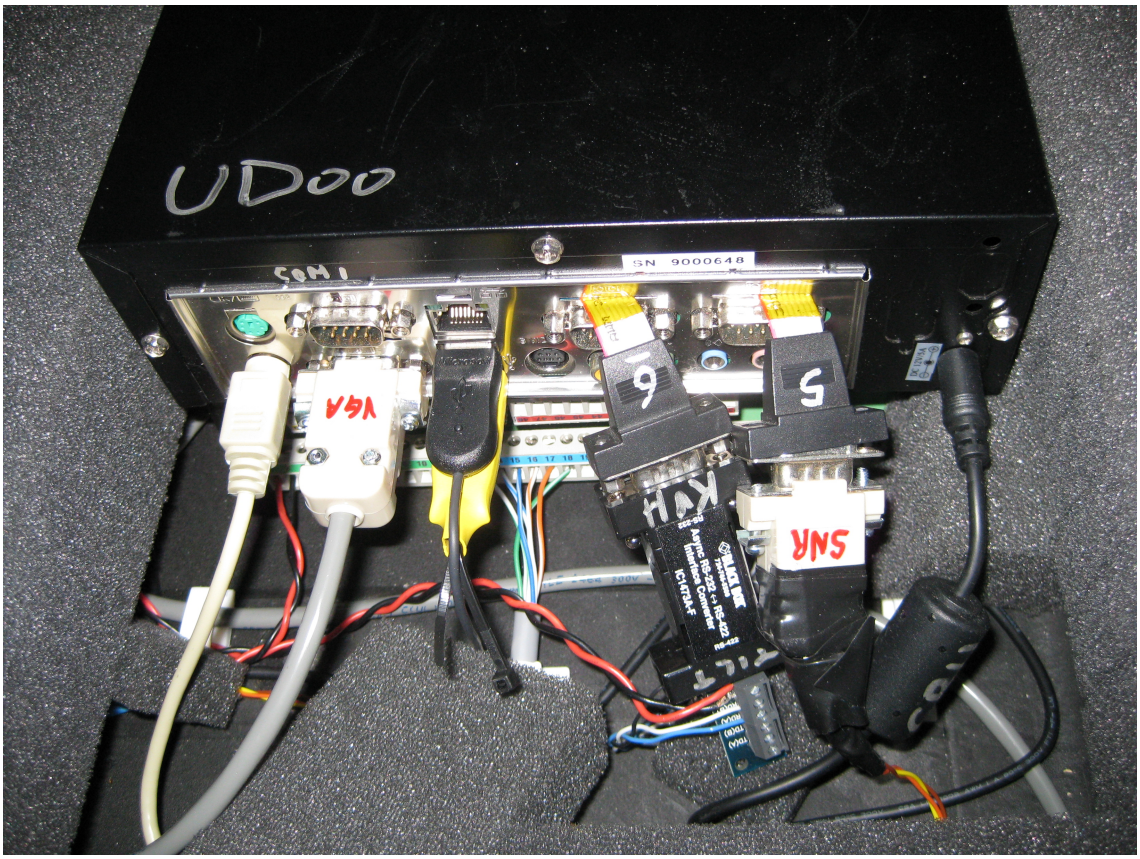

Figure A.6: Photograph of the rear panel of the UDoo computer, labeling uses the 3 letter abbreviations listed in Table A.1.

The GPS rover and antenna are not permanent components of the UDoo, the RTK GPS system is separate and is employed by the UDoo survey system. The rover sits inside the Big Box so that its antennae TNC connectors align with the TNC bulkheads. This alignment also allows the COM A (top comm port of the rover) of the rover easy connection with COM1 of the computer. Since it is not permanently connected, instructions for plugging the rover into the UDoo follow.

There are two antenna bulkheads, one located on top of the other; on the remote antenna and on the rover antenna stub the TNC connectors are located one on top of the other. For repeatability, always use the top bulkhead to connect the two top TNC antenna plugs, and the same for the bottom.

Schematics for wiring each of the components can be found as separate pages in this appendix.

A.4 Monitor Box

The small blue UK box with the clear lid contains the 7 inch widescreen monitor. Both power and signal come into the monitor box through the single 8-pin bulkhead connector. The monitor came from the factory with a rare type of digital input cable with pigtails for either component or VGA feed. Since we wanted to interface the monitor with a computer only, the component pigtails were cut, there are no ill effects from this streamlining. The male VGA connector that would normally plug directly into the back of a computer now connects to a female VGA connector wired from the bulkhead. Two of the bulkhead wires that do not carry VGA signal provide power to the monitor via a separate plug, similar to any other DC adapter plug. Refer to Figure A.7 for the schematic.

The monitor is pressed against the lid of the box to ensure easy viewing with plastic stands and compressed foam. The black plastic is free to move in the box when the lid is not closed, but while the lid is closed everything is held firmly in place, even under rigorous wave conditions. Hot glue can be used to repair any of these pieces that may become loose. There are a few silica gel desiccant packages in the monitor box to prevent fogging of the lid. The monitor becomes quite warm during operation, but no overheating has been observed. I have avoided filling the box with foam to allow sufficient air flow to try to limit heat buildup.

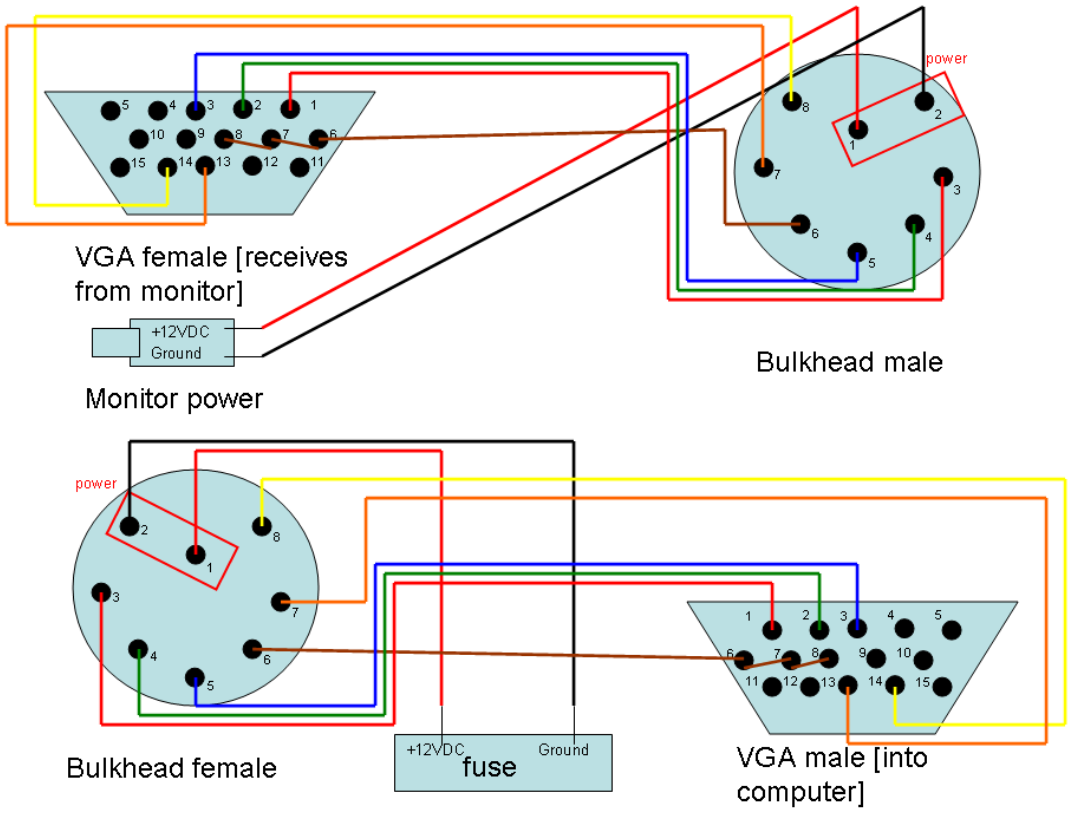

Figure A.7: Schematic of wiring of the VGA and MON bulkhead connectors.

A.5 KVH Box

The black UK 716 UltraCase ($17.6''x11.7''x7.1''$) houses the KVH motion sensing unit, and is referred to as the KVH box. It sits aft of the Big Box when equipped, and is fitted with two aluminum skis that get bolted onto the aluminum frame holding it securely in place. When mounting this box, the bulkhead connector should point to the port, and the handle of the box should point to the starboard, with the skis down.

Inside the box, the KVH unit is bolted into its factory mount, which is screwed to a separate piece of black plastic which is in turn glued to the bottom of the box with epoxy. This epoxy had proven difficult, and many re-applications have already been required. Prior to using the UDoo, check that the KVH motion sensing unit is firmly attached to the box. Careful alignment of the unit within the box is crucial to measuring proper heading information.

The connector that plugs into the back of the KVH is factory made. The factory cable was cut and the bulkhead pigtails were soldered to the wires. A schematic of this wiring can be found in Figure A.8.

A.6 Battery Box

The black UK 916 UltraCase ($17.6''x11.7''x8.6''$) contains the 12V marine gel deep cycle battery. Use extreme care when lifting this box, it weighs about 60 pounds. So far the handle of the UK box has been able to support the load, though no information regarding safe carrying capacity is available in the box specifications. Leads are soldered onto the bulkhead pigtails so that they may be bolted onto the battery terminals. Michael Davidson installed a diode on the positive (red) lead to prevent catastrophic discharging.

The battery box sits inside the aluminum frame on the aft deck of the UDoo. A safety bar gets bolted onto the frame to keep the battery from falling off during

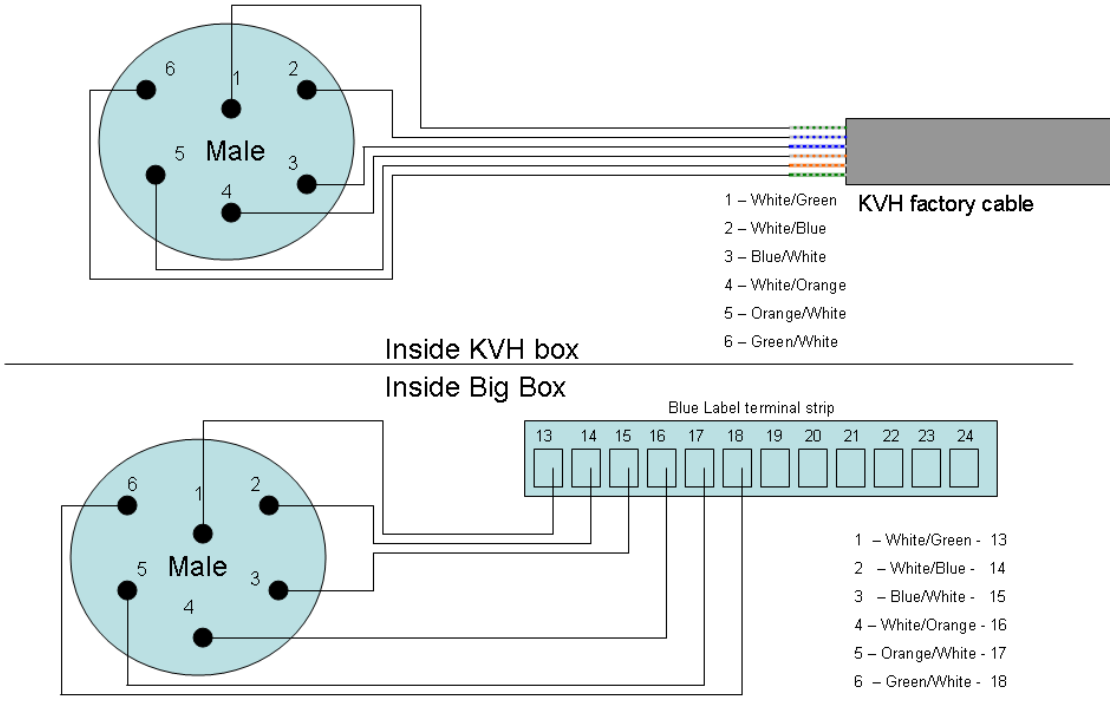

Figure A.8: Schematic of the KVH Box into Big Box wiring.

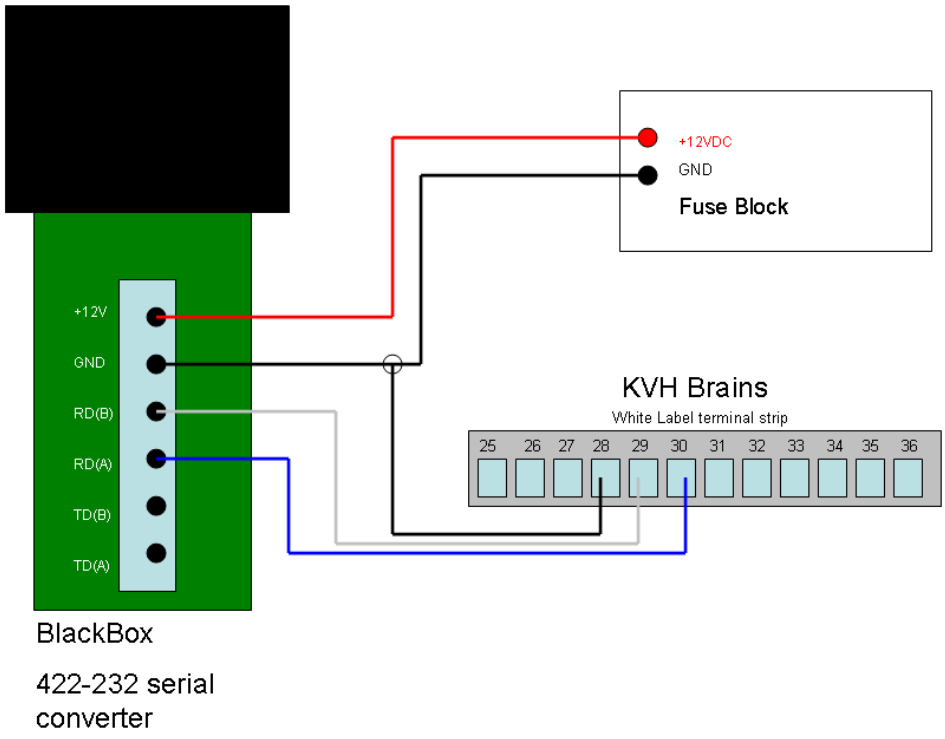

Figure A.9: Schematic of the communications between the KVH and the computer.

surveys, and nylon straps keep the box from moving even during intense maneuvering.

A.7 Keypad

The keypad currently sits inside a waterproof bag with its cable sealed in clear tubing. This configuration has been deemed sub-par and improvements are being made to encase the keypad in a rigid case with a soft top to allow the buttons to be depressed. The keypad connects to its designated bulkhead on the Big Box and then to the PS/2 connection on the back of the computer.

A.8 Sonar

The Tritech echosounder is held at the end of the survey stick by two complementary blocks of Delrin plastic. From the end of the echosounder the factory watertight plug gets screwed on to the transducer using 4 hex-key machine screws (this hardware and tool are in the echosounder box, along with spare o-rings to maintain watertight seal), and the cable runs up the aluminum frame to the appropriate Big Box bulkhead.

The echosounder is a Tritech PS500 Precision Miniature Altimeter, with a 500kHz sonic pulse and a 6° conical beam. The transducer is housed in a 316 stainless steel body rated for operation at depths up to 4000m. Its observation range is 0.5m to 50m, outputting data in an RS-232 format at 9600 baud. Inside the Big Box, a DB-9 connector is wired to the incoming sonar cable to facilitate communication between the computer and the transducer, a schematic of the wiring is shown in Figure A.12. The required 12V (9V-20V) power is supplied by the UDoo system's battery power described in Section A.3. The sonar echosounder begins recording as soon as power is supplied, and the stream should be visible across the COM5 port immediately provided the port is set up correctly.

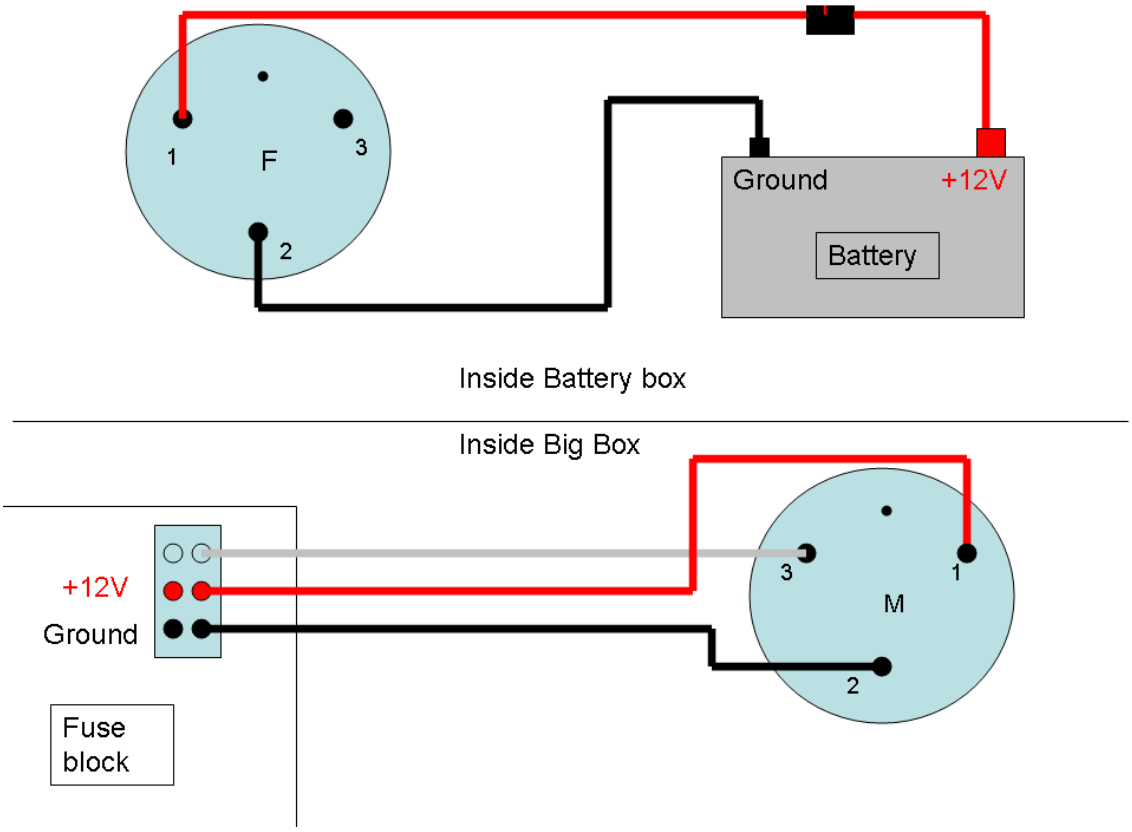

Figure A.10: Schematic of the wiring of the Battery Box into the Big Box.

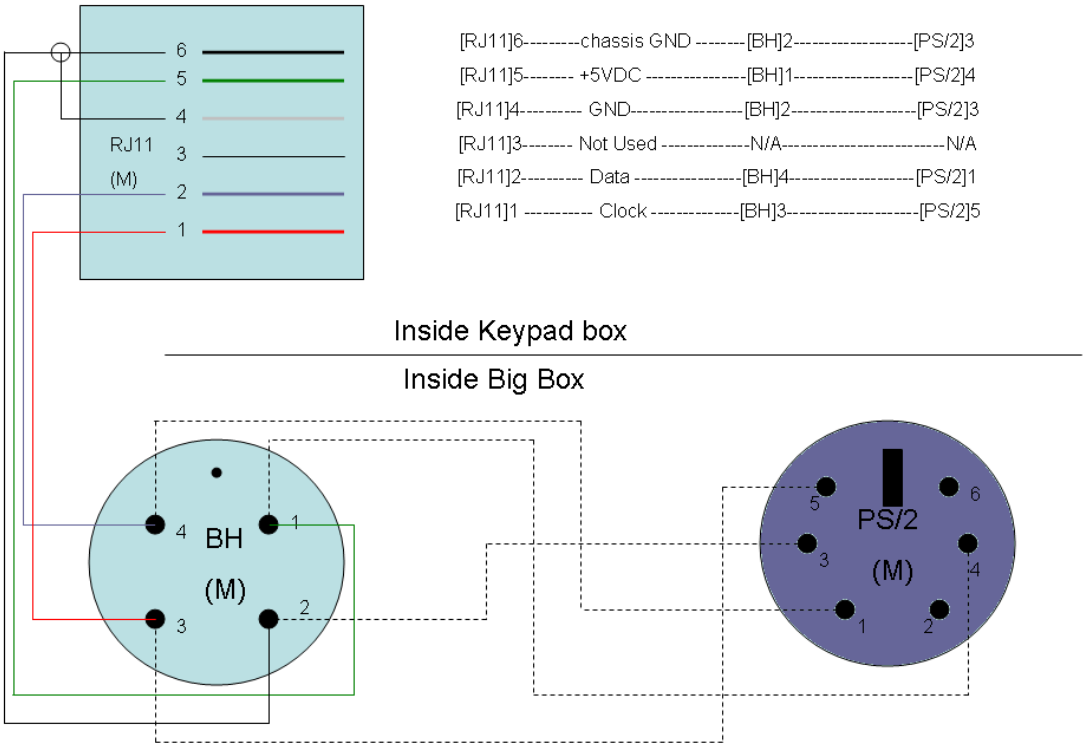

Figure A.11: Schematic of the keypad box into Big Box wiring.

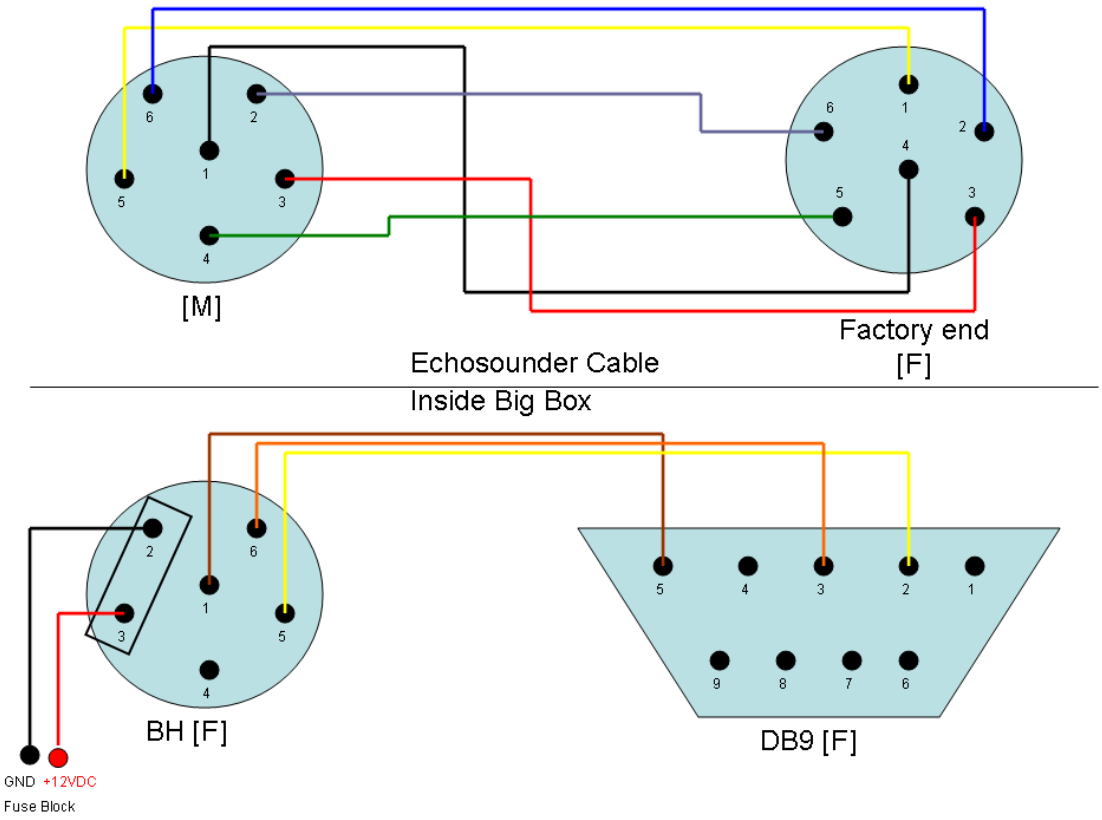

Figure A.12: Schematic of the hardwired echosounder cable into the Big Box.

A.9 GPS

The aft starboard mast features a stainless steel threaded rod that mates with most GPS antennae. The RTK GPS system used by the UDoo features a radio and GPS satellite antenna in one - and so only one mast is necessary. The remote antenna should be screwed onto the mast, then the TNC connections made to the Big Box according to the procedure above.

A.10 Hypack Survey Software

The best way to learn about the Hypack surveying software is to view the tutorial videos supplied by the company. These can be found via the Hypack website, or they also exist on the computer named *Wahoo* in the CACR.

The specifics of setting up Hypack for UDoo surveys follow, but you might be confused unless you have previously used Hypack or viewed the tutorials.

Some background maps of the Delaware coastline have been downloaded and exist in the "Nautical Charts and Maps" folder on the UDoo computer. Hypack can display a wide variety of background map types, similar to any other GIS program.

You can specify each device's location relative to the boat in the basic device setup dialog box in the user selected survey units. Distances are measured from the user selected origin of the boat, axes are positive to starboard, forward, and down (stand behind the boat facing it - right hand rule with thumb pointing down). For single beam surveys, suggested origin of boat is the transducer; when an MRU is present then Hypack suggests you use this as the origin. The UDoo is so small compared with typical survey boats, either should be acceptable.

A.10.1 Hypack Hardware Setup

The most important part of the setup procedure is telling Hypack how to read and implement the streaming data from your survey system. The UDoo employs 3

devices: an echosounder to collect depth information; RTK GPS for location, boat speed, and tides; and an MRU for heading, pitch, and roll.

To set up the drivers, first plug all devices into computer and then power everything up.

First add Tritech Echosounder device. Use generic device parser as driver. Gendevparse.dll should be used for data coming in that is delimited by comma, space, tab, or other - and need not be in columns of uniform width. If data is coming in in columns of uniform width, use gendevall.dll

In Hypack Hardware:

- Click Add Device, a window pops up with a long list of drivers, select gendevparse.dll
- You will use this driver only for Depth, so de-select all other options
- You can check the Use this to update Matrix box if you want Hypack to fill in your grid with depths as you survey, I check this box
- Select the method of communicating with the device, for UDoo it is COM5
- Ensure the proper COM settings are selected (9600, None, 8, 1)
- Click the Setup button, and the setup window pops up
- Check the Comma checkbox as the delimiter
- Make sure that the end of line indicator is $< cr >< lf >$
- Click OK
- Now click *Test..* button to test that the driver is setup properly and that the correct COM port is selected

The echosounder is not the origin of the vessel, so you have to tell Hypack where it is in relation to the selected origin. In this case the echosounder is $-0.3937m$ forward, $0.4239m$ starboard, and $0.9462m$ below the origin. NOTE: The last measurement listed here is the distance below the origin using the short survey stick, the long stick should be measured prior to use.

Second, add KVH pitch/roll/heading device. Again use the generic device parser as the driver. Before setting up Hypack to read the signal, you have to set up the KVH to send the right kind of signal to the computer. On the KVH ACU (the brains) located under the computer in the Big Box, there are 3 buttons and a small digital screen. Follow the instructions on page 27 of the KVH manual, reproduced in Figure A.13, to set the serial output to the KVH special 422 version (outputs Pitch, Roll, Magnetic Heading). The wiring is set up to communicate out of COM2 on the back of the KVH brains. These wires go into a BlackBox brand 422-232 converter, the schematic is available in Figure A.9. The 422-232 converter should then be plugged into COM6 on the UDoo computer. Now you're ready to set up the KVH driver.

In Hypack Hardware:

- Click Add Device
- Select gendevparse.dll from the list
- You will use this driver for Heave (pitch/roll) and Heading only
- Select COM6 as the method of communicating with the device
- Ensure the proper COM settings are selected (9600, None, 8, 1)
- Click Setup to get the setup window
- The KVH outputs Pitch, Roll, and Heading in that order, so check the appropriate boxes and order them accordingly

- Check the Comma as the delimiter
- The sentence has a "%" percentage symbol as the header, tell Hypack so that it knows how to read the sentence
- The "%" header is NOT a separate field
- Make sure that the end of line indicator is $< cr >< lf >$
- The pitch, roll, and heading data is output in tenths of degrees - so you have to tell Hypack what to multiply the information by - tell it to multiply the pitch/roll by 0.1, and the heading by 0.001.
- Click OK
- Now click Test to make sure you set up the KVH driver properly

The MRU, in this case called *KVH*, is the origin of the vessel. When measuring offsets, open the KVH box and measure to the letter *O* that is approximately at the center of the label on top of the unit. This *O* is considered the origin of the vessel.

Third, add the RTK GPS device. This time you will be using a special driver for GPS inputs. Both the kinematic.dll and gps.dll are valid, they are identical and can be used to handle inputs from the RTK GPS. The Ashtech RTK GPS only outputs a few of the sentences that this driver can read, so you will need to 1) find the 3-letter codes that can be output by the Ashtech, 2) ensure only these boxes are checked in the driver setup or else this device will not operate properly.

- Check the appropriate boxes to use the GPS for Position, Speed, and Tide
- Under Options, check all the boxes so that the raw data is logged also
- Select COM1 as method of communicating with the device

- Ensure the proper COM settings are selected (9600, None, 8, 1)
- Click Setup, note that this setup window is different from the gendevparse setup
- Change nothing under General Tab
- Under Alarms tab, select NMEA 3.0 status codes, typical for newer GPS - here you can also give threshold values for max HDOP and min Number of Satellites and have Hypack display an alarm or even stop logging when the threshold is crossed
- Under the GPS status codes tab, you can tell Hypack to show an alarm or even stop logging when certain status codes appear. I prefer to just show the alarm, as you can always go into the data file later and remove points
- Check the following boxes under Advanced Tab, make sure *only* these boxes are checked: GGA, GLL, RMC, VTG, GST
- Under the Graphs tab, you can select information to be displayed in Survey. Since we have a very small screen on the UDoo and limited controls, it is best to keep Survey uncluttered, at most I recommend displaying the number of satellites.
- Click OK
- Now Test that you have set up the GPS driver properly

Now you need to tell Hypack where the GPS antenna sits relative to the origin. Barring a redesign of the aluminum frame, the GPS antenna sits $-0.3937m$ forward, $0.3731m$ starboard, and $-0.64175m$ down. The negative down measurement means it is above the origin.

Still in Hypack Hardware you should have a "Boat" with 3 devices listed under it. Click on the word Boat and change the name to "UDoo" since that is the vessel you just set up.

Now it is important to test all of the instruments at the same time.

- Click *Options* - *Com* - *WCOM32* A window pops up with nothing in it
- Click *Port* - *Open Port* - *Com1* (this starts the GPS data streaming)
- Click *Port* - *Open Port* - *Com5* (this starts the Echosounder data streaming)
- Click *Port* - *Open Port* - *Com6* (this starts the KVH data streaming)

Make sure that all of the incoming data makes sense. You should also run a dry test in the Survey Program, just start logging and note if all of the values in the display area seem to make sense. NOTE: It can appear as though the devices are all working in the WCOM32 test while the drivers are not completely set up properly for Survey. The only way to ensure that they work in Survey is to test them in Survey, so do that.

If everything appears normal (devices should display some kind of nonsense data if their drivers are set up properly, not just zeros), then all your drivers are set and you're ready to survey.

A.11 GPS Specifics

Setting up the Ashtech Z-Family GPS to stream data from its serial port for Hypack to read. You should follow the step-by-step instructions for field operations written by Jack Puleo and Tom McKenna that are found in the big black binder that contains the GPS manuals.

In addition to these steps, you must have already saved a .txt file on the orange handheld GPS logger. That text file contains commands to tell the rover to output the NMEA 3.0 sentences that you selected under the Advanced tab of the

GPS.dll or kinematic.dll driver in Hypack. The text file should look exactly like this:

$PASHS,NME,GGA,A,ON
$PASHS,NME,GLL,A,ON
$PASHS,NME,RMC,A,ON
$PASHS,NME,VTG,A,ON
$PASHS,NME,GST,A,ON
$PASHS,NME,PER,1

These commands tell the rover to:

1. output the GGA sentence through COM A, GGA contains GPS fix data
2. output the GLL sentence through COM A, GLL contains position data
3. output the RMC sentence through COM A, RMC contains recommended minimum specific GPS data
4. output the VTG sentence through COM A, VTG contains course over ground and ground speed data
5. output the GST sentence through COM a, GST contains GPS pseudo-range statistics (I don't know what that means either)
6. output all of these sentences once per second.

A.12 RTK Tides in Hypack

There are a few options for using the RTK GPS to correct for tides in Hypack. There is a specific tutorial slideshow/video just on this topic. Most of these methods assume that surveys will reference a chart datum; this is not the case for most UDoo surveys which will most often reference data to the North American Vertical Datum of 1988 (NAVD88).

Since the UDoo will be operated in relatively small areas where the difference between geoid and ellipsoid can be assumed not to vary, and since it is designed to operate in various wave conditions — the survey vessel will be considered a floating survey rod of fixed length. The RTK GPS outputs very precise elevations relative to the ellipsoid, and thus if the precise distance between the antenna and the echosounder is known, then the depth recordings can be referenced to the ellipsoid as well. The local difference between the geoid (mean sea level) and the ellipsoid is given at tidal benchmarks, and can be applied to correct the depth data to the proper reference datum.

Since charts and maps are only used for background graphics in Hypack by UDoo operators, this storage of depth data relative to the ellipsoid simplifies post processing — as all interpretation of the data will employ the ellipsoid as a datum.

A.13 Reference

MacMahan, J. H., 2001. "Hydrographic Surveying from Personal Watercraft." *Journal of Surveying Engineering.* 127(1): 12-24.

Figure 2-20 Serial Port Configuration

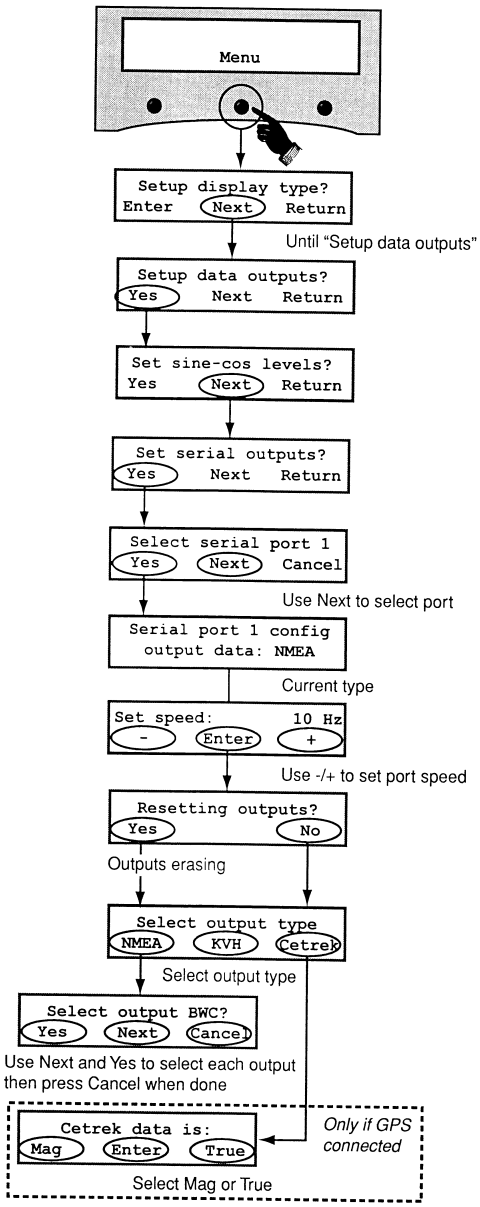

Figure A.13: Procedure to program serial output of the KVH ACU. Use serial port 2 and the KVH output stream.

Appendix B

TRAFFIC BOX CONFIGURATION

The aluminum enclosure that contains all of the power and communication components of the BBSMS is commonly known as the *Traffic Box*. This box was purchased from supplier DDB Unlimited along with the four shelves contained within. Off the shelf features of the box included a thermostat controlled vent fan, louvered side vents, and an electrical outlet. The interior dimensions of the box are limited by the standard 19 inch wide racks that act as shelf supports, though there is ample space outside the racks to route cables. The shelves are movable up and down the racks, but are currently spaced to allow access to the middle two shelves which hold the computers and communication components for the underwater instruments. Four large diameter bolts anchored in a 4 inch think concrete pad hold the Traffic Box in place, the pad is also anchored into the sand with lengths of rebar.

To the untrained eye, the Traffic Box could appear confusing, or even like an untamed wilderness (see Figure B.1); however, the configuration follows an elegant logic comparable to a Monday morning New York Times Sudoku puzzle. In other words, do not be afraid — you can probably figure it out in an hour or so.

For a detailed description of the instruments and their operation, see section 3.2 on page 59. The components inside the Traffic Box serve as support for the deployed tilt sensors, current profilers, and scanning sonar. One mini-PC controls the sonar and ADCP for the south pier, the other mini-PC is reserved for the north pier. The tilt sensors feed data to the Campbell Scientific logger, which interfaces

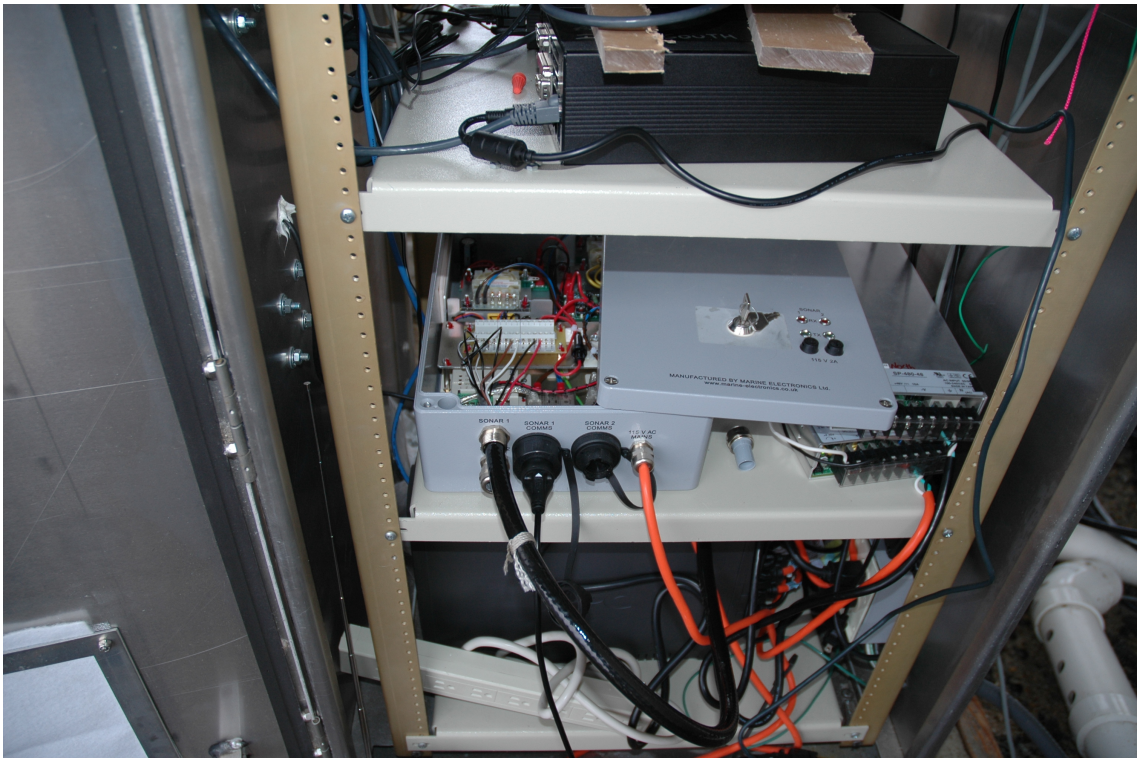

Figure B.1: Photograph of shelves 1,2, and 3 (numbered from bottom) in the Traffic Box, the maze of cables is explained more clearly in Fig. B.2

with the laptop computer. All of the computers and the data logger are connected to the secure network which allows data to be transferred to the University, and allows limited remote access to the machines in the field.

The mini-PC computers are marked with *North* and *South* to indicate the instruments they control. The incoming cable ports are also designated with North and South markings, as the incoming cables are separated according to their pier of origin — note that the incoming ports appear vertically stacked in the drawing in Figure B.2, while in reality they are horizontally stacked, refer to their markings for North/South designation.

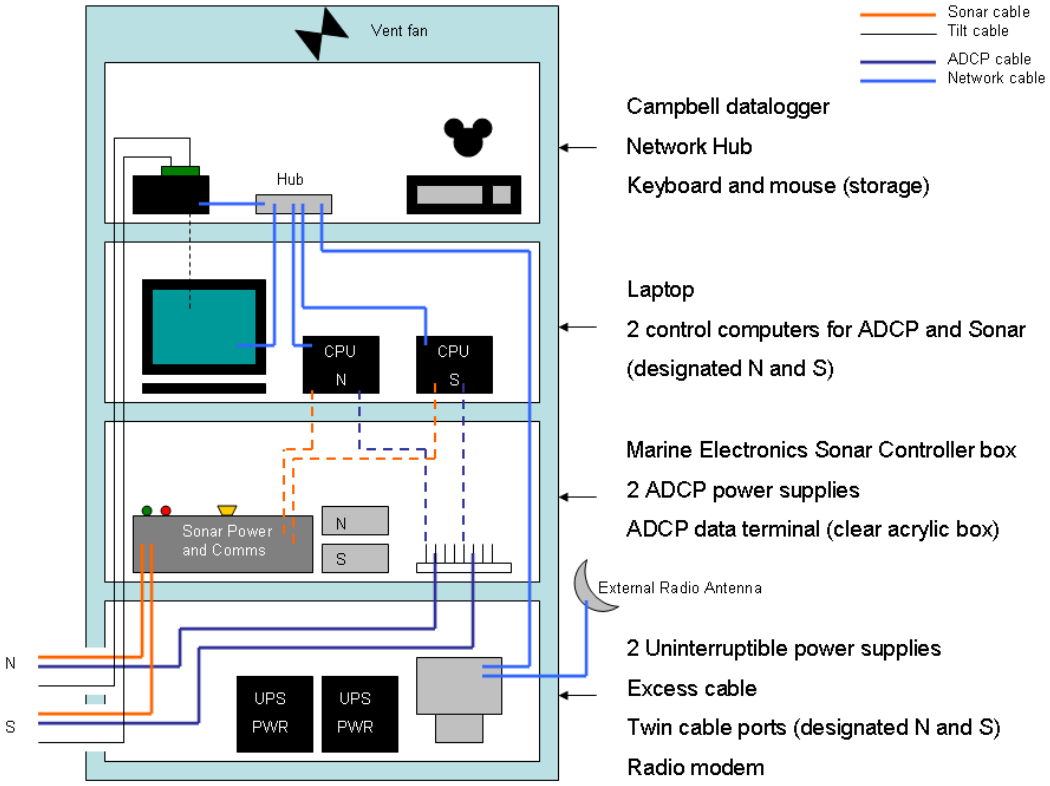

Figure B.2: Schematic of shelves and cabling inside the Traffic Box, for simplicity power cables have been omitted.

Power enters the box via a separate smaller port, and was wired by a DelDOT

electrician through the old cathode protection system (the galvanized steel box that sits next to the Traffic Box). In order to provide the BBSMS with robust operation, no devices should be plugged directly into the wall outlet; computers and instruments should be plugged into a battery backup outlet on one of the UPS boxes. These provide enough juice to the whole system to overcome short disruptions in power, which happen often during summer storms.